TRANSPORTATION RESEARCH RECORD 1000

Surface Properties–Vehicle Interaction

TRB
TRANSPORTATION RESEARCH BOARD
NATIONAL RESEARCH COUNCIL
WASHINGTON, D.C. 1984

Transportation Research Record 1000
Price $8.20
Editor: Julia Withers
Compositor: Joan G. Zubal
Layout: Theresa L. Johnson

modes
1 highway transportation
4 air transportation

subject areas
24 pavement design and performance
51 transportation safety

Transportation Research Board publications are available by ordering directly from TRB. They may also be obtained on a regular basis through organizational or individual affiliation with TRB; affiliates or library subscribers are eligible for substantial discounts. For further information, write to the Transportation Research Board, National Research Council, 2101 Constitution Avenue, N.W., Washington, D.C. 20418.

Printed in the United States of America

Library of Congress Cataloging in Publication Data
National Research Council. Transportation Research Board.
Surface Properties–Vehicle Interaction

(Transportation research record; 1000)
1. Pavements–Surface–Addresses, essays, lectures.
2. Motor vehicles–Skidding–Addresses, essays, lectures.
I. National Research Council (U.S.). Transportation Research Board. II. Series.
TE7.H5 no. 1000 [TE250] 380.5 s [625.8] 85-10046
ISBN 0-309-03809-X ISSN 0361-1981

Contents

Addresses of Authors

Agrawal, Satish E., ACT-310, Aircraft Safety and Airport Technology, Federal Aviation Administration Technical Center, Atlantic City, N.J. 08405

Bester, Christo J., Council for Scientific and Industrial Research, National Institute for Transport and Road Research, P.O. Box 395, Pretoria 0001, Republic of South Africa

Cap, Jerome C., Sandia National Laboratory, ORG 1251, P.O. Box 5800, Albuquerque, N. Mex. 87185

Daiutolo, Hector, ACT-310, Aircraft Safety and Airport Technology, Federal Aviation Administration Technical Center, Atlantic City, N.J. 08405

Davit, P. S., Ketron, Inc., Hickory Hill Plaza, 131 South Warner Road, Wayne, Pa. 19087

Henry, J. J., Pennsylvania Transportation Institute, Pennsylvania State University, Research Building B, University Park, Pa. 16802

Her, Innchyn, Pennsylvania Transportation Institute, Pennsylvania State University, Research Building B, University Park, Pa. 16802

Huebner, Richard S., Pennsylvania Transportation Institute and Department of Civil Engineering, Pennsylvania State University, University Park, Pa. 16802

Huft, David L., South Dakota Department of Transportation, 700 Broadway Avenue, East, Pierre, S. Dak. 57501-2586

Ivey, Don L., Texas Transportation Institute, Texas A&M University System, College Station, Tex. 77843-3582

Janoff, Michael S., Ketron, Inc., Hickory Hill Plaza, 151 South Warner Rd., Wayne, Pa. 19087

Marks, G. Warren, Pennsylvania Transportation Institute and Department of Civil Engineering, Pennsylvania State University, University Park, Pa. 16802

Nick, J. B., Ketron Inc., Hickory Hill Plaza, 151 South Warner Road, Wayne, Pa. 19087

Reed, Joseph R., Pennsylvania Transportation Institute and Department of Civil Engineering, Pennsylvania State University, University Park, Pa. 16802

Wambold, J. C., Automotive Research Program, Pennsylvania Transportation Institute, Pennsylvania State University, Research Building B, University Park, Pa. 16802

Wang, Jiunnjyh, Pennsylvania Transportation Institute, Pennsylvania State University, University Park, Pa. 16802

Zimmer, Richard A., Texas Transportation Institute, Texas A&M University System, College Station, Tex. 77843-3582

South Dakota Profilometer

DAVID L. HUFT

ABSTRACT

In order to provide accurate and consistent pavement roughness measurements for its pavement management system, the South Dakota Department of Transportation designed and constructed a profilometer system during the fall and winter of 1981-1982. A linear accelerometer and a noncontact ultrasonic ranging device mounted on a standard automobile and controlled by an onboard microcomputer measure a vehicle's independent profile at normal urban and rural highway speeds. In approximately 10 weeks of operation during the summer of 1982, more than 8,000 lane-miles of highway were tested; because of the high degree of automation in processing the measurements, the entire state highway system's roughness ratings were computed and entered into the Department's central highway data base within 3 weeks following completion of field measurements. The roughness measurements are a major input component in the analysis the Department uses to assign priorities and program construction projects.

Because pavement roughness has long been recognized as one of the most significant indicators of overall pavement condition and performance, most states have established roughness measurement programs. A variety of systems have been devised to perform the measurements, but most currently used are response-type road roughness measurement systems that measure the severity of a test vehicle's response to the profile of the roadway being tested. Although such systems have some usefulness, they generally suffer one serious drawback: because the responses of different test vehicles (and even of the same vehicle at different times) vary widely, it is difficult to establish and maintain calibration. In addition, the roughness ratings, usually in inches per mile, are often difficult to relate to pavement properties. Before 1981 the South Dakota Department of Transportation used a response-type system.

A second group of roughness measuring systems includes those devices that are designed to measure the actual roadway profile instead of a vehicle's response to the profile. Both low- and high-speed profilometers have been designed. Because the measurements obtained from these systems are essentially independent of the test vehicle suspension characteristics, calibration is more easily established and maintained. During the fall and winter of 1981-1982, the South Dakota Department of Transportation (SDDOT) designed, constructed, and tested a high-speed, noncontact profilometer that was used to test the entire state highway system during the summer of 1982. The profilometer and the current use of profile measurements are described in this paper.

PRINCIPLE OF OPERATION

In order to understand the principles involved in high-speed profilometery, it is useful to consider a vehicle's response to a step in a roadway profile (Figure 1). In this discussion, the lower front corner of the vehicle body is chosen as the vehicle's point of reference.

Before encountering the profile step, the vehicle body maintains an equilibrium position at some distance above the roadway surface. When the wheel encounters the step, the wheel and then the vehicle body are driven upward. Depending on the characteristics of the vehicle suspension, the body assumes a damped periodic motion, until it again attains its equilibrium position. The record of the vehicle's vertical position is described by the curve u(x), where x is the roadway distance coordinate.

The vehicle height above pavement h(x), the distance between the vehicle reference point and the roadway surface, depends on both the profile and the vehicle motion. Before encountering the step, the height is the equilibrium distance; from the time the reference point is above the step until the vehicle's periodic motion is completely damped, the height varies, dependent on both the height of the profile step and the vehicle's response. Finally, the equilibrium height is again attained.

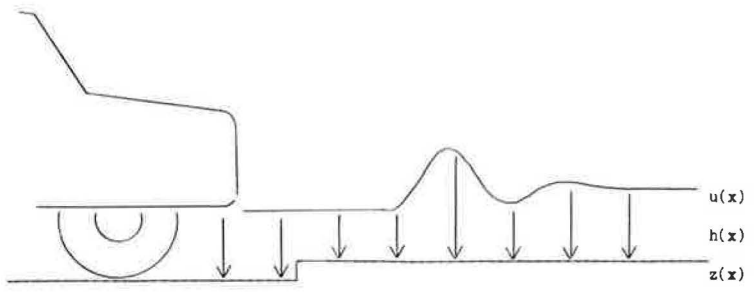

$$z(x) = u(x) - h(x)$$

FIGURE 1 Profile measurement principle.

It is apparent that the vehicle height above pavement at any position x is given as the difference between the vehicle's position u(x) and the roadway profile z(x). That is:

$$h(x) = u(x) - z(x) \quad (1)$$

It can be concluded that if both u(x) and h(x) can be measured, then the profile z(x) may be computed as

$$z(x) = u(x) - h(x) \quad (2)$$

Most important, although both measurements u(x) and h(x) depend on the vehicle's response, their difference z(x) representing the roadway profile does not. Indeed, for any vehicle response motion u(x), a corresponding vehicle height h(x) is measured such that their difference corresponds to the roadway profile z(x). In summary, if vehicle position u(x) and vehicle height above pavement h(x) can be measured, the profile z(x) can be computed.

INSTRUMENTATION

The profilometer consists of a standard full-size automobile equipped with a microcomputer and associated electronic instrumentation to measure and record a single profile.

A Digital Equipment Corporation LSI-11/23 microcomputer riding on the back seat of the test vehicle forms the basis of the profilometer instrumentation system. Executing profile measurement software written by the SDDOT, the computer controls the devices that measure the vehicle's horizontal distance, vertical position, and height above pavement, then computes and records the highway profile in real time as the vehicle moves at normal traffic speeds.

The microcomputer is equipped with flexible diskette (floppy disk) drives for storage of operating programs and profile data, a handheld typewriter-style keyboard-display terminal for operator interaction, and a line printer. A 500-watt sine wave inverter located in the trunk of the vehicle provides 115 V AC power to the entire system.

VEHICLE DISTANCE MEASUREMENT

To make the measured profile distance-based, that is, to record profile elevations at equally spaced intervals, the microcomputer is equipped with a horizontal distance-measuring interface. The device, constructed on a single wirewrap prototype development board and installed directly in the computer's backplane, has the capability to accept a desired measurement interval distance under software control. By counting electrical pulses generated by a magnetic pickup that senses magnets attached to the vehicle's left front wheel, the device accurately measures distance and informs the microcomputer each time the vehicle moves the specified distance. For normal roughness survey purposes, the device is programmed to detect 1-ft intervals; for special purposes, any other interval may be selected.

VEHICLE POSITION MEASUREMENT

The vertical position u(x) of the vehicle reference point is determined by using a linear accelerometer, the voltage output of which is proportional to the vertical acceleration of the vehicle body (Figure 2). The acceleration signal is filtered by an analog lowpass filter to remove high frequency (greater than 25 Hz) components corresponding to spurious

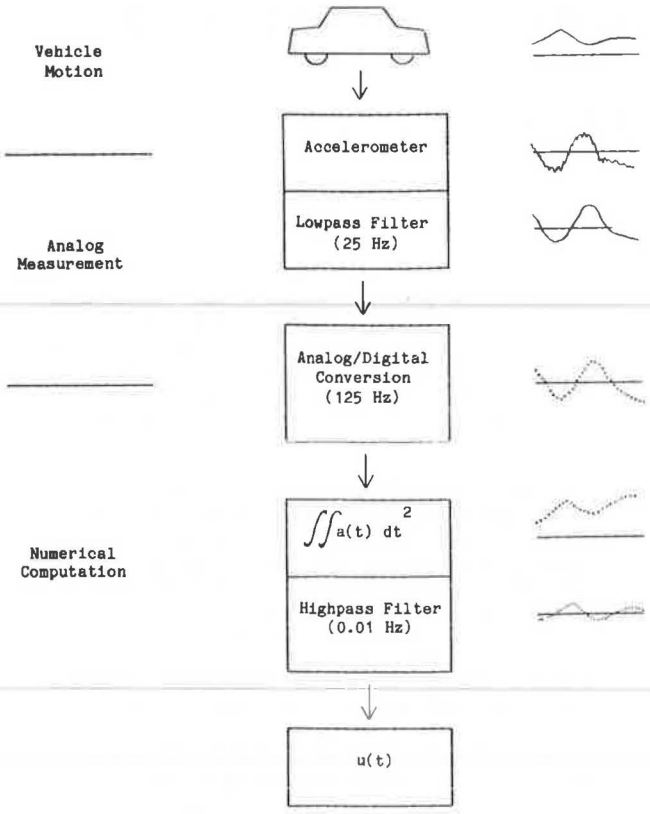

FIGURE 2 Measurement of vehicle position.

vehicle body vibrations, then sampled by the microcomputer's analog-to-digital converter at a programmable clock-controlled rate of 125 Hz. Because acceleration is inherently temporal, the vehicle position record is computed as a function of time rather than distance, as the double integral of acceleration with respect to time:

$$u(t) = \int\int a(t)\, dt^2 \quad (3)$$

Two considerations dictate that this integration be modified by highpass filtering to remove extremely low frequency acceleration components that correspond to long wavelength profile features such as hills and valleys. First, offsets induced by accelerometer tilt and electronic drift also appear as low frequency, nearly constant terms in a(t); these would generate errors in u(t) proportional to the square of time, quickly overwhelming the true long-term profile. Furthermore, even if offset errors were not present, true profile measurement would be possible only if the vehicle's initial conditions--elevation and vertical velocity--were precisely known. Such instrumentation would increase system cost by at least one order of magnitude. By removing signal components corresponding to both offset errors and true long wavelength profile features, highpass filtering forces the computed vehicle position u(t) to remain numerically close to zero, in effect making the long-term vehicle position record an assumed horizontal line.

After the acceleration is digitized, a single numeric operation simultaneously performs both the double integration and highpass filtering. The nominal 3 db cut-off frequency of 0.01 Hz corresponds to a wavelength of approximately 8,000 ft at 55 miles per hour. Because longer wavelength features such as hills, valleys, and long inclines are

essentially removed from the vehicle position record, they are missing from the computed surface profile as well. For computation of roughness ratings, these features are not important anyway; it must be remembered that the measured profile does not represent an accurate long distance survey, however.

VEHICLE HEIGHT MEASUREMENT

The record of vehicle height above pavement is measured by an ultrasonic ranging device mounted directly beneath the linear accelerometer (Figure 3). The transducer transmits a 150-microsecond pulse of 50 KHz sound waves downward to the pavement surface, which reflects the sound to the same transducer.

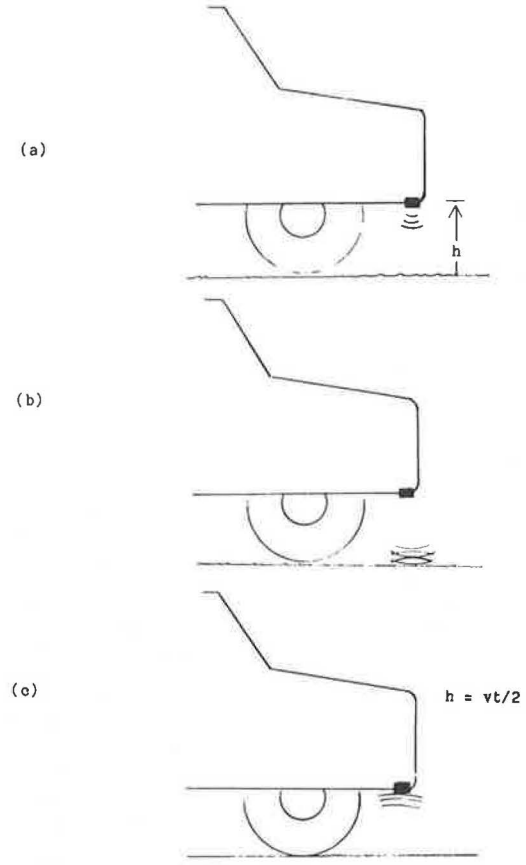

FIGURE 3 Measurement of vehicle height.

The elapsed time between transmission and detection of the reflected echo is proportional to the vehicle height, according to the relation:

$$h = vt/2 \quad (4)$$

where v is the velocity of sound in air, approximately 1,090 ft per second.

Ultrasound transmission and echo detection are controlled by a custom interface constructed on a single wirewrap prototype board installed in the microcomputer's electrical bus. The interface is capable of initiating a height measurement under software control, generating a program interrupt when the measurement is complete, and providing a count representing the elapsed time. Although the count is recorded in microseconds, allowing very fine measurement resolution, the accuracy of the ultrasonic ranging device is limited by the ability to cleanly detect the 50 KHz echo. On sound pavement surfaces, variations in the surface macrostructure can induce echo phase shifts, leading to an uncertainty of one half-period (10 microseconds) in the time measurement, corresponding to a distance uncertainty of 0.005 ft.

Extremely irregular surfaces may scatter the ultrasound so severely that the echo is detected either very late or not at all. Although this problem occurs less than one measurement in one thousand on most asphalt and concrete pavements, it is troublesome on coarse chip sealed pavements. Work is in progress to improve operation on this surface type. Meanwhile, the profile measurement software detects and counts poorly received echos, and flags each affected profile measurement. Subsequent software may then replace these measurements with interpolated values, if desired.

The ultrasonic transducer is an instrument grade version of the transducer used by Polaroid on autofocusing cameras, mounted in 1.5-in. Polyvinyl chloride pipe fittings. It withstands temperature extremes and dust, and is insensitive to wheel, engine, and other traffic noises. It is not waterproof, however, and although the unit will work in conditions of light mist, operation must be suspended during rain showers.

PROFILE DETERMINATION

Because vehicle position is computed at equal intervals of time while vehicle height above pavement is computed at intervals of distance equal to the desired profile data interval, the two records must be merged by software methods. At the conclusion of each vehicle height measurement, the height is subtracted from the most recently computed vehicle position, giving the profile value at that point. The difference between that value and the previous profile value is then stored on diskette. Comparison of successively measured profiles of the same highway section reveals the measurement repeatability over both short (Figure 4) and long distances (Figure 5). Although it is somewhat difficult to ensure identical vehicle paths for repeated test runs, the repeatability of both plotted profiles and computed roughness ratings has been very good.

OPERATION

Because system efficiency and ease of use are important considerations, the profilometer instrumentation and controlling software are designed to maximize machine work and minimize operator effort. There are no calibrations or field adjustments to be made, and the computer is "friendly"--the operator is prompted whenever input is required. Simplified operational procedures enable a two-man crew to achieve a consistently high level of production.

Preparation

The crew, consisting of driver and operator, is responsible for planning test routes so the greatest number of lane-miles are tested for the number of miles driven. In rural test areas, a daily route of approximately 350 to 400 miles is planned; of these, an average of 200 miles are tested. (This is largely the result of having a limited number of access

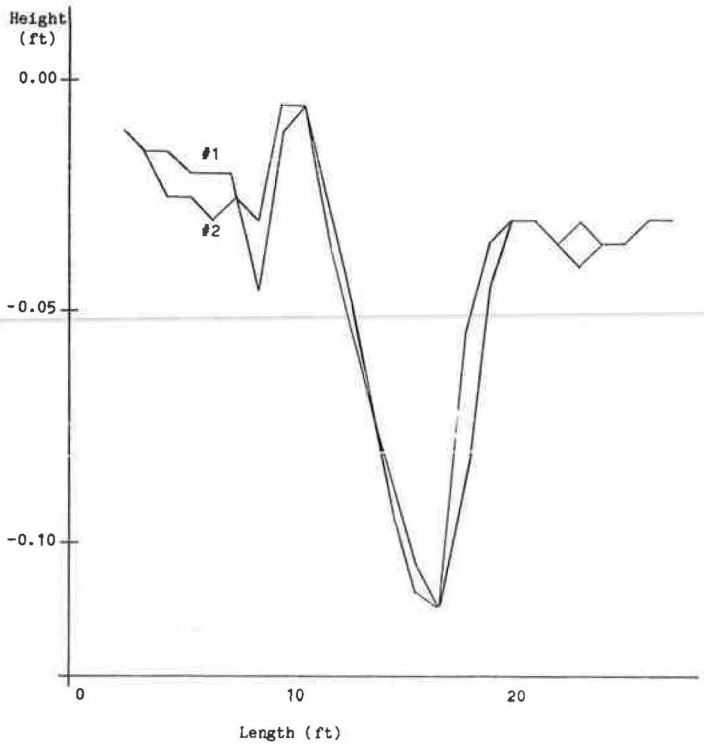

FIGURE 4 Short distance profile repeatability.

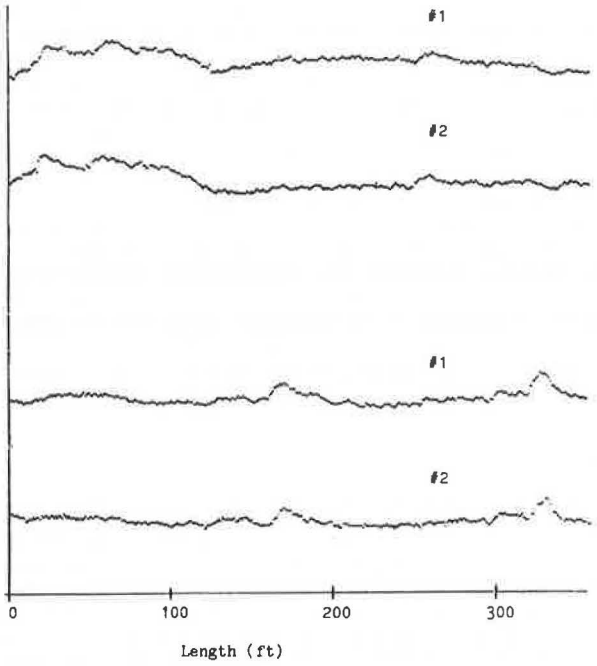

FIGURE 5 Long distance profile repeatability.

routes from the central office to the state perimeter areas.) Before beginning a 4-day workweek, the entire week's route is mapped and overnight layover locations are determined.

The crew is also responsible for routine system maintenance, including verifying the equipment's operation using quickly executed diagnostic programs at daily intervals, checking the appearance of exposed instrumentation and wiring, and ensuring that adequate supplies of computer paper and diskettes exist.

Test Procedure

Before beginning profile measurement, the operator must identify the highway to be tested and verify that sufficient disk storage exists to record the intended test length. After being informed that the system is ready to begin profile measurement, the driver initiates car motion. At the beginning point, the operator enters the begin command, optionally specifying the mileage reference marker (MRM) of that point. As subsequent MRMs are encountered, the operator enters their identification, continuing until the end of the project is reached.

After the entire profile is measured, the operator identifies the project location and may enter remarks concerning pavement condition, weather, or any other pertinent information. The existence and order of MRMs are verified against the computer's master MRM file, and the operator is given opportunity to correct errors. Figure 6 shows the operator action required on a short test project.

OUTPUTS

When roadway profiles are measured, they are recorded on magnetic media and documentation of test activity is printed. Although the profiles may be further analyzed in the field, plotting and roughness rating computations are normally performed later in the laboratory.

Raw Profile Data Files

The measured profile and associated information for each project are placed on a flexible diskette in a

```
PRF001:  SDDOT Profilometer System

Operators?  OVERBAY & SCHAACK

Highway  1014 W                                  (Identify highway)

72.5 miles remain on disk 110                  (Verify that sufficient
Change disk?  NO                                 space exists on disk)

PRF001 ready--

*B                                             (Begin recording profile)
*M233                                          (Locate Mileage Reference
*M235                                        Markers as they are passed)
*M231
*E                                                     (End profile)

Lane?  2                                         (Identify lane number)

Project?  EAST OF PIERRE                            (Identify location)
Remarks?  EXAMPLE                              (Miscellaneous remarks)

MRM changes/deletions?                         (Correct MRM error above)
From?  235
  To?  232

Highway?                                      (Next highway, if desired)

PRF001 done
```

FIGURE 6 Typical operator input.

file named after the project's highway and approximate MRM. Each diskette contains up to 94 miles of profile data, assuming a data spacing of 1 foot. All further analysis is based on the information contained in these files.

Field Activity Reports

For each test project, a record of field test activity is printed on the line printer (Figure 7). The highway, lane, and project identification as well as the date and time of test are indicated first; other parameters relating to the test conditions follow. These include identification of the test vehicle and specification of the average test speed, data interval, vertical resolution of the recorded profile, total number of data points, and number of data points at which no valid ultrasonic echo was received.

A list of project location events follows, including the location of the test beginning and ending and the occurrence of mileage reference markers throughout the project. For sections between MRMs, the ratio of distance measured by the profilometer system to the distance recorded in the MRM inventory is computed and printed; deviations exceeding 5 percent are flagged, providing a check on the system's distance measurement and enabling seriously misplaced MRMs to be detected.

Normally, field activity reports are sorted and filed in order of highway and MRM. The identification of the disk number and project file name then enable the project profile to be easily referenced for further analysis.

Profile Plots

Measured profiles may be plotted on the system's line printer (Figure 8). Each profile data point is

```
PRF001:  Profilometer Field Activity Document

Highway: 1014 W
Lane:    2
Project: EAST OF PIERRE
Remarks: EXAMPLE
   Date:  16-NOV-83
   Time:  15:13:26

      Test Vehicle:  000476
Average Speed (mph):  49.383
 Data Interval (ft):   1.000
    Resolution (ft):   0.005
  # of Data Points:   18100
 # of Bad U/S Data:       1

Project                          Distance
 Event        MRM       Disp       Ratio

 Begin      233.00     0.864
            223.00
            232.00                  1.001
            231.00                  0.997
End         231.00     0.574

Disk:    110
File:  0140W0.233
Operators:  OVERBAY & SCHAACK
```

FIGURE 7 Profilometer field activity document.

```
PRF010: Profile Plot
25-NOV-83 20:50:58

Highway: 1014 W
   Lane: 2
Project: EAST OF PIERRE
Remarks: EXAMPLE
   Date: 16-NOV-83
   Time: 15:13:26

      Test Vehicle: 000476
Average Speed(mph): 49.383
 Data Interval(ft):  1.000
    Resolution(ft):  0.005
  # of Data Points:  18100
 # of Bad U/S Data:      1

Filtered Profile Plot
Highpass wavelength: 500.00
(Profile 1/4 actual scale)

231.00
```

FIGURE 8 Profile plot.

represented by a single dot; tic marks indicate each interval of 50 data points. The plotting software includes highpass filtering to eliminate long wavelength features if desired. Those profile features of wavelength longer than the specified cutoff wavelength are attenuated, while those of shorter wavelength are unaffected (Figure 9).

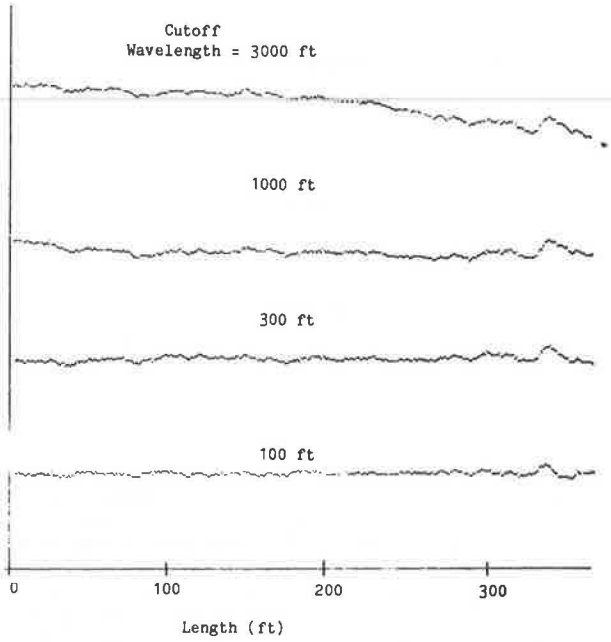

FIGURE 9 Profile filtering.

Although profile plots are useful for verification of system operation and for detailed analysis of specified highways, they are not routinely generated for roughness surveys. Visual inspection of several thousand miles of profile is simply not practical.

Roughness Ratings

Roughness ratings are computed as a function of the mean square power present in the measured profile at wavelengths shorter than 50 ft (Figure 10). The profile is first filtered to remove longer wavelength components, then the power is computed as

$$P = (1/L) \int^2 z(x)\, dx \quad (5)$$

where L is the length of the section being considered. Finally, a roughness rating between zero and five is computed as

$$5 \exp \left\{ -[\ln(P) + 13.42/4.38]^3 \right\} \quad (6)$$

This formula, derived through comparison of power P to a panel's subjective roughness ratings for a diverse sampling of pavement surfaces, assigns a roughness rating of five for extremely smooth pavements, whereas ratings lower than one are given to the roughest pavements on the state highway system. Figures 11 and 12 show roughness ratings for a highway section composed of two distinct pavement types; although most of the roadway is an older asphalt pavement, the last three quarters of a mile are 2-year-old concrete pavement. Comparison of the two figures reveals the degree of repeatability in the ratings.

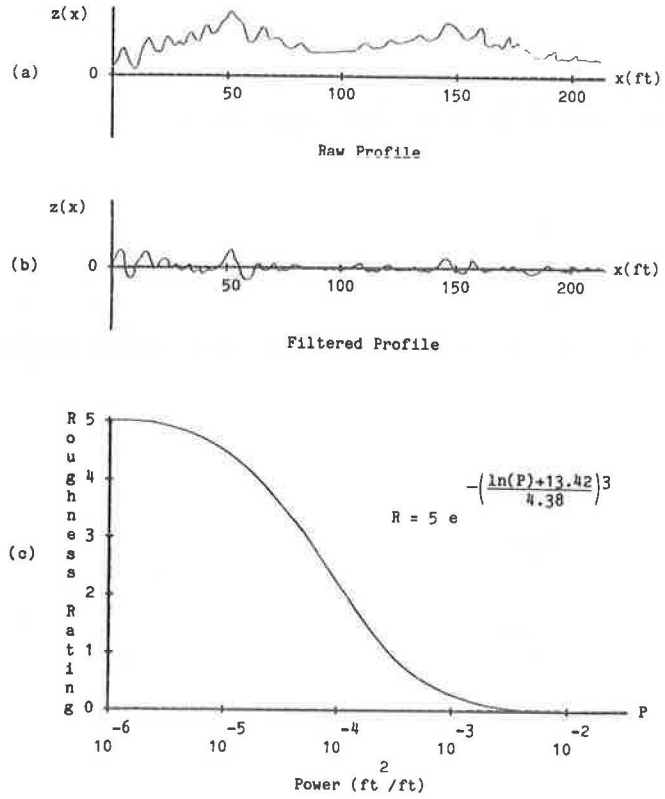

FIGURE 10 Roughness computation.

```
PRF020:  Roughness Rating Document
25-NOV-83 20:50:58

Highway:  1014 W
   Lane:  2
Project:  EAST OF PIERRE
Remarks:  EXAMPLE
   Date:  16-NOV-83
   Time:  15:13:26

      Test Vehicle:  000476
Average Speed (mph):  49.383
 Data Interval (Ft):   1.000
   Resolution (Ft.):   0.005
   # of Data Points:   18100
  # of Bad U/S Data:       1

Roughness Analysis

        From      To     Rough-       Very
 MRM    Disp      Disp    ness      5 Good  4 Good  3 Fair  2

231.00 -0.574   -0.287    2.22      ************************
       -0.287    0.000    2.95      ******************
231.00  0.000    0.250    2.46      ***********************
        0.250    0.500    3.10      ******************
        0.500    0.750    3.05      ******************
        0.750    1.000    4.14      ********
232.00  0.000    0.250    3.73      ************
        0.250    0.500    2.96      ******************
        0.500    0.750    4.02      *********
        0.750    1.000    3.29      ***************
233.00  0.000    0.288    4.94      *
        0.288    0.576    4.22      *******
        0.576    0.864    3.90      *********

Project Average           3.29      ***************

Disk: 110
File: 0140W0.233
Operators:  OVERBAY & SCHAACK
```

FIGURE 11 Roughness rating document.

```
PRF020:  Roughness Rating Document
25-NOV-83 21:12:06

Highway:  1014 W
   Lane:  2
Project:  EAST OF PIERRE
Remarks:  EXAMPLE
   Date:  16-NOV-83
   Time:  16:08:50

      Test Vehicle:  000476
Average Speed (mph):  49.972
 Data Interval (Ft):   1.000
   Resolution (Ft.):   0.005
   # of Data Points:   17974
  # of Bad U/S Data:       0

Roughness Analysis

        From      To     Rough-       Very
 MRM    Disp      Disp    ness      5 Good  4 Good  3 Fair  2

231.00 -0.569   -0.284    2.28      ************************
       -0.284    0.000    2.93      ******************
231.00  0.000    0.250    2.55      ************************
        0.250    0.500    3.13      ******************
        0.500    0.750    3.08      ******************
        0.750    1.000    4.10      ********
232.00  0.000    0.250    3.80      ************
        0.250    0.500    3.02      ******************
        0.500    0.750    3.89      ***********
        0.750    1.000    3.19      ****************
233.00  0.000    0.282    4.94      *
        0.282    0.563    4.40      ******
        0.563    0.845    4.24      *******

Project Average           3.33      ***************

Disk: 110
File: 0140W0.232
Operators:  OVERBAY & SCHAACK
```

FIGURE 12 Roughness rating document.

PAVEMENT MANAGEMENT SYSTEM INPUT DATA

The primary use of the profilometer system is to supply the SDDOT's construction priority assignment analysis with pavement roughness measurements. The computerized analysis determines the sufficiency of the current pavement, estimates the year of construction need, and arranges proposed construction projects in order of priority; the priorities so determined may be overruled only with strong justification. Because roughness measurements constitute one of the primary components involved in the analysis (others include visually determined surface condition, in-place pavement thickness and design, roadway strength, current maintenance cost, and traffic load), timely, accurate, historically consistent measurements are mandatory. The present schedule calls for annual testing of the entire state highway system.

For every project tested, single-lane roughness ratings are computed over approximate quarter-mile sections and recorded on a floppy disk in a format acceptable for input to the central mainframe computer. Because no manual data coding is required, the ratings are quickly available. In 1982 approximately 8,000 lane-miles of roughness ratings were computed and entered into the central roadway data base within a period of 3 weeks following completion of field testing.

COSTS

An important requirement of a profilometer system is that its acquisition, operation, and maintenance costs be low.

Acquisition Cost

Although development costs of the profilometer have been substantial, the actual cost of duplicating the present system is reasonable. The hardware and installation costs may be summarized:

Hardware	Cost ($)
Microcomputer system	9,000
Handheld alphanumeric terminal	500
Line printer	600
Linear accelerometer	1,000
Acceleration lowpass filter*	100
Analog-to-digital converter	800
Programmable clock	600
Ultrasonic ranging transducer/interface*	400
Vehicle distance interface*	400
500-watt, 12-V DC to 115-V AC inverter	1,500
Hardware, connectors, wiring	500
Total	15,400

The items followed by an asterisk are not commercially available, and require construction. For these items, only the cost of materials (components, foundation boards, enclosures, etc.) is shown. Although labor costs for assembly and system installation are not included, a total cost estimate of $20,000 appears adequate.

Operation Cost

Based on 1982 experience, the average cost of measuring and recording highway profiles in a program of statewide testing can be estimated as follows:

	Cost per Mile Tested ($)
Personnel	1.00
Meals and lodging	0.40
Automobile mileage	0.45
Supplies	0.05
Total	1.90

These costs were experienced in a statewide, primarily rural test program, using 4-day, 40-hr workweeks. On the average, slightly more than one-half of the total mileage driven was tested.

The cost of computing roughness ratings and entering the data into the central data base is less than $0.40 per mile tested, including both personnel cost and mainframe computer charges.

Maintenance Cost

It is difficult to estimate average system maintenance costs based on one year's experience. In that time, one of the microcomputer's floppy disk units required replacement at a cost of $400; because the linear accelerometer was dropped in the laboratory, it required $200 to repair. Finally, a transistor in the 115-V AC inverter was replaced at a cost of $20.

Routine replacement of the ultrasonic transducer is required because of accumulation of dirt on its surface. During the year, two replacements were made at a cost of $30 each. No other periodic system maintenance is required, nor is extra vehicle maintenance necessary.

CONCLUSION

The profilometer developed by the South Dakota Department of Transportation has proved to be an efficient instrument for economically measuring pavement surface roughness independent of test vehicle characteristics. Because of the system's speed and high level of automation, it is the intention of the Department to use it to perform annual statewide roughness surveys and to continue to determine construction priorities based largely on the measurements obtained.

Development of a Data Acquisition Method for Noncontact Pavement Macrotexture Measurement

INNCHYN HER, J. J. HENRY, and J. C. WAMBOLD

ABSTRACT

Pavement texture is the controlling factor in the skid-resistance level of roadway surfaces. To obtain more complete data on texture, a noncontact high-speed method was developed to permit the collection of pavement data from a vehicle moving at highway speeds. This method combines existing designs with new processing concepts and hardware improvements and is believed to be promising for the measurement of macrotexture. The system uses a light-sectioning technique in which a strobed band of light with high infrared content is projected onto the pavement. A camera with high sensitivity to the infrared portion of the spectrum views the band at an angle. The pictures resulting from each strobe are stored in a frame grabber and subsequently processed by detecting the shadow along the leading edge of the band to produce a macrotexture profile. The method was evaluated using a prototype system operated both in the laboratory and in the field at 40 mph. The results are encouraging, and recommendations for improvement are made that will result in a practical noncontact macrotexture profile acquisition system.

It is generally agreed that the skid resistance of a pavement is controlled by the surface texture characteristics. Therefore, by measuring the relevant parameters describing texture, or by measuring a physical process dependent on texture, regression techniques can be applied to relate skid resistance to the chosen texture parameter or process. Two scales of texture are of particular importance, microtexture and macrotexture. Pavement microtexture is the deviation of a pavement surface from a true planar surface with characteristic dimensions of wavelength and amplitude less than 0.5 mm. Pavement macrotexture is the deviation of a pavement surface from a true planar surface with characteristic dimensions of wavelength and amplitude from 0.5 mm up to those that no longer affect tire-pavement interaction (1).

A number of pavement texture measurement systems are currently in use or are under development both in the United States and abroad. However, they are still not adequately reliable, are expensive, and are not easy to operate. A project was conducted at the Pennsylvania Transportation Institute to develop a prototype high-speed, noncontact texture measurement technique for both microtexture and macrotexture. The system had to be inexpensive, self-sufficient (which implies that some decisions must be made automatically), and capable of being operated from a moving vehicle at normal highway speeds. Be-

TABLE 1 Comparisons of the Rating Score Levels and Capabilities of the Recommended Texture Measurement Systems

Recommended Texture Measurement Systems	Measurement				Rating Score Levels				
	Macrotexture		Microtexture		Technical Feasibility	Operational Feasibility	Cost Score	Functional Feasibility	Cost-Effectiveness
	Direct	Indirect	Direct	Indirect					
Ensco vidicon system	X				High	High	Medium	Highest	Medium
Ribbed versus blank tire skid-test concept		X		X	High	High	High	Medium	High
Light depolarization		X			Medium	High	High	Medium	Medium

cause the system was expected to measure the texture profile down to about one-half of the lowest wavelength for the macrotexture, high-resolution hardware was required.

BACKGROUND

Many noncontact measuring techniques have been developed and evaluated during the past decade (2), but most are not suitable for operation on a moving vehicle (3). Table 1 presents comparisons of the rating score levels and capabilities of three feasible basic systems. Among them, Goodman's method (4) was considered the most promising system for a noncontact scheme for the high-speed acquisition of pavement texture data. This scheme consists of forming and directing an extremely narrow, fan-shaped, stroboscopic light beam vertically downward onto the surface, and detecting the resultant single-line profile with a camera viewing the light beam at an angle.

In 1976 Goodman's experiments were repeated and enhanced with computerized image processing facilities for the Maryland Department of Transportation (5). The system used a high-intensity, short-duration flash of light projected vertically onto the pavement through a very thin optical slit. The resulting image on the pavement was a fine line approximately 100 mm long and 0.25 mm wide. The sampling frequency was 10 Hz, which provided a reading every 1.8 m at a vehicle speed of 40 mph. The results had a very poor resolution and were restricted to relatively low vehicle speeds, typically below 40 mph. Blooming of the video image was a serious problem whenever an adjustment to the system was required to compensate for the lack of contrast between the image and the background, caused by high levels of ambient light and by the pavement color. The pavement being measured had to be fairly smooth in order to minimize the vertical motion of the vehicle so that the optics of both the projecting system and the television camera were in proper focus. It was also reported that the system should be operated at night, because the thin slit of light projected on the pavement tended to be masked by the ambient illumination.

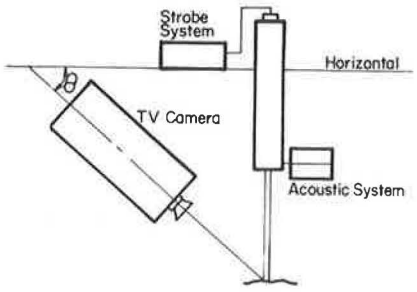

FIGURE 1 Profile acquisition system—schematic.

PROPOSED SCHEME

To overcome the limitations of existing techniques, much effort has been directed in the past few years to develop methods that embrace new concepts and existing designs. Figures 1 and 2 show the basic concept composed of several separate subsystems that are described individually in the following paragraphs.

Strobe System

The entire system is designed to be operated from a vehicle moving at a highway speed of at least 40 mph, or about 25 mm per millisecond. In order to freeze a picture at these speeds, with no more than

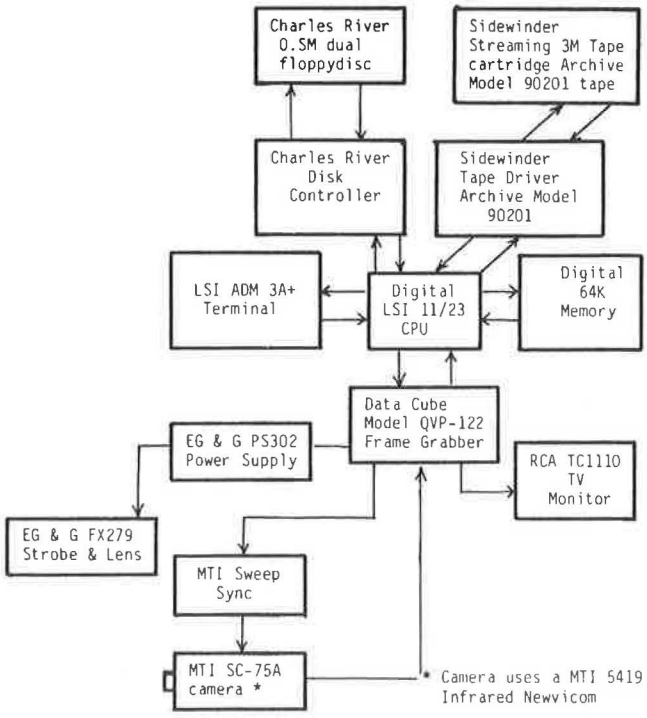

FIGURE 2 Profile acquisition system—block diagram.

a one-half-millimeter smear (the required tolerance for macrotexture), a stroboscopic light source with a flash duration as short as 20 microseconds is required. A bulb-type xenon flashtube (EG & G Fx-201) was selected for the prototype version of the system design, although a linear xenon flashtube is suggested for further improvement of the prototype. The entire spectral output of the flashtube is not useful because only the near-infrared range is used. To ensure that the system functions well during daylight as well as at night, image inputs are filtered to pass only the near-infrared before they enter the television camera to improve the contrast (S/N ratio) between the profile and the background. Figures 3 and 4 show the average daytime background

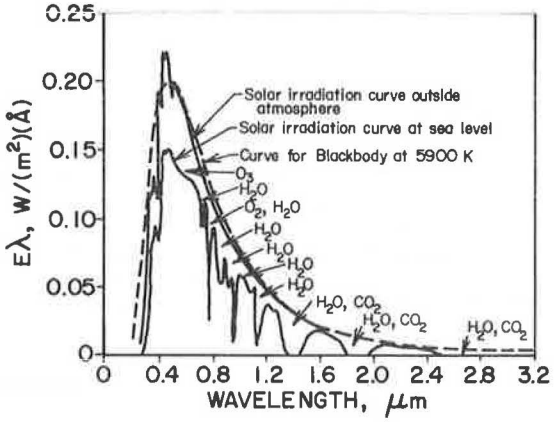

FIGURE 3 Spectral distribution on the sun.

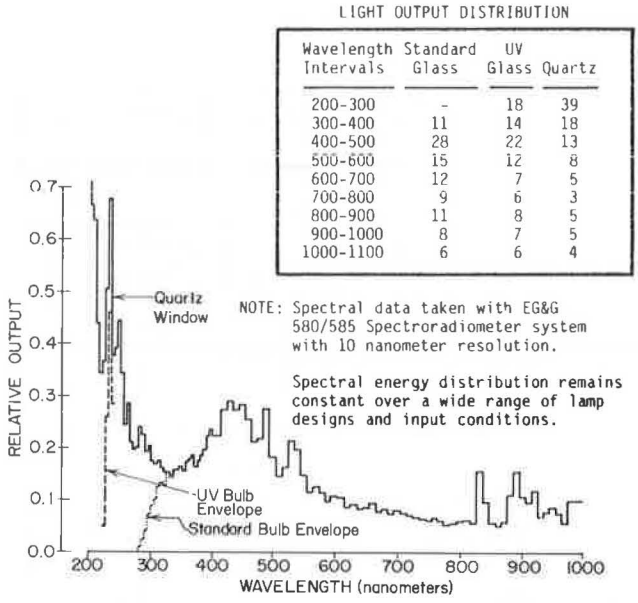

FIGURE 4 Spectral distribution for a bulb-type flash lamp.

radiation spectrum and the power spectrum of the present flashtube. Less than 20 percent of the flashtube output passes through the present filter (Figure 5), a waste of energy that could be reduced by using a more suitable infrared source.

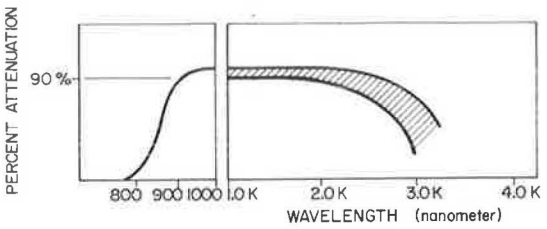

FIGURE 5 Characteristics of filter used in the profile acquisition system.

Optical System

The light source generated by the flash tube is collected, directed, and focused to form a concentrated strip of light on the pavement. To achieve this, the optical system is composed of a concave reflection mirror that makes use of the upward light beams, a pair of optical condensers, a sharp-edged band slit (no longer a thin slit), pairs of projection lenses, and some adjusting mechanisms. Several arrangements were incorporated to increase the performance of the optical system. First, the position of the condensers was accurately adjusted so that a semi-focused image of the discharging arc of the strobe was formed on the slit. Instead of forming an evenly illuminated disc on the slit, this method allows for a concentration of the light to pass through the slit. Second, a pair of orthogonal cylindrical lenses was implanted in front of the projection lenses.

The effect of the cylindrical lenses is to permit linear expansion of the projected image only in the desired direction, and thus refine the sharpness of the edges of the slit. Because the output of the whole system is filtered before it enters the television camera, the chromatic aberration, which is usually inevitably associated with wide-band continuous light sources passing through different media, is therefore reduced to a negligible amount.

Acoustic System

This system, which provides a major technical advance over other existing designs, serves as a system synchronizer to continuously provide synchronization signals to each subsystem processor; it gives commands to other systems while it detects suitable conditions for taking pictures, for example, when each subsystem is ready and the picture is in focus. It is equivalent to a built-in automatic focusing device that relieves the television camera and the optical system of the constraint of having a large depth of focus. This provides an advantage of higher magnification for the acquisition system, and thus consequently permits a higher degree of precision to be obtained with the entire system (6).

Television Camera

Because the system is required to process low intensity pictures, due to the filtering effects and the short duration of the stroboscopic light source, an extremely light-sensitive camera with the ability to capture short-duration images is required. An infrared-enhanced Newvicon camera (MTI 75 series) was used with a 2-in., f/10 close-up lens. Charge-coupled device (CCD) cameras were considered early in the development of the system, but were rejected because they do not have the desired infrared sensitivity. Because the television camera has analog resolution along each raster line, analog signals represent more important information, which, in this case, is

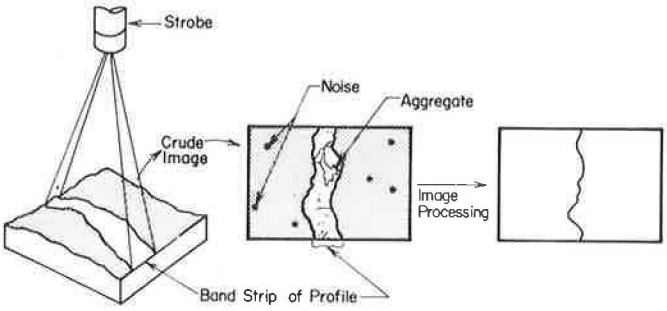

FIGURE 6 Picture acquisition.

the amplitude of the pavement texture. The camera was mounted in the system in such a way that a 2-in. slit on the pavement could be displayed vertically on the screen of the television monitor. With the aid of the acoustic system, the depth of the focus of the television camera was reduced to as small as 0.25 in., and the camera will take pictures only when it is in focus.

Frame of the System

The mechanical supporting frame must be rigid because only a small amount of relative motion can be tolerated between the components of the system. It is also designed to allow easy adjustment, both vertically as well as horizontally, to allow for possible changes of tire inflation and pavement roughness, and for routine maintenance of the system. The frame is mounted perpendicular to the direction of the vehicle, and the slit is positioned to be in a wheel track. The design provides easy mounting of the frame and promises less profile smear and more accurate results than the other alternatives that were considered.

PICTURE PROCESSING

After the television camera has taken a picture containing a pavement line profile, as shown in Figure 6, a series of image processing techniques is applied to obtain usable data and reasonable interpretations of the pictures. These procedures are digitization, preprocessing, profile refinement, and postprocessing. Each of these procedures is discussed below.

Digitization

To analyze and translate the raw analog outputs from the television camera, an image digitizer is needed to provide readable formats for the processors. For the first version, two cards of the high-speed frame grabber (Datacube QVG-120/QAF-120) with 320h*240v resolution and 256 black-and-white intensity on each picture element, were linked to a minicomputer (Digital LSI-11/23). These cards enable the system to process pictures at a speed of less than 5 seconds per picture or, equivalently, 15 to 20 processed profiles per mile of highway pavement.

Preprocessing

Trimming

After digitization, the picture is stored pixel-by-pixel in the random access memory of the frame grabber. Before the profile is taken out and transmitted into the core of the minicomputer for refinement, it is suggested that some preprocessing be performed to help eliminate unnecessary transmission. Figure 7 shows that while the vehicle bounces slightly up and down within the depth of focus of the acoustic system, the image moves from left to right on the monitor. It is clear that there are limits for horizontal pixel coordinates where the acoustic system shuts off the trigger signals. It is straightforward to calculate the limits and to program the frame grabber to transmit only the picture elements located between the bounds. This process reduces some of the noise by eliminating spikes, which sometimes are indistinguishable from data points.

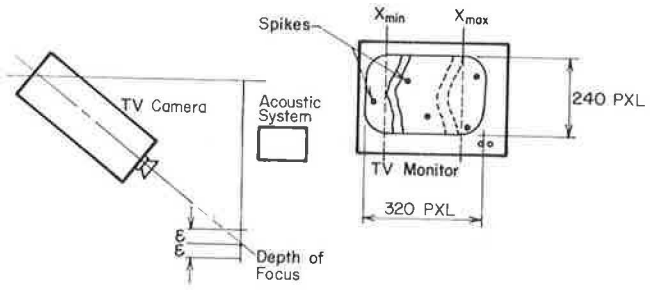

FIGURE 7 Effect of variations in range.

Thresholding

Thresholding is one of the simpler kinds of image-processing techniques. By simply discarding the points for which the intensities are below a certain level, as shown in Figure 8(a) and (b), a rough profile of the picture with some remaining noise is obtained. The threshold level need not be very close to the peak intensity of the profile, as shown in 8(c). Because the distance between the threshold point and the actual profile position is almost constant (with deviation less than dx/2, where dx is the distance between two horizontal picture elements), tracing along the threshold points could be regarded as equivalent to tracing along the actual profile, with only very small errors. Although it may appear that there is great latitude in setting the threshold level, the contrary is true in most cases. Because pavements are usually composed of multicolor textures and aggregates, as shown in parts 8(d)-(f), it is a tedious task to find the right threshold level in various background illumination conditions such that the algorithm traces neither along the edges of dark stones [TS' as shown in 8(e)] nor along the edges of bright stones (TS").

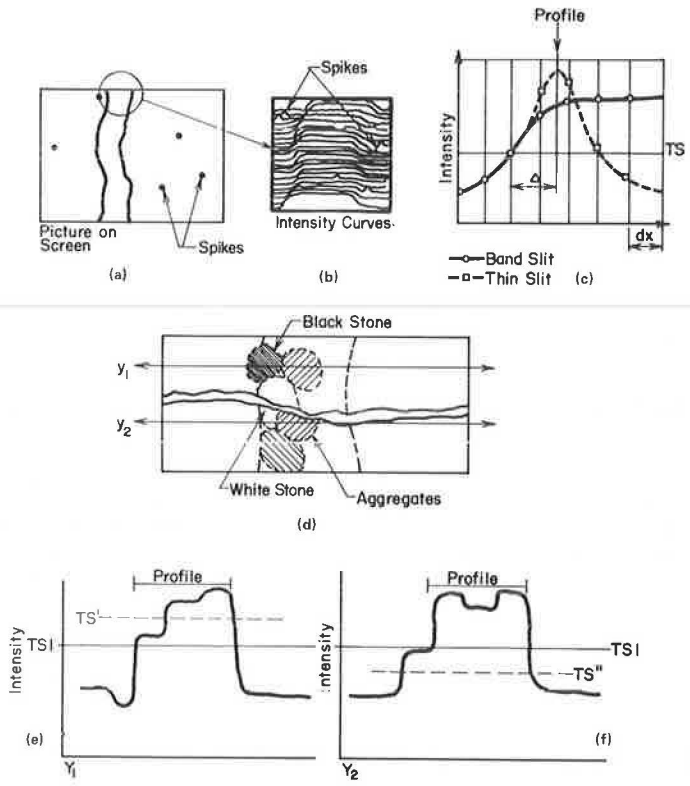

FIGURE 8 Thresholding: (a) picture on screen; (b) intensity curves; (c) threshold level; (d) effect of color of aggregate on pictures; (e) profile for section Y_1; and (f) profile for section Y_2.

An automated thresholding technique will be discussed in the recommendations.

Profile Refinement

A typical result of the system is shown in Figure 9. The raw profile, after thresholding the video output at 80 percent of the maximum intensity (that is, a value of 200 out of 256 maximum) is presented in 9(a). Note that there are several noise points and a few extra segments shown in this figure. The profile as originally generated already displayed discontinuity because the light strip was not evenly illuminated and because the discharge arc moved, due to the intensity of the bulb-type flash system in the prototype. Almost all the noise is removed as shown in 9(b), because the program allows no more than one data point on each horizontal line. By setting a reasonable value for the maximum slope in the preprocessing algorithm, the next processing step [as shown in 9(c-1) and 9(c-2)] is essentially free of all noise. It should be noted, however, that this processing procedure can affect the profile continuity in some cases. The final profile is then created by connecting the remaining points, as shown in 9(d). Line generation is a common technique for which many complete algorithms can be found (7). This final profile is clean-looking and has an accuracy directly proportional to the resolution of the entire system.

Postprocessing

It should be noted that postprocessing procedures are not usually programmed to run in real time with the acquisition system working on the highway. In practice, sequential-access memory peripherals are used to record the processed profiles via parallel logic connections. There are many post-processing techniques available to analyze image profiles. An existing quasi-pattern-recognition scheme developed

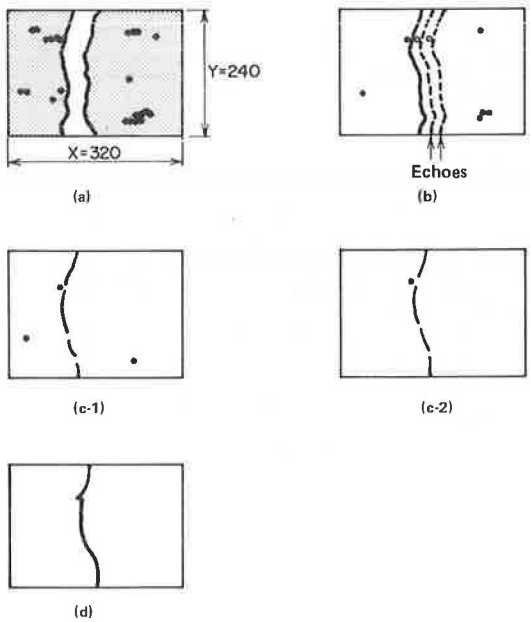

FIGURE 9 Steps in profile refinement.

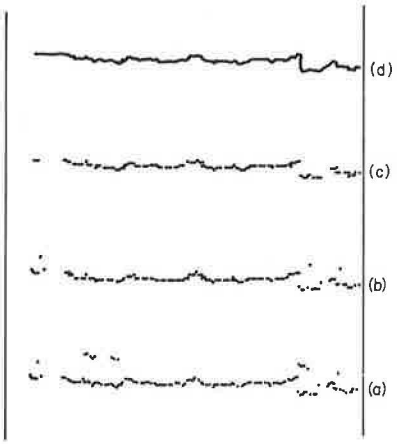

FIGURE 10 Steps in profile refinement for an actual sand surface: (a) raw data; (b) after rejection of outliers; (c) after slope limitation criteria; and (d) final profile.

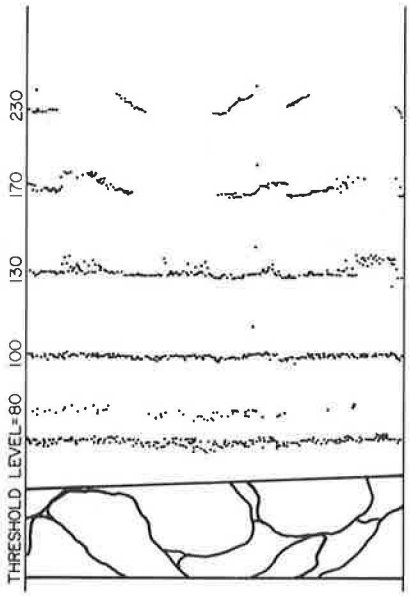

FIGURE 11 Effects of threshold level on raw profile data.

at the Pennsylvania State University was examined for application, but only a small portion of this scheme was directly applicable to this project. Other commonly used profile manipulation techniques include simple root-mean-square (RMS) computation, fast Fourier transformation, and least-square curve processing, but they were not included.

RESULTS AND CONCLUSIONS

A typical result of the system is shown in Figure 10. A raw profile after thresholding the video output at 80 percent (200/256 maximum) of maximal intensity is represented in 10(a). There are some noise points and a few extra segments shown in the picture. The profile is discontinuous because the light strip is not evenly illuminated and also because the discharging arc moves as a result of the instability of the bulb-type flash tube. Almost all of the noise is removed in 10(b) because the program allows no more than one data point on each horizontal line. By setting a reasonable value of MaxSlope in algorithm Clean, 10(c) is expected to be free of noise, although these procedures sometimes affect the profile continuity. The final profile is clean and has an accuracy directly proportional to the resolution of the entire system.

Figure 11 shows an interesting relationship between picture quality and the threshold level in measuring a sample with aggregates having a wide range of color variation. How the sample looked on the television monitor screen is shown in 11(a). There are many kinds of aggregate in which infrared reflecting ability may vary over a wide range. By changing the threshold level, the results are dramatically altered. But if the threshold level is too high, the program follows the more highly reflective stones and the picture no longer represents a line profile of the pavement texture.

Compared with the actual profile of the pavement texture, the results turned out to be quite credible. As shown in Figure 12, the main difference in appearance between the actual profiles and the processed optical results is due to the low resolution of the prototype frame grabber and the unavoidable high-frequency noise generated by the power system of the strobe. A comparison of the RMS values of several different typical core samples, obtained with a contact profiler and the noncontact prototype system, is given in Table 2. This table gives only a rough indication of the capabilities of this system, because the core samples were moved at high speed under the stationary system to simulate actual conditions on a highway. It was difficult to detect accurately on what part of the sample the system took a measurement. Also, the calculated RMS value from the results of the prototype system represents only a particular local texture (2 in. long) of the sample. To obtain as full an RMS range representation

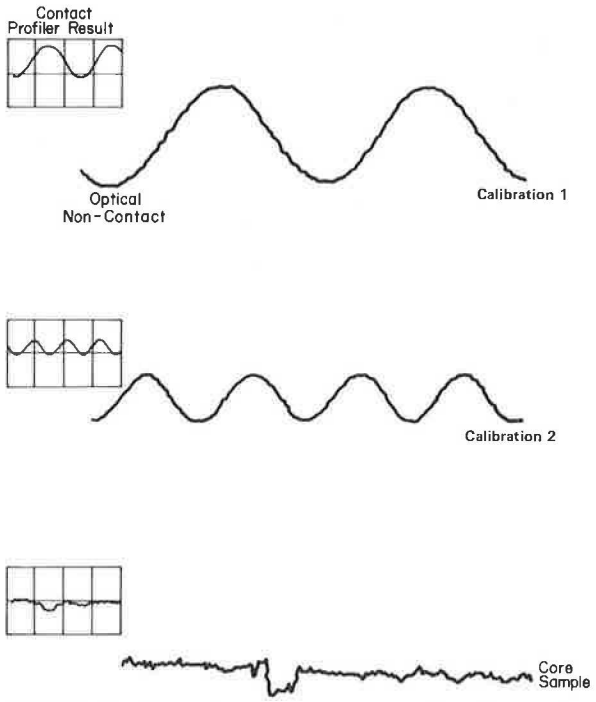

FIGURE 12 Comparison of noncontact profile with actual profile obtained by a contact profile for two calibrated samples and a core sample.

TABLE 2 Comparison of RMS Values of Seven Samples Using a Contact Profiler Versus the Noncontact Prototype

Sample	RMS Value in mm: Contact Tracer	Prototype
1	0.374 to 0.497	0.388
2	0.951 to 0.968	0.438
3	0.847 to 1.014	0.819
4	0.447 to 0.550	0.570
5	0.597 to 0.769	0.693
6	1.188 to 1.490	1.274
7	0.831 to 0.922	0.959

as that obtained with a contact profiler, the results of a sequence of measurements of a sample must be integrated. A positive side effect of moving the samples is that the background texture is blurred and consequently the contrast level of the data signals is increased.

RECOMMENDATIONS

The techniques presented here are by no means a complete solution for measuring pavement microtexture and macrotexture. Improvements in this method, currently being developed at the Pennsylvania Transportation Institute, are as follows:

The hardware system should include a fast microcomputer with hard disk and/or magnetic tape storage capability, a fast, high-resolution picture acquisition system, a strong and steady infrared light source (which can be achieved by using a properly designed linear Kr or Xe flashtube), and a robust, adjustable design of the mechanical supporting frame.

Some work is being done in developing an automated method to choose the optimal threshold level for the frame grabber. The aim is to take a calibration picture each time at the beginning of a run before any real profile is processed. Because correct information on the calibration texture has been stored in memory before the testing, the computer can automatically compare the results and improve the threshold level until it detects when the processed profile matches the stored values. Another possible improvement is to increase the picture resolution by interpolation. Although in this design the computer is no longer connecting the "peaks" of each raster scan to constitute the line profile [as shown in Figure 8(c)], an interpolation routine (for example, cubic spline) can still help to determine at which position the threshold occurs. By expressing the discretized intensity levels by a continuous approximation, better resolution can be obtained. Recommendations for other refinements to the prototype system can be found in Wambold and Henry (8).

ACKNOWLEDGMENTS

This paper is based on a research study conducted at the Pennsylvania Transportation Institute, Pennsylvania State University, under the sponsorship of the Federal Highway Administration, U.S. Department of Transportation. A full discussion of the study may be found in the final report for the project.

REFERENCES

1. Definitions and Nomenclature: Standard Definitions of Terms Relating to Traveled Surface Characteristics. Report E 867-82. American Society for Testing and Materials, Philadelphia, Pa., 1982.
2. M.C. Leu and J.J. Henry. Prediction of Skid Resistance as a Function of Speed from Pavement Texture. In Transportation Research Record 666, TRB, National Research Council, Washington, D.C., 1978, pp. 7-13.
3. J.J. Henry and J.C. Wambold. Pavement Surface Texture--Significance and Measurement. Report 8008. Pennsylvania Transportation Institute, Pennsylvania State University, University Park, 1980.
4. H.A. Goodman. Pavement Texture Measurement From a Moving Vehicle. M.S. thesis. Pennsylvania State University, University Park, March 1970.
5. C. Cantor. Automation of the Schonfeld Method of Highway Surface Texture Code Assignment. Report MD-R-76-8E. FHWA, U.S. Department of Transportation, 1976.
6. J. Wang. Microprocessor-Based Non-Contact Distance Measuring Control System. Department of Mechanical Engineering, Pennsylvania State University, University Park, May 1983.
7. W. Newman and R. Sproull. Principles of Interactive Computer Graphics. McGraw-Hill, New York, 1973.
8. J.C. Wambold and J.J. Henry. Evaluation of Pavement Surface Texture: Significance and Measurement Techniques. Report 8312. FHWA, U.S. Department of Transportation, May 1983.

Traction of an Aircraft Tire on Grooved and Porous Asphaltic Concrete

SATISH K. AGRAWAL and HECTOR DAIUTOLO

ABSTRACT

The Federal Aviation Administration is engaged in an experimental program to determine the effectiveness of various surface treatments to eliminate aircraft hydroplaning when landing on wet runways. The surface treatments included saw-cut grooves, reflex-percussive grooves, and porous friction overlays in the asphaltic concrete runways. Experiments were conducted on a 1.25-mile long track that included a 300-ft test bed containing concrete with 40-ft sections of various surface treatments. Test speeds between 70 and 150 knots were achieved by the use of a jet-powered pusher car that also supported a dynamometer and tire-wheel assembly. The test tire was similar to one that is used on a Boeing-727 aircraft. The results showed that the porous friction overlay, the reflex-percussive grooves, and the saw-cut grooves of various spacing provided similar friction levels under wetness conditions that were either "wet" or "flooded." However, for the "puddled" condition (intermediate wetness between wet and flooded), the saw-cut grooves spaced at 1.25 in. provided the maximum improvement in friction level over a nongrooved or nontreated surface. Thus, although hydroplaning is delayed to a speed higher than 150 knots for all the surface treatments included in the program, the selection of a particular type of surface treatment can be based on whether the rainfall intensities in a region create predominantly wet, puddled, or flooded water conditions on the runway.

The total distance required for bringing a landing aircraft to a complete stop can fluctuate widely, depending upon the friction level available at the tire-runway interface. When this interface is dry, the friction level is high and the aircraft can be brought to a stop quickly; however, the presence of water at the interface reduces the available friction level significantly, and results in hazardous conditions that can cause overrun and hydroplaning.

Runway grooving has been recognized as an effective means of minimizing the danger of hydroplaning. The grooves provide escape paths for water from the tire-runway interface during the passage of the tire over the runway. Runway grooves are usually cut by diamond-tipped rotary blades. Various groove configurations have been used on the runways; however, square grooves of 0.25 in. at groove-spacing between 1 and 1.5 in. have been widely used. Recently, a few runways have been grooved at a spacing of 3 in. Other reportedly effective methods of surface treatment include porous friction overlays and grooving by the reflex-percussive cutting process.

The grooves provided by the reflex-percussive cutting process are still in an experimental stage; however, their cost-effectiveness has been demonstrated by the Federal Aviation Administration (FAA) in the portland cement concrete (PCC) surface by full-scale tire tests under controlled dynamic conditions (1). Because 80 percent of all the runways in the United States are of asphaltic concrete construction, it is important to evaluate the effectiveness of these experimental grooves cut in asphaltic concrete. It is also necessary to determine the relative braking performance of an aircraft tire, under controlled dynamic conditions, on saw-cut grooves cut in the asphaltic concrete surface, particularly in the absence of any such investigation in the past. Full-scale aircraft tests have been conducted on asphaltic concrete surfaces by the National Aeronautics and Space Administration (NASA); however, groove-spacing was not a variable in that study. A direct comparison of the reflex-percussive grooves, saw-cut grooves, and porous friction overlay in asphaltic concrete is the primary objective of this paper. It is expected that such a comparison will provide information about a cost-effective surface treatment for asphaltic concrete runways.

HYDROPLANING AND GROOVING

Aircraft Tire Hydroplaning

The magnitude of the coefficient of friction is influenced by many parameters. The important ones are: speed of operation, water depth, runway surface texture and drainage capacity, condition of tire tread, and the characteristics of the braking system. In general, an aircraft experiences an increase in available friction on a water-covered runway as it is decelerated by the action of brakes. A high level of available friction at the start of the deceleration process will provide better braking and directional control; a low level of available friction at the start of the deceleration process will adversely affect the braking and directional control of the aircraft. A complete loss of braking and directional control results when the available friction at the tire-runway interface approaches zero. Such a condition exists when the aircraft encounters the state of hydroplaning.

Hyroplaning is a peculiar tire-to-runway condition where the aircraft tire is physically separated from the runway surface by a layer of water that supports the aircraft weight by developing hydrodynamic and viscous pressure within the water layer. Hydrodynamic and viscous pressures are associated with fluid density and fluid viscosity, respectively. Thus, when runways are flooded with water, fluid density effects cause predominantly dynamic hydroplaning, whereas the fluid viscosity effects that cause viscous hydroplaning are predominant when smooth runways are covered with only a thin film of water. In all cases of water-covered runways, however, both effects are present to some degree.

In dynamic hydroplaning, the buildup of hydrodynamic pressures in the tire-runway interface causes inward buckling of the tire surface. The

space so created between the tire and the runway is filled with water. A relief in fluid pressures is necessary to regain contact between the aircraft tire and the runway surface for developing higher friction forces for effective braking action and directional control of the aircraft. Partial relief in the hydrodynamic pressures can be obtained by cutting circumferential grooves on the aircraft tire and transverse grooves in the runway surface; grooves of various shapes and sizes can be designed for optimum braking performance. Transverse runway grooves provide a longer-lasting solution to alleviating hydroplaning than the circumferential grooves on the aircraft tire.

In viscous hydroplaning, a thin film of water separates the tread rubber from the aggregate and binder of the runway surface. The deformation of the tire surface within the tire-runway interface is not as large as in dynamic hydroplaning. For an intimate contact to occur between the tire tread rubber and aggregate material, fine-scale asperities (or microtexture) in the aggregate material are desirable. These asperities can break through the thin water film and relieve the viscous pressures.

Runway Grooving

Grooves are small channels of geometrical cross-section cut into the runway surfaces usually by means of diamond-tipped rotary blades. A square cross-section is the most widely used shape for the grooves; however, other promising designs have been investigated by researchers (1).

Pavement grooves were introduced by the British (2) and have been investigated by NASA (3) and the FAA (4). The basic objective of the NASA investigation had been to determine the groove configuration that provided the best cornering and braking performance under wet operating conditions. Investigating various groove widths and depths and three groove spacings (1 in., 1.5 in., and 2 in.), NASA concluded that all groove configurations provided improved cornering and braking performances relative to nongrooved surfaces; however, 0.25-in. square grooves spaced 1 in. apart provided the greatest increase in available friction (3). Based on these and further tests by NASA (5), the FAA has recommended (6) a standard groove configuration of 0.25-in. depth x 0.25-in. width x 1.5-in. spacing and has encouraged airport operators, managers, and owners to groove runways where the possibility of hydroplaning exists. However, many runways remain nongrooved. The major deterrents to the use of runway grooves are the high cost of grooving by the conventional saw-cutting method and the availability of only limited evidence as to the effectiveness of the grooved surfaces at the touchdown speeds of jet aircraft.

In its efforts to find a cost-effective groove configuration for the runways, the FAA completed a test program on PCC in 1981 (4). The study compared the braking performance of an aircraft tire on the reflex-percussive grooves and on the conventional saw-cut grooves. The general conclusion was that the conventional saw-cut grooves, spaced up to 3 in., will provide acceptable braking performance to an aircraft on water-covered runways, and that the cost of installation of grooves at 3-in. spacing can be up to 25 percent less than that of the grooves spaced at 1.25 in. (7). It also concluded that the braking performance on reflex-percussive grooves (spaced at 4.5 in.) was equivalent to that on conventional saw-cut grooves spaced at 2 in., and that the installation cost of the reflex-percussive grooves could be as low as one-half the cost of conventional saw-cut grooves spaced at 1.25 in. However, this information requires verification on asphaltic concrete surfaces. In addition, other promising methods of groove installation or surface treatments should be continuously investigated.

Grooving, Drainage, and Hydroplaning

The improved braking performance of an aircraft on a grooved runway is the result of a dual process of water removal from the tire-runway interface. First, the grooves influence the surface water drainage (runoff) by providing channels through which water can flow freely. How an increase or decrease in the groove-spacing influences the drainage is a subject not clearly understood. However, results from an analytical study (8) show that a decrease in water depth occurs with decreasing spacing for the saw-cut grooves of square cross section. Second, the grooves provide forced water escape from the tire-runway interface when the aircraft travels on a water-covered runway. Because the maximum amount of water that can be removed from the runway in a given time is limited, both the free flow and the forced water escape are important.

Groove roughness plays an important role in determining the flow of water out of the interface. Being laminar in nature, the free flow is enhanced if the groove channels are smooth; forced water escape is essentially turbulent and requires a rough groove channel to provide a shallow velocity profile for increased flow. The free flow, however, may also be turbulent during rain because of the mixing of the pelting rain. Thus, neither a smooth nor a rough groove alone will provide optimum out-flow of water from the interface.

Effectiveness of grooving in providing forced water escape is influenced by the amount of water on the runway and the speed of the aircraft. As mentioned earlier, runway grooves can provide relief in the hydrodynamic pressure developed within the tire-runway interface. Because fluid pressures are predominantly hydrodynamic when runways are flooded, grooves will be very effective on these runways. On the other hand, when the runways are covered with only a thin film of water, where predominantly viscous pressures are developed within the tire-runway interface, grooves are less effective than the sharp-textured aggregates in the runway surface because the pressure relief is accomplished by sharp aggregates breaking the thin water film between the tire and the runway. In the intermediate condition, between thin film and flooding, both grooves and sharp-microtexture aggregates are desirable.

TESTING APPROACH

The measurement of hydroplaning of an aircraft tire is a complex problem that involves simulating the braking operation of an aircraft tire on a wet or flooded runway. The coefficient of friction, as computed by dividing the tangential forces developed at the tire-runway interface by the vertical load on the tire, determines the relative performances of the surfaces tested. As the coefficient of friction decreases, so does the braking capability. In the limiting case, when the coefficient approaches zero, hydroplaning is said to occur. However, the friction coefficient cannot be equal to zero because of the presence of small viscous and hydrodynamic drag forces (at the tire-runway interface), which are difficult to measure accurately. Thus, a direct measurement of the speed at which hydroplaning occurs is difficult. Various indirect methods have been used in the past (9) to identify the onset of hydro-

planing. In the present study, incipient hydroplaning is indicated when the measured coefficient of friction is 0.05 or lower. In comparison, the average coefficient of friction between the aircraft tire and the dry runway is approximately 0.7.

Fractional forces are developed as a result of relative motion between two surfaces; the tire-runway combination is no exception. It is well-documented that as the tire slips in the contact area, a progressively increasing friction coefficient is developed. Tire slip is an indication of the departure of the angular velocity of the braked tire from the free-rolling velocity. Thus, a locked tire represents 100 percent slip whereas a free-rolling tire is under no slip. A slip of between 10 and 20 percent has been identified as the value beyond which the coefficient of friction starts to decrease. This behavior is more pronounced when the tire-runway interface is dry. For wet interfaces, the coefficient of friction remains level over a wide range of slip value; this makes it more difficult to determine the maximum value of friction coefficient under wet interface conditions. There are two methods by which a meaningful comparison of various surface treatments can be accomplished: (a) measurement of coefficient of friction when the tire is locked and slides over the test surfaces, or (b) measurement of maximum available value of the coefficient of friction on each test surface. The present study uses the second method, even though it requires many more tests than the first method.

The disadvantage with the first method is an accelerated treadwear of the tire that may require frequent tire changes; danger of tire blowout is also present in the first method. The advantage with the second method is that it represents a realistic simulation of the braking process of an aircraft. To obtain the maximum coefficient of friction available for a given set of speed, water depth, and surface type (treatment), multiple tests were performed. The first test was conducted at a relatively low brake pressure to assure that wheel lock would not occur. Subsequent tests were conducted at gradually increasing brake pressures. In each test, the magnitudes of the coefficient of friction and tire slip were monitored. Initially, both the coefficient and the slip increased with increasing brake pressure. Later on, a drop in the coefficient or sudden increase in the slip indicated that the maximum value of the coefficient of friction had been obtained in the previous test. This procedure was followed throughout the test program. To eliminate undesired sliding of the test tire, automatic brake release was initiated just beyond the test section in question.

EXPERIMENTAL PROGRAM

Test Facility and Equipment

The experimental program was conducted at track No. 3 of the Naval Air Engineering Center, Lakehurst, New Jersey. The track is 1.25 miles long and has guide rails spaced 52.25 inches apart running parallel to the track centerline. The last 300 feet of the track were used for installing the test bed over the existing PCC surface. The test bed was 2.25 in. thick and 30 in. wide and was made of asphaltic concrete. An aircraft arresting system is located beyond the test track to recover the test equipment at the completion of a test run.

The major components of the test equipment are: the four-wheeled jet car, the dead-load carriage, which supports the dynamometer and wheel assembly, and the measuring system. The jet car (Figure 1) is powered with four J48-P-8 aircraft engines developing a total thrust of 24,000 pounds. The jet car is used to propel the dynamometer and wheel assembly and the carriage from the launch end at a preselected speed. The jet car is disengaged after the test speed is attained, and the dynamometer assembly and the carriage are allowed to coast at this speed into the test bed.

The dynamometer and wheel assembly was designed and fabricated by the FAA and is capable of simulat-

FIGURE 1 Jet-powered pusher car for providing preselected speed to test equipment.

ing a jet transport tire-wheel assembly under touchdown and rollout conditions. The dynamometer is similar in design to one developed by NASA for the Langley Test Facility (10). Figure 2 shows the dynamometer and wheel assembly and the details of the instrumentation for measuring vertical and horizontal loads at the axle. The dynamometer is instrumented to measure the vertical load on the tire, the horizontal force developed at the tire-runway interface, the angular velocity of the test tire, and the vertical motion of the dynamometer assembly relative to the dead-load carriage.

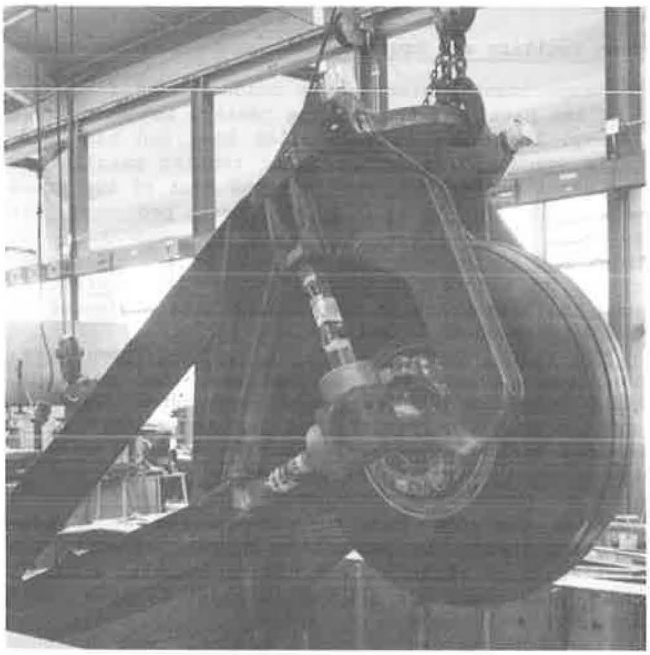

FIGURE 2 Dynamometer and wheel assembly showing vertical and horizontal load links.

Test Sections

The 300-ft test bed (Figure 3) at the end of the track was divided into seven 40-ft sections following a 20-ft section. The 20-ft section was intended for ensuring proper approach of the test wheel into the test section. The dimensional tolerance of the test surface was held within 0.031 in. from horizontal level throughout the test bed.

Various surface treatments installed in the test bed are shown in Figure 4. Section 2, which is not shown in the figure, contained reflex-percussive grooves having the same dimensions as those in the PCC surface that was tested earlier (1); section 1 contains reflex-percussive grooves with different dimensions (Figure 5).

The original grooves have a V-angle of 13 degrees and a groove spacing of 4.25 in. The new configuration has a 20-degree V-angle and the spacing is reduced to 3 in. The flow area per unit length for the two configurations is approximately equal. This is the first improvement to the reflex-percussive grooves originally developed by Klarcrete Limited, London, England and Ontario, Canada; however, other changes may be required to develop an optimized geometry. The square grooves of 0.25-in. size were spaced at 1.25 in., 2 in., and 3 in. between centers. Typical dimensions of the saw-cut grooves are shown in Figure 5.

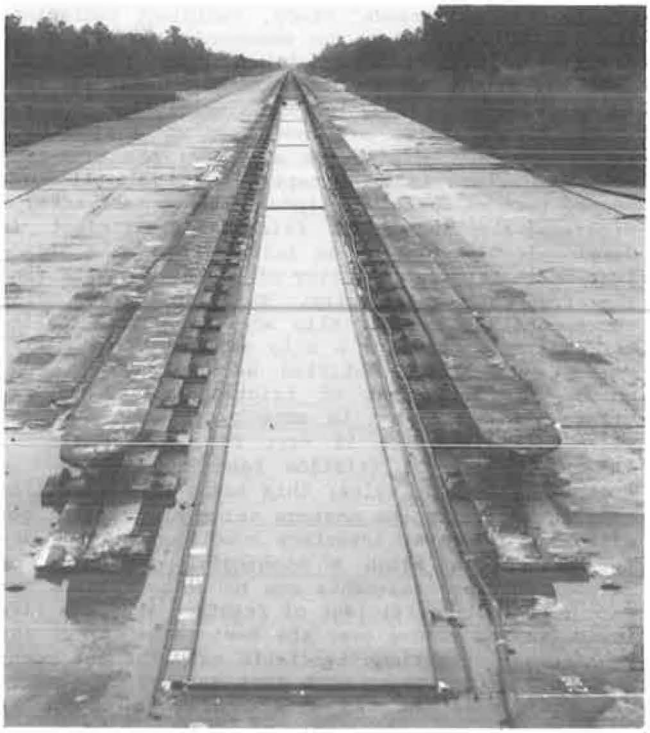

FIGURE 3 300-ft test bed at the end of the test track.

The plastic state grooving technique refers to grooving PCC while it is still in an uncured plastic state. Use of a ribbed vibrating float constructed on a bridge spanning the pavement width, and use of a roller with protrusions, or ribs, which form the grooves in the plastic concrete are two methods used in the United Kingdom and the United States (6). Another method uses steel combs of various dimensions and tine spacing to form a groove-like texture in the plastic concrete pavement. The grooves are approximately 0.125 x 0.125 in., spaced at 0.5-in. intervals center-to-center. The configuration provided in section 6 (Figure 4) has the groove dimensions of the wire comb technique.

The porous friction course was installed in section 7 (Figure 4). Porous friction course is a thin asphaltic concrete overlay about 0.75-in. thick characterized by its open-graded matrix. It consisted of a 0.5-in. maximum size aggregate mix.

Test Parameters

The following is a summary of the test parameters investigated in this research:

Tire Parameters	
Vertical load	: 35,000 lb
Inflation pressure	: 140 lb/sq in.
Tread design	: Worn and treaded 6-in. groove
Tire size and type	: 49 x 17, 26 ply, type VII
Pavement Parameters	
Type of surface	: Asphaltic concrete
Microtexture	: 0.014 nongrooved surface; grease smear test
Types of surface	: Saw-cut grooves, reflex-percussive

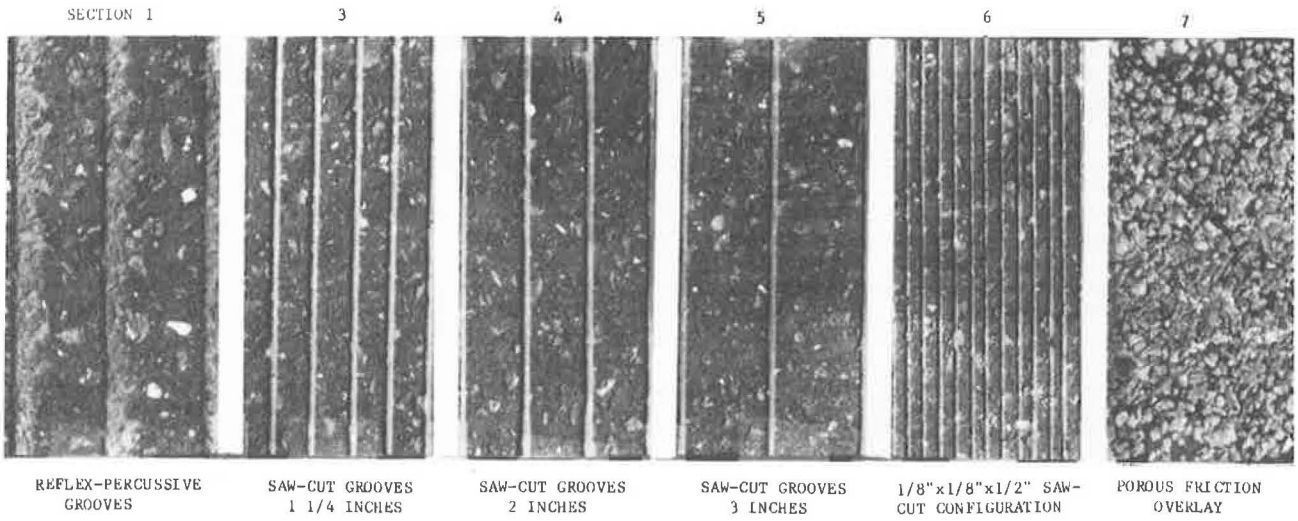

FIGURE 4 Various test sections of the 300-ft asphaltic concrete test bed (each section is 40 ft long).

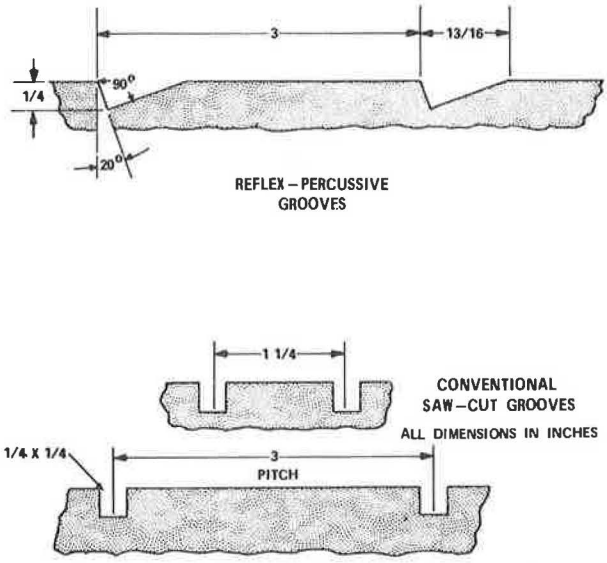

FIGURE 5 Dimensions of reflex-percussive grooves and conventional saw-cut grooves.

Treatment	: V-grooves, porous friction overlay
Groove spacing	: Saw-cut grooves 0.25-in. square: 1.25-in., 2-in., 3-in. spacing 0.125-in. square: 0.5-in. spacing Reflex-percussive V-grooves: 20° groove angle, 3-in. spacing
Environmental Parameters	
Average water depths	: Less than 0.01 in.-wet 0.10 0.01 in.-puddled 0.25 0.01 in.-flooded
Operational Parameters	
Wheel operation	: Rolling to locked
Brake pressure	: 200 lb/sq in.-2,200 lb/sq in.
Speeds	: 70 knots to 150 knots

Test Procedure

The dynamometer assembly, with mounted tire, was positioned at the launch end for the tests. A complete braking test consisted of the following steps:

1. Desired water depth was obtained on the test sections at the recovery end.
2. The jet engines were started at the launch end and set at the performance level to provide the preselected speed in the test section.
3. The jet car was released to propel the test equipment (dead load and dynamometer carriage). The test tire remained in a free rolling state during this maneuver.
4. The jet car was braked and separated from the test equipment several hundred feet ahead of the test bed. This allowed the dead load and dynamometer to enter the first test section at the preselected speed. The test speed in the remaining sections were within 1 to 2 knots of the speed in the first section as computed from the analog traces.
5. Before the dynamometer assembly entered the first test section, the hydraulic systems were activated to apply the vertical load and brake pressure on the tire. (The magnitude of each was preselected.)
6. The wheel entered the test sections at preselected test conditions. The instrumentation was activated and the data were recorded.
7. As the wheel left the test bed, unloading and brake release were initiated and the test equipment was recovered by the use of arresting cables.

Data Collection and Analysis

The results on the asphaltic concrete surfaces are given in Table 1. The coefficients of friction in this table represent the maximum available under each set of operating conditions; many more tests were conducted to obtain this maximum. A least-square fit was obtained between speed and coefficient of friction. A second order fit was found satisfactory because of a small scatter of data.

DISCUSSION

Braking Performance

Wet runway surfaces are normally encountered during or after a light or moderate rain. These surfaces

TABLE 1 Coefficient of Friction–Speed Relationships

Surface Treatment	Wet Surface		Puddled Surface		Flooded Surface	
	Speed, Knots	Friction Level μ x 100	Speed, Knots	Friction Level μ x 100	Speed, Knots	Friction Level μ x 100
Nongrooved (worn tire)	44	34	33	31	33	32
	54	31	55	23	57	22
	90	26	70	18	68	16
	125	20	90	14	90	12
	151	18	110	11	110	10
			130	8	133	8
			143	5	143	4
Nongrooved (new tire)	54	40	42	38	42	40
	70	37	54	29	54	30
	90	33	72	25	72	26
	108	30	90	24	90	16
	131	24	108	16	110	13
	149	27	131	12	131	11
			149	6	149	5
Conventional saw-cut grooves (worn tire)	71	48	70	44	71	39
	109	49	110	21	90	24
	144	45	128	17	90	25
1.25-in. spacing	147	44			110	13
					128	10
					130	10
					147	10
2-in. spacing	72	46	66	41	70	39
	111	44	68	39	89	19
	144	40	106	19	90	20
			128	15	108	10
					110	10
					110	10
					128	8
					148	8
3-in. spacing	72	42	67	35	68	33
	112	39	72	35	70	33
	146	40	106	15	85	20
			128	9	86	20
			147	10	110	8
					128	8
					147	8
Reflex-percussive grooves (worn tire)	70	44	70	33	70	33
	90	41	111	15	86	20
	144	38	129	10	107	10
			147	9	129	8
					145	9
Plastic state grooves (0.125 x 0.125 x 0.5 in.)	73	48	72	34	72	30
	109	39	110	14	90	23
	147	40	128	8	110	8
			147	9	130	9
(worn tire)					148	9
Porous friction course	73	49	–[a]	–[a]	72	33
	109	40			72	33
	147	43			90	19
(worn tire)					91	19
					130	9
					148	9

[a]No data.

may be saturated with water but would not have measurable water depth present on them. The puddled and flooded surfaces are representative of conditions that can be expected immediately after heavy rains of short and long durations, respectively.

On the wet nongrooved surface, a new tire performs better than a worn tire. Although predominantly viscous pressures are developed in the entire contact area of a worn tire, a more complex pressure distribution develops under a new tire; the viscous pressure under the tire groove is lower than under the rib. In addition, the water particles that try to escape (from the contact area of the worn tire) and cannot do so because of high tire side-wall pressures, find immediate relief in the circumferential grooves of the new tire. This results in a "drier" contact area and correspondingly a higher friction coefficient for the new tire (top solid line curve in Figure 6).

The data for the puddled and flooded conditions on a nongrooved surface (two bottom curves) show that the braking performance is significantly lower than for the wet surface (upper curves). The reduction in performance on puddled and flooded surfaces is due to the presence of hydrodynamic forces in the contact area, which along with the viscous forces have forced a partial separation of the tire from the runway surface. This effect is more pronounced at speeds in excess of 140 knots where conditions of imminent hydroplaning exist for both the new and worn tire.

When the wet runway surface is subjected to treatments included in this study, the braking performance of a worn tire is significantly better than

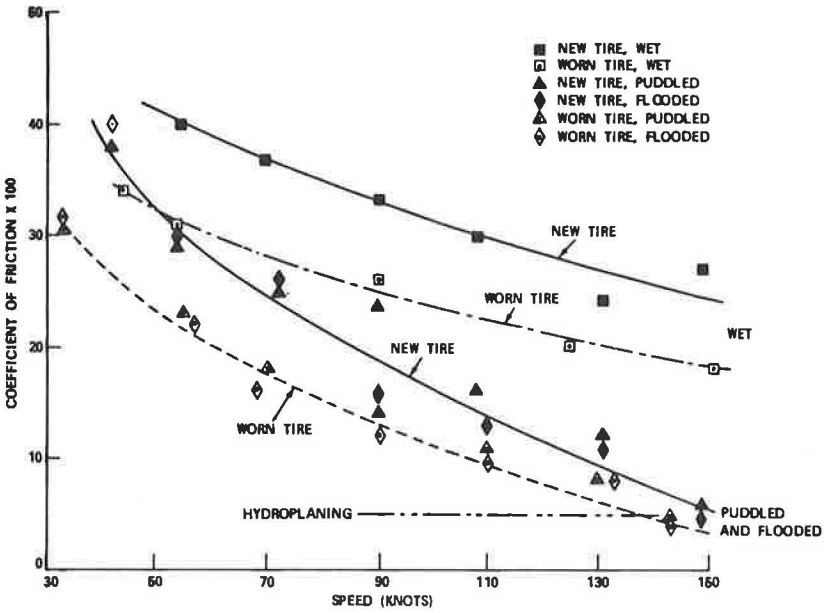

FIGURE 6 Braking test on nongrooved surfaces with new and worn tires.

on a nongrooved surface as shown in Figure 7. Even the performance of the new tire on a nongrooved surface is lower than that of the worn tire on treated surfaces. It should be pointed out that a single curve has been drawn for the performance of worn tires on all the treated surfaces. This choice is based on the high available friction level for all the treated surfaces for the entire range of test speeds.

The braking performance of the worn tire on puddled surfaces with saw-cut grooves is shown in Figure 8. Figure 8 shows that for the 0.25-in. square grooves, the spacing has a distinct effect on the available friction level: for a given speed, the larger the spacing, the smaller the value of available friction level. However, even with the largest groove spacing included in the test program (3 in.), the condition of hydroplaning is not reached within the speed range tested (70 to 150 knots).

The performance on the reflex-percussive grooves, and on 0.125-in. square saw-cut grooves is shown in Figure 9. A single curve adequately represents the average performance of the two treatments.

Figures 10 and 11 show the braking performance of a worn tire on flooded surfaces. In each case, a single curve shows the average performance on the surfaces tested.

Friction Coefficient and Stopping Capability

An interesting characteristic of the friction speed curve--its slope--in Figures 6, 8, 10, and 11 can provide additional information about the overall improvement the surface treatments have over nongrooved surfaces. The slope of the friction-speed curve is continuously decreasing for all the sur-

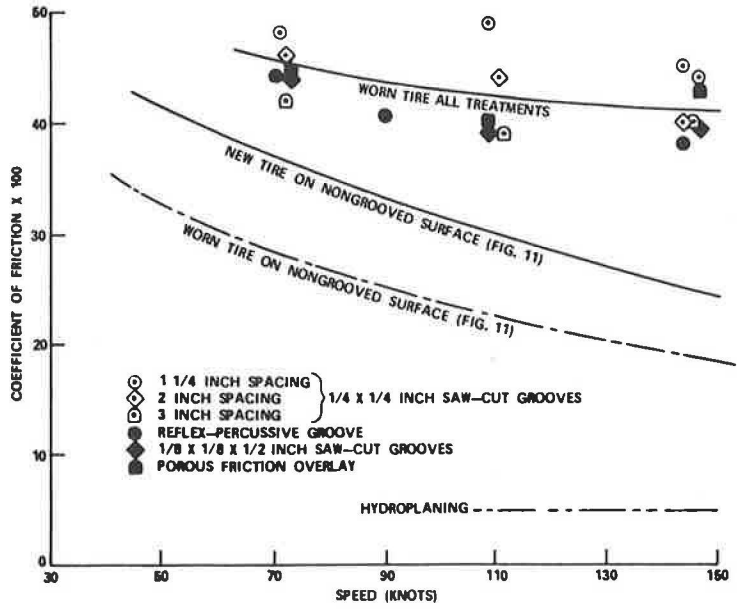

FIGURE 7 Braking performance of worn tire on wet surface.

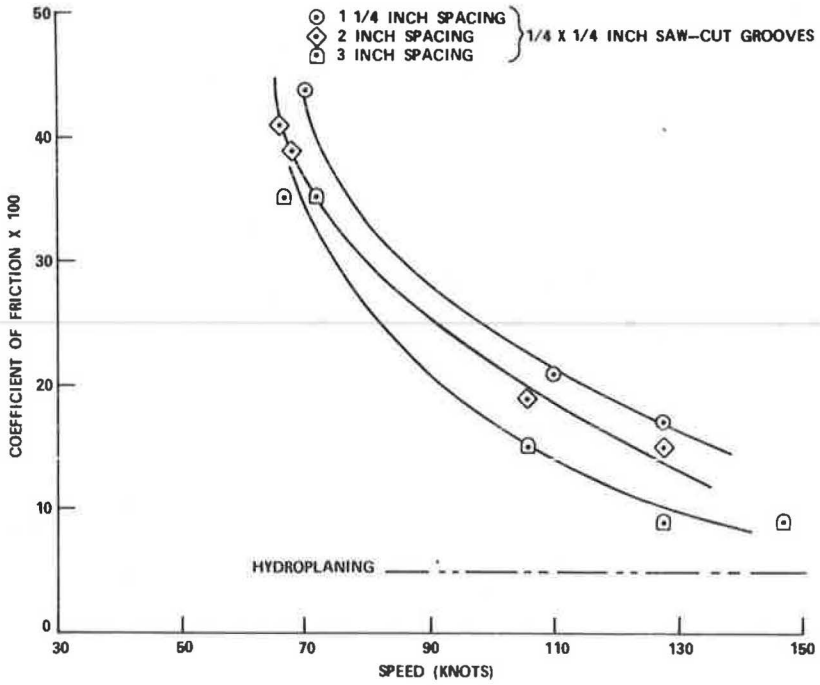

FIGURE 8 Braking performance of a worn tire on saw-cut grooves under puddled conditions.

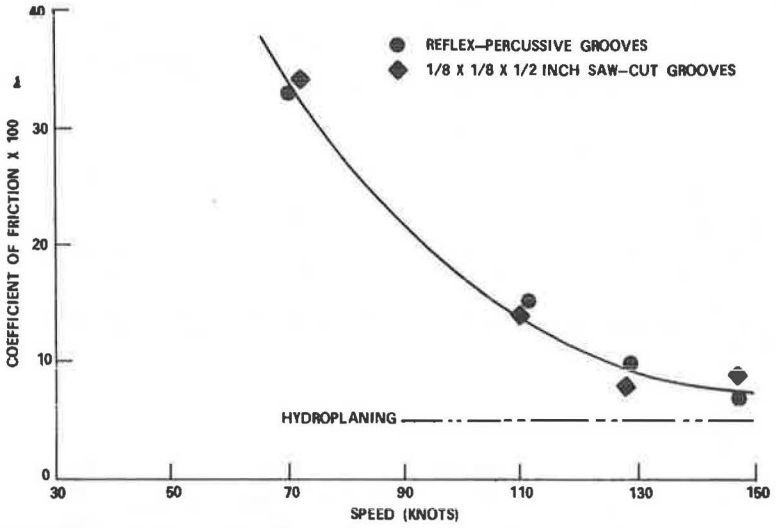

FIGURE 9 Braking performance of a worn tire on reflex-percussive grooves under puddled conditions.

faces--treated or nongrooved. However, although not enough data are available, Figures 8, 10, and 11 indicate that the slope is changing asymptotically beyond 140 knots and below 70 knots for treated surfaces. Thus, in a situation where a landing is attempted at a speed higher than normal, the wheel will not immediately experience friction levels corresponding to hydroplaning. Also, as the aircraft is being braked and going through successively lower speeds, it is encountering a gradually increasing rate of friction level change. This enables a shorter overall stopping distance. In comparison, the friction-speed curve for the nongrooved surfaces (Figure 6) uniformly decreases near the high speed end and a state of hydroplaing will exist should the landing speed be higher than normal.

Forced Water Escape

Water is forced out of the tire-runway interface when the tire travels on the runway. Escape of water takes place in all directions; however, a large amount of water escapes from the rear and the sides of the contact area between the tire and the runway.

Although this research did not include instrumentation to measure the water escape paths or the amount of water escaped, an attempt is made here to explain how the grooves help water escape. When a worn tire travels over a wet (0.01-in. depth) surface having grooves, the pressures in the contact area are predominantly viscous. Because only a small amount of water is present in the contact area, all

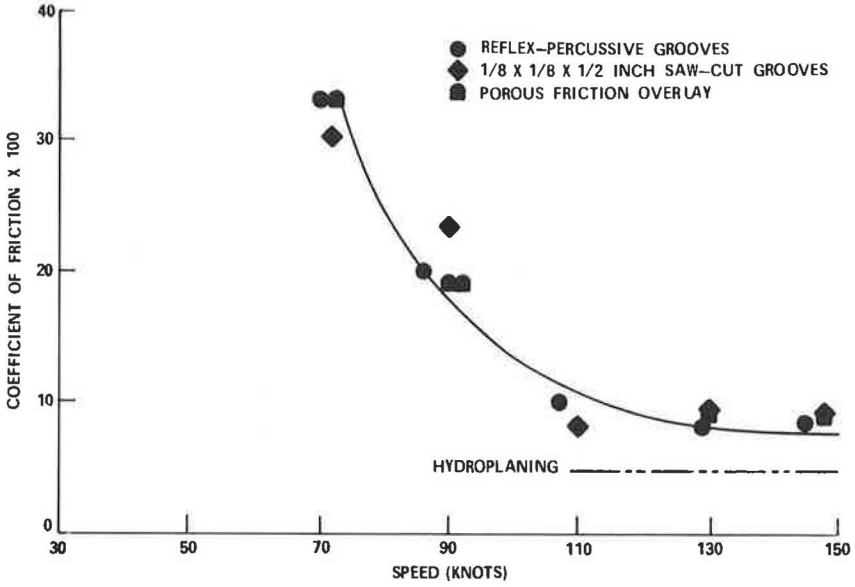

FIGURE 10 Braking performance of worn tire on saw-cut grooves under flooded conditions.

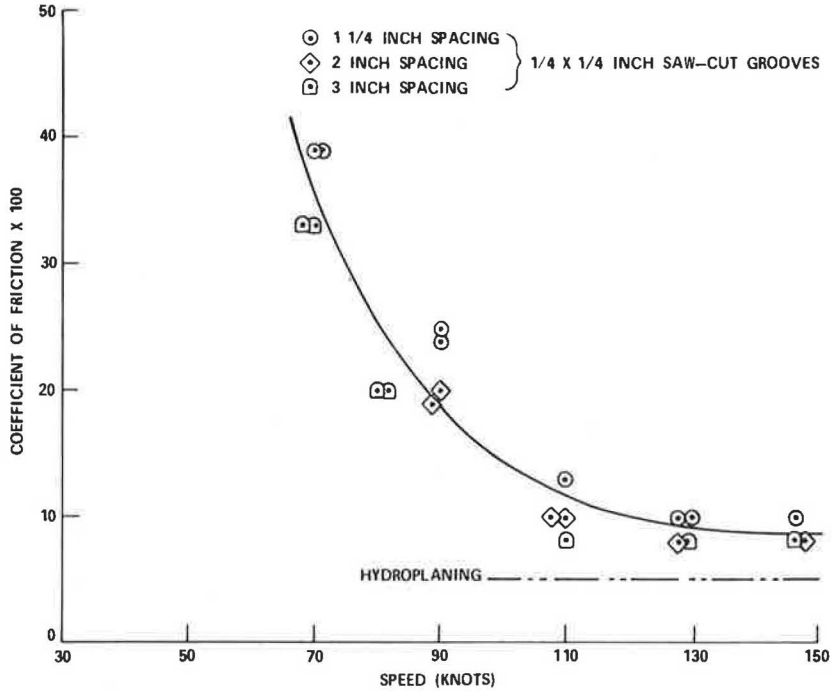

FIGURE 11 Braking performance of worn tire on reflex-percussive grooves and porous-friction course under flooded conditions.

of it is expelled through grooves. Thus, all the surfaces provide high friction levels as shown by the solid-line curve in Figure 12 (curve 1). The data scatter can be seen in Figure 7. But because the friction levels are high for the entire range of test speed, data scatter is irrelevant and all surface treatments (included in this study) will provide adequate safety in terms of stopping the aircraft quickly.

When the grooved surfaces are puddled, the hydrodynamic pressures become important. The additional water in the contact area must be removed to reduce the buildup of hydrodynamic pressures and to ensure high friction levels. When the grooves are spaced closer, water particles trying to escape through the rear of the contact area will find it easier to escape through the grooves and develop a drier contact area. However, a large spacing will be completely ineffective in forcing the water out of the contact area because it will simulate a nongrooved surface and the friction forces will approach a hydroplaning level as shown by curve No. 5 in Figure 12. An optimum condition would be when all the water is expelled from the contact area in such a way that the water-carrying capacity of the grooves is fully exhausted. This condition could be obtained by a certain combination of groove-spacing and the amount of water. Thus, for the same amount of wetness for

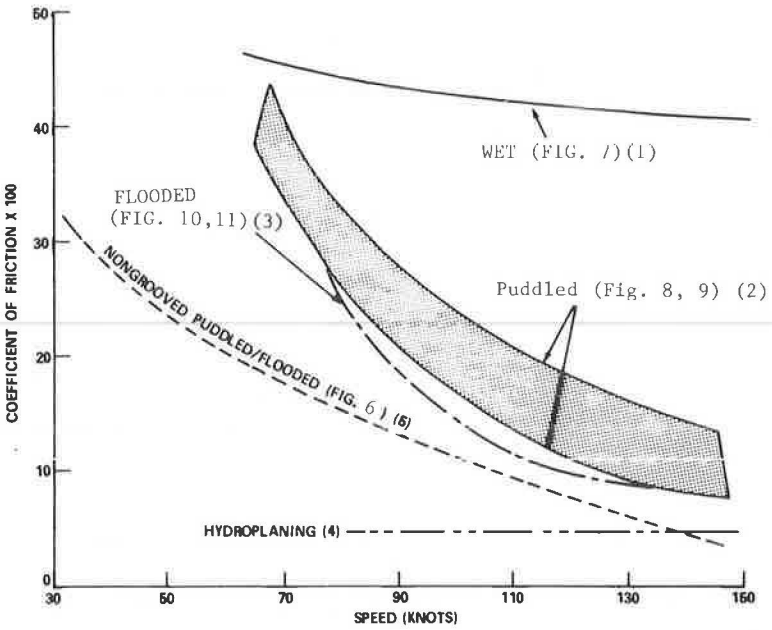

FIGURE 12 Comparison of all surface treatments under wet, puddled, and flooded conditions.

which the capacity of 3-in. spaced grooves is exhausted, the capacity of 1.25-in. spaced grooves will not be and these grooves will provide a drier contact. The results on puddled surfaces with grooves verify this phenomenon: curve No. 2 shows these results. The shaded area bounded by two lines shows the extent of the forced water escape as a function of groove spacing: The top boundary represents the 1.25-in. groove spacing and the bottom boundary represents the grooves spaced at 3 in.

The puddled condition in this study (water depth 0.10 in.) represents a water condition where groove-spacing is a factor in determining the maximum friction levels available. Clearly, the grooves at 1.25-in. spacing provide better braking action. However, the spacing of 3 in. will provide sufficient braking to allow a gradual reduction in speed to develop further braking. It should be noted that hydroplaning is avoided for all spacings.

When the grooved surfaces are flooded, the reduced groove spacing does not improve the available friction levels. It can be seen from curve No. 3 (Figure 12) that the available friction levels are slightly below the bottom of the shaded area for the puddled condition. Also, only a single curve represents the performance on all treated surfaces. For the flooded surfaces, the grooves are filled with water even before the passage of tire over them. Then, the inertia of water particles retards the escape of water in all directions when the tire does travel over the grooves. The result is that the available friction levels are insensitive to the groove spacing.

Saw-Cut Grooves, Reflex Percussive Grooves, and Porous Friction Overlay

For the asphaltic concrete surface under wet and flooded conditions, the reflex-percussive grooves, the porous friction overlay, the 0.125-in. x 0.125-in. x 0.5-in. saw-cut grooves, and the 0.25-in. square saw-cut grooves of various spacings perform alike in terms of available friction levels when a full-scale aircraft tire is braked on these surfaces. However, the spacing of the 0.25-in. square saw-cut grooves influence the available friction levels on "puddled" surfaces: The smaller spacing provides higher friction levels. The reflex-percussive grooves, the 0.125-in. x 0.125-in. x 0.5-in. saw-cut grooves and the 3-in. spaced saw-cut grooves provide similar results on puddled surfaces.

Because a previous study (4) has included the cost analysis of various grooving methods, it would be necessary in this study to accept those results. However, another cost analysis would be desirable to reflect new developments during the past several years. The previous study had shown that the saw-cut grooves spaced 3 in. apart in PCC could provide a cost savings of approximately 25 percent over the grooves spaced 1.25 in. apart. It also showed that the reflex-percussive grooves in PCC offer even higher cost savings: these grooves could cost as low as half the cost of saw-cut grooves at 1.25-in. spacing.

The reflex-percussive grooves need refinements to offer a cut as clean as in PCC. This may require a modified cutting head and a different impact frequency for the head. These changes may be necessary to compensate for the viscoelastic nature of asphaltic concrete surface. With proper modifications, the reflex-percussive cutting process would be a viable cost-competitive method to the saw-cut grooves. But, realistic cost estimates and full savings potential can only be affirmed after application of these grooves on an operating airport.

CONCLUSIONS

The following conclusions are drawn from the findings of this research. These conclusions are valid for asphaltic concrete surfaces and for the operating parameters included in the test program.

1. Where the seasonal and topographical conditions consistently produce puddled water conditions on the runways, the type of surface treatment has a significant influence on the braking performance of an aircraft tire. Although all the surface treat-

ments alleviate hydroplaning, the saw-cut grooves spaced at 1.25 in. provide the maximum values of friction levels.

2. Where the seasonal and topographical conditions consistently produce either wet or flooded water conditions on the runways, the type of surface treatment has an insignificant effect on the braking performance of an aircraft tire.

3. The reflex-percussive grooves (spaced at 3 in.), the porous friction overlay, and the saw-cut grooves spaced at 3 in. perform comparably at all wetness conditions, and all alleviate hydroplaning.

4. If performance were the only criterion for the selection of a surface treatment, it is only at those airports where seasonal and topographical conditions produce puddled water conditions that the choice of one treatment will be more beneficial than another. However, if performance were not the only criterion, any surface treatment could be selected based on cost, because all the treatments provide sufficient braking to allow a gradual reduction in the speed of the aircraft and thus develop further braking.

REFERENCES

1. S.K. Agrawal and H. Daiutolo. Reflex-Percussive Grooves for Runways: an Alternative to Saw-Cutting. In Transportation Research Record 836, TRB, National Research Council, Washington, D.C., 1981, pp. 49-55.
2. R.F.A. Judge. A Note of Aquaplaning and Surface Treatments Used to Improve the Skid Resistance of Airfield Pavements. Report 8556/PS. British Ministry of Public Building Works, London, Oct. 1965.
3. T.J. Yager. Comparative Braking Performance of Various Aircraft on Grooved and Ungrooved Pavements at the Landing Research Runway, NASA Wallops Station. NASA SP-5073. National Aeronautics and Space Administration, Washington, D.C., 1968.
4. S.K. Agrawal and H. Daiutolo. The Braking Performance of an Aircraft Tire on Grooved Portland Cement Concrete Surfaces. Report FAA-RD-80-78. Federal Aviation Administration Technical Center, Atlantic City Airport, N.J., Jan. 1981.
5. T.A. Byrdsong, J.L. McCarty, and T.J. Yager. Investigation of Aircraft Tire Damage Resulting from Touchdown on Grooved Runway Surfaces. NASA TN D-6690. National Aeronautics and Space Administration, Washington, D.C., March 1972.
6. Method for the Design, Construction and Maintenance of Skid Resistant Airport Pavement Surfaces. Advisory Circular No. 150/5320-12. FAA, U.S. Department of Transportation, Washington, D.C., 1983.
7. S.K. Agrawal and H. Daiutolo. Effects of Groove Spacing on Braking Performance of an Aircraft Tire. In Transportation Research Record 836, TRB, National Research Council, Washington, D.C., 1981, pp. 55-60.
8. J.R. Reed, D.F. Kibler, and S.K. Agrawal. Mathematical Model of Runoff From Grooved Runways. Presented at 62nd Annual Meeting of the Transportation Research Board, Washington, D.C., Jan. 1983.
9. S.K. Agrawal and J.J. Henry. Technique for Evaluating Hydroplaning Potential of Pavements. In Transportation Research Record 633, TRB, National Research Council, Washington, D.C., 1977, pp. 1-7.
10. U.T. Joyner, W.B. Horne, and T.J.W. Leland. Investigation on the Ground Performance of Aircraft Relating to Wet Runway Braking and Slush Drag. Report 429. Advisory Group for Aeronautical Research and Development, Paris, France, Jan. 1963.
11. W.B. Horne and R.C. Dreher. Phenomena of Pneumatic Tire Hydroplaning. NASA TN D-2056. National Aeronautics and Space Administration, Washington, D.C., Nov. 1963.

Holes in the Pavement—An Assessment of Their Influence on Safety

RICHARD A. ZIMMER and DON L. IVEY

ABSTRACT

A hole must be relatively large to constitute a significant safety influence when rim or tire damage are the guiding criteria. A hole must be in excess of 60 in. long and 3 in. deep to constitute a threat to the smallest automobiles at highway speeds in excess of 40 mph. On urban streets, with traffic speeds as low as 20 mph, holes must still be greater than 30 in. long and greater than 3 in. deep to have the potential of damaging tires and rims, or both. Damage to tires and rims, with the associated potential for a tire blowout, is the only significant safety-related influence of holes identified in this study. Holes are atypical of most highway surface discontinuities in that the lower the vehicle speed, the greater the potential for causing damage. Problems can arise if a driver reacts to the hole inappropriately. For example, it is counterproductive to react to a hole in the vehicle's path by braking or extreme cornering. In general, a hole of a given size is more likely to cause damage if speed is reduced. Losses of control can occur if extreme braking is produced at highway speed. Extreme cornering can have two results: (a) if a driver reacts with a large steering input to avoid a hole, he may produce a loss of control on a low friction surface; and (b) the vehicle may be put in a hazardous position with respect to other traffic. It is probably the latter that accounts for most of the accidents where holes are identified as contributing factors.

The nature of a hole (also known as "pothole" and "chuck hole") is to be hard on tires, vehicles, and drivers' tempers, but are holes really a significant direct threat to safety, or is their influence on safety highly inflated by many accident reports reflecting driver frustrations and excuses?

Accident reports state that "holes" are a causative factor in many accidents. In 1976 Ivey and Griffin (1) reported a rank ordering of various types of roadway disturbances based on 15,968 accidents in North Carolina. Of these, the narratives of 566 stated that the accident was either caused or aggravated by some kind of roadway disturbance, for example, holes, ruts, soft shoulders, or water. Hole was mentioned in 59 reports ranking it 5th of 19 disturbances behind the key words water, dropped, soft, curb, and edge. In a Delphi ordering developed by the same authors, holes appeared more important to the drivers of wrecked vehicles in North Carolina than they did to the engineers involved in the Delphi study.

It appears clear, whether justified or not, that holes are perceived to be a significant threat to safety. It is also clear that the perception of the public is not shared by many engineers with significant knowledge of vehicle handling and stability characteristics. One way of more accurately defining the problem is by controlled vehicle-hole interactive tests. The experiments conducted as part of this project reflect an effort to separate folklore, personal perceptions, and societal opinion from fact.

TEST PROGRAM

A comprehensive test program was developed to evaluate the safety-related effects of roadway surface discontinuities in the form of holes in pavement, commonly referred to as potholes. Because there is an infinite number of pothole shape, area, and depth combinations, and a large number of vehicle suspension system and tire combinations, a program to examine all conceivable combinations was deemed impractical. The research approach here was to determine a worst-case condition, or a condition that would produce a definite safety hazard. This condition was defined as an upper boundary and sublimit tests were performed to evaluate the potential influence on safety.

Hazardous Condition Determination

Knowing the drop rate of various wheel and suspension systems and the initial ride height of the rim (bottom of the rim to the ground distance), it is possible to predict the minimum length and depth of a pothole (with a relatively square edge) that will produce a possible hazardous condition at any particular speed.

To test the theoretical methods developed to determine safe pothole sizes, several runs were made at 20 mph using the mini-compact and intermediate sized vehicles, dropping the left wheels into the 36-in. diameter test hole set to a depth of 6 in. The speed of 20 mph was arbitrarily selected as a lower limit for this study because it was believed that any lower speeds should not produce safety-related problems. This speed then becomes the worst-case condition because lower speeds should not produce significant problems and higher speeds do not allow the wheels to drop as far for a given length.

It was found during field and test track testing that directional stability was not affected by impacting single holes up to and including 3 ft in diameter and 6 in. deep. According to the test driver, even the run that bent the rim of the intermediate vehicle did not change the vehicle path or force the steering wheel to turn.

The chart shown in Figure 1 is conservative in that the square edge hole is the most critical of the hole edge geometries. Three bands of safety are shown based on the four test vehicles evaluated. The first band, left and lower, defines hole length and depths referred to as being reasonably safe or where a prudent driver of a reasonably maintained vehicle would experience no significant problem in traversing the hole. The middle band, which is bounded by

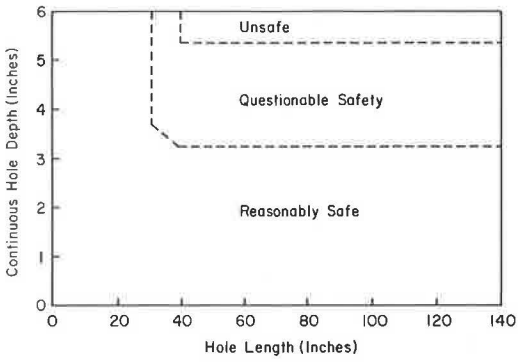

FIGURE 1 Pothole safety as a function of size.

the upper and lower extremes of vehicles tested, represents a questionable safety area where a vehicle could sustain tire, rim, or suspension damage when traversing a hole with the defined dimensions. Finally, the unsafe band defines length-depth combinations that could produce a hazardous condition for any of the four vehicles tested.

Limitations of Test Program

Although the choice of vehicles would appear adequate to define a fairly wide spectrum of vehicle characteristics, this has not been experimentally verified. Parameters such as inertial properties, spring stiffness, and tire stiffness should be considered in order to objectively evaluate the spectrum of vehicles encompassed. Other factors such as vehicle loading and the influence on vehicles other than four-wheeled passenger vehicles were not considered. As with snowflakes, there are probably no two potholes alike in terms of shapes, edge slopes, and bottom contours. This study used a definable square edge with vertical sides and a level bottom. This approach provided insight into a worst-case situation that may encompass only a small number of real world potholes. It does, however, permit conservative safety predictions because any sloping of the sides will only produce a safer condition for a given-size hole.

CONCLUSION

It is apparent that a hole must be relatively large to constitute a significant safety influence when rim or tire damage are the guiding criteria. A hole must be in excess of 60 in. long and 3 in. deep to constitute a threat to the smallest automobiles at highway speeds in excess of 40 mph. On urban streets, with traffic speeds as low as 20 mph, holes must still be greater than 30 in. long and greater than 3 in. deep to have the potential of damaging tires and rims, or both.

Damage to tires and rims, with the associated potential for a tire blowout, is the only significant safety-related influence of holes identified in this study. Holes are atypical of most highway surface discontinuities in that the lower the vehicle speed, the greater the potential for causing damage.

Problems can arise if a driver reacts to the hole inappropriately. For example, it is counterproductive to react to a hole in the vehicle's path by braking or extreme cornering. In general, a given-size hole is more likely to cause damage if speed is reduced. Losses of control can occur if extreme braking is produced at highway speed. Extreme cornering can have two results: (a) if a driver reacts with a large steering input to avoid a hole he may produce a loss of control on a low-friction surface; and (b) he may put his vehicle in a hazardous position with respect to other traffic. In the authors' opinion, it is probably the latter that accounts for most of the accidents where holes are identified as contributing factors.

The purpose of this work is certainly not to conclude that holes in highway surfaces should be tolerated. The many disadvantages of these flaws dictate their elimination within the bound of financial constraints. The purpose is to put the safety influence of holes into a reasonable perspective, so that maintenance activities can be assigned the appropriate priority.

REFERENCE

1. Don L. Ivey and Lindsay I. Griffin III. Driver Vehicle Reaction to Road Surface Discontinuities and Failures. Proc., International FISITA Conference, Tokyo, 1975.

Effect of Pavement Type and Condition on the Fuel Consumption of Vehicles

CHRISTO J. BESTER

ABSTRACT

The effect of pavement type and condition (roughness) on the rolling resistance of vehicles is investigated. By means of the relation between the energy requirements and the fuel consumption of vehicles, this effect is used to predict the fuel use on different pavements. It is found that, except for gravel surfaces, pavement type has a minor effect on fuel consumption. Roughness, however, correlates strongly with rolling resistance and therefore with vehicle fuel consumption. This is important for the economic justification of major road maintenance projects.

As a result of two oil crises in the past 10 years, the importance of the fuel consumption of vehicles cannot be overemphasized. Fuel has strategic importance. Moreover, its cost rose to such an extent that it not only caused high inflation rates, but also seriously affected the balance of payments of importing countries. Because fuel is high on the list of expenses of the vehicle owner, savings in fuel consumption play a major role in the economic justification of new road projects. In the past, this was usually the case where geometric improvements were being considered. There is little information available from which the effect of pavement improvements on fuel consumption can be predicted, yet such predictions are imperative for the evaluation of major maintenance operations.

Because of the numerous variables that affect fuel consumption, it is difficult to isolate the specific effect of pavement type and condition (1). This is mainly because the effect is rather small (2). It was therefore decided to determine the relationship between the pavement type and condition and the rolling resistance of vehicles. This relationship can then be used to predict the effect on fuel consumption.

A procedure for determining the rolling resistance of vehicles, which is then related to the type and condition of the pavement, is described. The latter is expressed in terms of road roughness as measured by a Linear Displacement Integrator (LDI). This road roughness value can also be related to the quarter car index (QI) scale developed in Brazil (3).

From the rolling resistance, the fuel consumption of the test vehicles is then predicted by means of the relationship between the energy requirements and fuel use of a vehicle.

FUEL CONSUMPTION AND ENERGY REQUIREMENTS OF VEHICLES

It has been shown that the fuel consumption of a vehicle is directly related to the energy necessary for the movement of the vehicle (4). The different resistances that must be overcome by the energy supplied by the engine are:

- Rolling resistance, R_r;
- Air resistance, R_a; and
- Gradient resistance, R_g.

Energy is also used to overcome transmission losses and the internal friction of the engine.

If

$R_r = (A + BV^2)M$,
$R_a = 0.5\rho C_D A_F V^2$, and
$R_g = MgG$,

then the fuel consumption at constant speed is:

$$F = p_1 + p_2/V + p_3V^2 + p_4G \quad (1)$$

where

R_r = rolling resistance (N),
R_a = air resistance (N),
R_g = gradient resistance (N),
F = fuel consumption (mℓ/km),
V = speed (m/s),
G = gradient (m/m),
$p_1 = bAM/\eta$,
p_2/V = idling fuel consumption (mℓ/km),
$p_3 = (bBM + 0.5b\rho C_D A_F)/\eta$,
$p_4 = bMg/\eta$,
b = fuel conversion factor (mℓ/kJ),
A,B = rolling resistance coefficients,
M = mass (kg),
η = drive-line efficiency,
ρ = air density (kg/m³),
C_D = aerodynamic drag coefficient,
A_F = frontal projected area (m²), and
g = gravitational acceleration (m/s²).

It is clear that the pavement type and condition can only affect fuel consumption through the rolling resistance and therefore through p_1 and p_3 in Equation 1.

ROLLING RESISTANCE TESTS

Theoretical Background

The combined effect of air and rolling resistance can be determined by using a coasting vehicle (that is, a vehicle running freely, with the engine disengaged) (5). Under these circumstances, there are only three forces acting on the vehicle:

- Rolling resistance,
- Air resistance, and
- Gradient resistance.

From Newton:

$$Ma = R_r + R_a + R_g \quad (2)$$

where a represents deceleration (m/s²). Therefore

$$Ma = (A + BV^2)M + 0.5\rho C_D A_F V^2 + MgG \quad (3)$$

and

$$a = (A + gG) + (B + 0.5\rho C_D A_F/M)V^2 \quad (4)$$

This is of the form:

$$a = C_1 + C_2 V^2 \quad (5)$$

where

$$C_1 = A + gG \quad (6)$$

and

$$C_2 = B + 0.5\rho C_D A_F/M \quad (7)$$

To determine the rolling resistance of a vehicle, the speed is measured at regular intervals (for example, every 10 seconds) during coasting, starting from a maximum speed on a relatively flat section of road with a constant gradient. This is done for both directions. If the decelerations are plotted against the square of the speeds, the values of C_1 and C_2 in Equation 5 can be obtained through a linear regression analysis for both directions. The rolling resistance coefficient A is then equal to the average of the two values of C_1, and the difference between the two values is equal to 2gG.

The rolling and air resistance coefficients contained in C_2 cannot be calculated separately. However, if the value of C_2 differs for different road surfaces, it must be as a result of a change in the value of B, because the air resistance is a constant.

An example of this procedure is shown in Figure 1 for the test car on section 1. The equations for the north- and southbound tests were:

Northbound

$$a = 0.0946 + 4{,}344.10^{-4}\ V^2 \quad (r = 0.992)$$

Southbound

$$a = 0.2118 + 4{,}147.10^{-4}\ V^2 \quad (r = 0.997)$$

From the values of C_1, the rolling resistance coefficient

$$A = (0.0946 + 0.2118)/2 = 0.1532\ N/kg$$

and the gradient

$$G = (0.2118 - 0.0946)/(2 \times 9.81) = 0.0060\ m/m.$$

The last value is the same as that given in the construction plans for that specific section of road.

If the value of B from Bester (4) is assumed, the aerodynamic drag coefficient can be calculated from the average of the two values of C_2. In this case:

$B = 6.86 \times 10^{-5}\ m^{-1}$
$M = 1322\ kg$
$A_F = 2.3\ m^2$
$\rho = 1.059\ kg/m^3$ (at an altitude of 1500 m above sea level)

Therefore, from Equation 7:

$$C_D = (C_2 - B)M/(0.5\rho A_F) = 0.386.$$

Test Procedures

To determine the effect of road roughness and pavement type on the rolling resistance of vehicles, eight different road sections were chosen for the tests. Each section had to have a sufficient length (±400 m) of uniform gradient and roughness. The pavements on which sections were chosen were as follows: two were of asphaltic concrete, one was a portland cement concrete pavement, four had surface treatments, and one was unpaved. The roughness of each section was determined by using a Linear Displacement Integrator (LDI) developed by the National Institute for Transport and Road Research. These roughness values could be related to the QI scale through the correlation developed by Visser (6). The details of the test sections are given in Table 1.

Two vehicles were used for the tests--a passenger car and a truck with respective masses of 1322 and 7200 kg. The passenger car was fitted with radial tires and the truck was fitted with cross-ply tires. Both vehicles were instrumented to yield accurate speed measurements at fixed time intervals.

For reliable results, the tests had to be conducted in windless conditions, with the correct tire

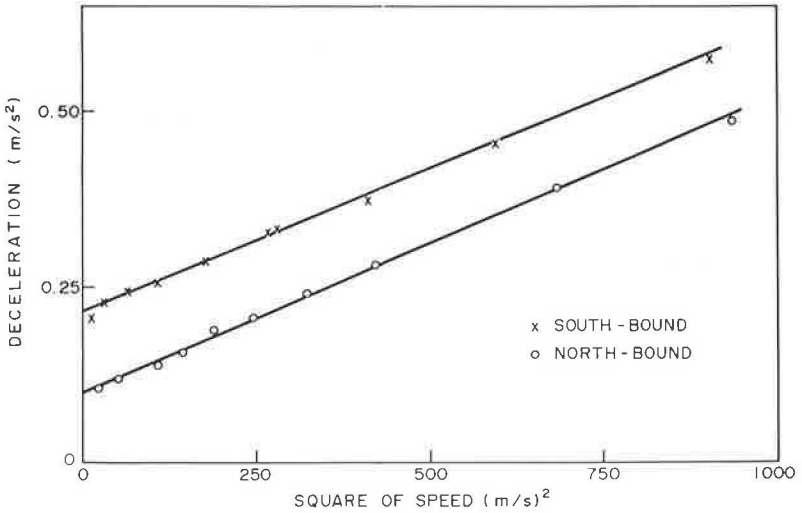

FIGURE 1 Deceleration versus square of speed during coasting.

TABLE 1 Details of Test Sections

Section No.	Pavement Type	Length (m)	Roughness LDI	Roughness QI[a]
1	Asphaltic concrete	1000	0.73	11.8
2	Asphaltic concrete	900	0.69	10.9
3	Concrete	700	0.94	16.5
4	Surface treatment	300	0.73	11.8
5	Surface treatment	600	1.27	23.9
6	Surface treatment	500	1.61	31.6
7	Surface treatment	400	2.34	48.0
8	Unsurfaced	350	3.53	74.7

[a]QI = −4.6 + 22.46 LDI from Visser *(6)*.

pressure and with the tires having been well warmed-up in advance. Because of the limited length of the test sections, all tests had to be repeated with different initial speeds to cover a full range of speeds.

Test Results

The speed of the vehicles during coasting was determined at 10-second intervals. From these speeds, the deceleration over the interval and the average speed during the interval were calculated. Linear regression analyses (see Equation 5) were then performed for both directions of each test section. The average values for both directions are given in Table 2 for the passenger car and in Table 3 for the truck.

TABLE 2 Test Results for Passenger Cars

Section No.	Roughness LDI (m/km)	A (N/kg)	C_2 ($0.10^{-4}m^{-1}$)	r
1	0.73	0.1532	4.246	0.994
2	0.69	0.1532	4.232	0.996
3	0.94	0.1521	4.182	0.995
4	0.73	0.1533	4.268	0.983
5	1.27	0.1583	4.267	0.994
6	1.61	0.1585	4.336	0.996
7	2.34	0.1649	4.410	0.990
8	3.53	0.2418	5.469	0.964

TABLE 3 Test Results for Trucks

Section No.	Roughness LDI (m/km)	A (N/kg)	B ($0.10^{-4}m^{-1}$)	r
2	0.69	0.0877	2.866	0.984
4	0.73	0.0979	3.179	0.931
5	1.27	0.1074	3.189	0.995
7	2.34	0.1213	2.880	0.922
8	3.53	0.1454	3.073	0.769

From these values, the following relationships between road roughness and the various coefficients were established:

Passenger Car

For all surface roads:

$$A = 0.1475 + 0.0073R \text{ (N/kg)} \quad (r = 0.965) \quad (8)$$

$$C_2 = (4.149 + 0.108R) \times 10^{-4} \text{ (m}^{-1}\text{)} \quad (r = 0.884) \quad (9)$$

Truck

For all roads:

$$A = 0.0808 + 0.0182R \text{ (N/kg)} \quad (r = 0.984)$$

$$C_2 = 3.04 \times 10^{-4} \text{ (m}^{-1}\text{)} \quad (10)$$

where R represents road roughness in m/km as measured by the LDI. These relationships are shown in Figures 2, 3, and 4.

Discussion

The roughness of paved roads has an effect, although small, on the rolling resistance coefficients of a passenger car. Unpaved roads have a much greater effect. For a truck, however, only the constant rolling resistance coefficient, A, shows a meaningful relationship with road roughness.

From Figures 2, 3, and 4 it appears that concrete and asphaltic concrete pavements have (for cars and trucks) a lower rolling resistance than roads with a surface treatment. These differences, however, are small and will be disregarded in further calculations. It should be mentioned that concrete and asphaltic concrete pavements with rougher surfaces were not available in the vicinity of Pretoria.

ROLLING RESISTANCE AND FUEL CONSUMPTION

From Equations 1 and 7:

$$p_1 = bAM/\eta$$
$$p_3 = bC_2M/\eta$$

By using the following values of constants for typical South African vehicles, the total fuel consumption at constant speed can be calculated for the two test vehicles (7):

b = 0.085 mℓ/kJ (for cars with petrol engines)
  = 0.070 mℓ/kJ (for trucks with diesel engines)
η = 0.90 (for cars)
  = 0.86 (for trucks)
p_2 = 450 mℓ/1000s (for cars)
  = 600 mℓ/1000s (for trucks).

Passenger Car

On surfaced roads:

$$F = 18.4 + 0.91R + 450/V + (0.0518 + 0.0013R)V^2 + 1224G.$$

On the unpaved road (gravel road) tested (Roughness = 3.53 m/km):

$$F = 30.2 + 450/V + 0.0683V^2 + 1224G.$$

Truck

On all roads:

$$F = 47.4 + 10.67R + 600/V + 0.178V^2 + 5750G$$

where

F = fuel consumption (mℓ/km),
R = road roughness (m/km) as measured by the LDI,
V = speed (m/s), and
G = gradient (m/m).

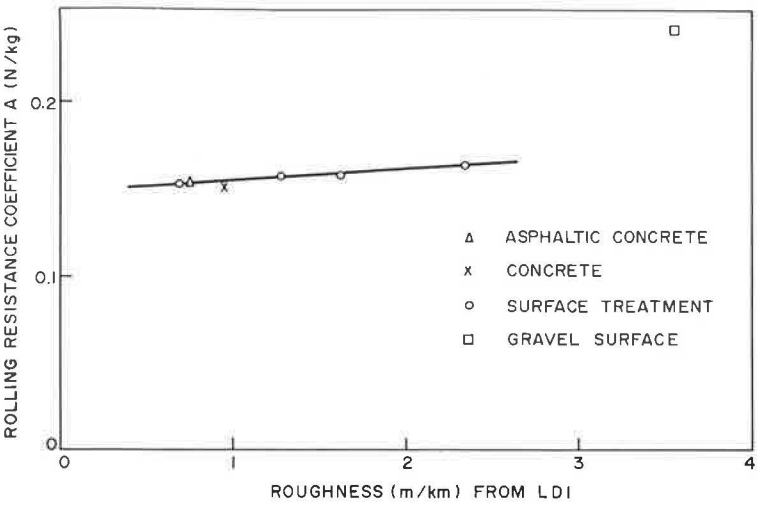

FIGURE 2 Rolling resistance coefficient, A, versus road roughness for test car.

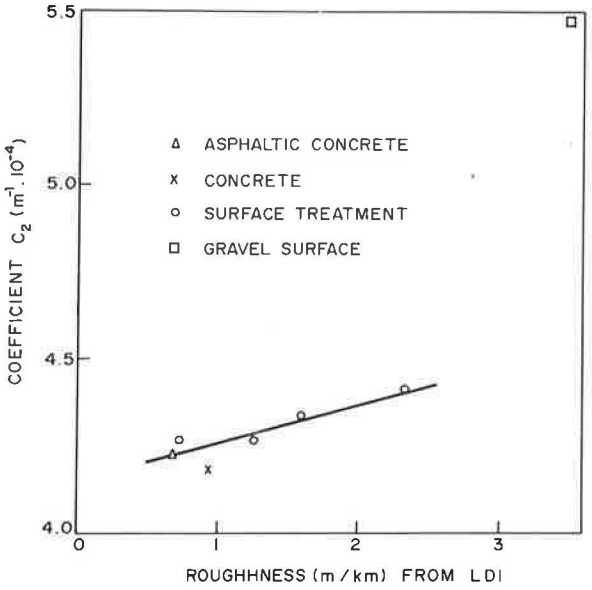

FIGURE 3 Speed-related coefficient, C_2, versus road roughness for test car.

Note that on negative gradients the minimum fuel consumption is p_2/V. When V=0, the distance-based fuel consumption, as in Equation 1, would be infinite and the time-based idling fuel consumption is equal to $p_2/1000$ (mℓ/s).

These formulas can now be used to determine the savings in fuel consumption that will result from improving the condition of pavements, either by new construction or by rehabilitation. So, for instance, if the pavement condition is improved from R = 3.0 to R = 0.6 m/km, the fuel saving will be 3210 liters/year/km for an annual average daily traffic of 1,000 vehicles per day including 20 percent heavy vehicles. Figures 5 and 6 show the fuel consumption of the test vehicles for different road conditions.

CONCLUSIONS

1. The pavement type has a small effect on the rolling resistance and, therefore, on the fuel consumption of vehicles.
2. Both the constant and speed-related rolling resistance coefficients for passenger cars are affected by the condition (roughness) of the pavement.
3. At 80 km/h, a passenger car can use 29 percent more fuel on a gravel road than on a paved road

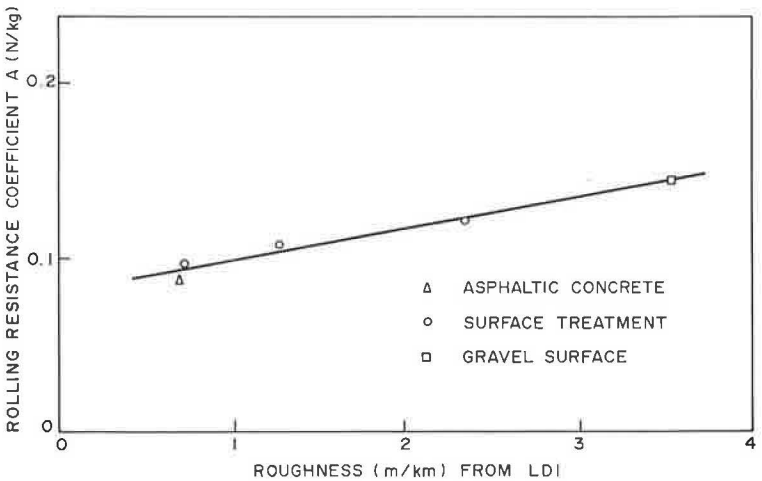

FIGURE 4 Rolling resistance coefficient, A, versus road roughness for test truck.

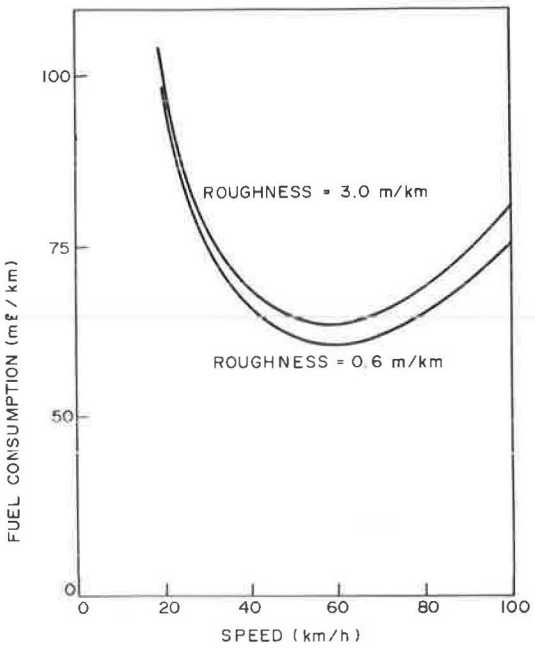

FIGURE 5 Fuel consumption of test car under different road conditions.

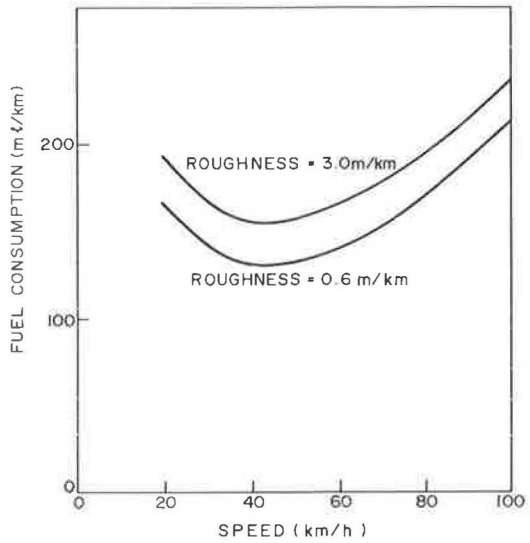

FIGURE 6 Fuel consumption of test truck under different road conditions.

in good condition. It should, however, be remembered that lower speeds are maintained on gravel roads.

4. Only the constant rolling resistance coefficient for trucks is affected by the condition of the pavement.

5. At 80 km/h, a truck can use 18 percent more fuel on a gravel road than on a paved road in good condition.

ACKNOWLEDGEMENT

This paper is published with the permission of the Chief Director of the National Institute for Transport and Road Research, Council for Scientific and Industrial Research, Pretoria, Republic of South Africa.

REFERENCES

1. G. Morosiuk and S.W. Abaynayaka. Vehicle Operating Costs in the Caribbean: An Experimental Study of Vehicle Performance. Laboratory Report 1056. Transport and Road Research Laboratory, Crowthorne, Berkshire, England, 1982.
2. J.P. Zaniewski. Fuel Consumption Related to Roadway Characteristics. In Transportation Research Record 901, TRB, National Research Council, Washington, D.C., 1983, pp. 18-29.
3. C.A.V. Queiroz. Calibrating Response-Type Roughness Measurement Systems Through Road-and-Level Profiles. In Transportation Research Record 898, TRB, National Research Council, Washington, D.C., 1983, pp. 181-188.
4. C.J. Bester. Fuel Consumption on Congested Freeways. In Transportation Research Record 801, TRB, National Research Council, Washington, D.C., 1981, pp. 51-54.
5. A.D. St. John and D.R. Kobett. Grade Effects on Traffic Flow Stability and Capacity. NCHRP Report 185. TRB, National Research Council, Washington, D.C., 1978, 110 pp.
6. A.T. Visser. A Correlation Study of Roughness Measurements With an Index Obtained From a Road Profile Measured with Rod and Level. Technical Report RC/2/82. National Institute for Transport and Road Research, Council for Scientific and Industrial Research, Pretoria, Republic of South Africa, 1982.
7. C.J. Bester. Fuel Consumption of Highway Traffic. Ph.D. dissertation. University of Pretoria, Pretoria, Republic of South Africa, 1981.

ACKNOWLEDGMENT

This paper is based on a research study conducted at the Pennsylvania Transportation Institute, Pennsylvania State University, under partial sponsorship of the Pennsylvania Department of Transportation. A full discussion of the study may be found in the final report for the project.

REFERENCES

1. J.R. Ingram. The Effects of Road Roughness on the Friction of a Slipping Tire. M.S. thesis. The Pennsylvania State University, University Park, 1972.
2. B.E. Quinn and S.E. Hildebrand. Effect of Road Roughness on Vehicle Steering. Highway Research Record 471, HRB, National Research Council, Washington, D.C., 1973, pp. 62-75.
3. F.J. Benvin. The Redesign of a Circular Track Apparatus for Traction Testing with Steering and Braking. Master of Engineering Paper. The Pennsylvania State University, University Park, 1976.
4. K.T. Cheng. Instrumentation and Data Processing System for Dynamic Tire Force Measurement. Report in Mechanical Engineering. The Pennsylvania State University, University Park, 1980.

Abridgment

Effect of Vehicle and Driver Characteristics on the Psychological Evaluation of Road Roughness

M. S. JANOFF and J. B. NICK

ABSTRACT

The objective of this paper is to summarize the results of an experiment that evaluated the effects of vehicle size, vehicle speed, residence of rating panel, and training of rating panel on the subjective evaluation of road roughness. The results of the panel ratings indicated that there was no significant effect of the different vehicle sizes or vehicle speeds used on the subjective evaluation of road roughness, and that trained raters (i.e., experts) evaluated roads the same as untrained raters (i.e., laymen). A small but significant effect of panel residence was found.

All panel ratings used the Weaver/AASHO scale employed in previous research (1). Five panels of 21 licensed drivers each--four of Pennsylvania residents and one of Florida residents--were used to obtain the subjective ratings.

Two groups of bituminous test sections--34 in Pennsylvania and 31 in Florida--that span a wide range of roughness were selected for the study. Table 1 summarizes the experimental plan and Table 2 provides an overview of the key variables and the hypotheses that were tested. The test sections spanned a range of roughness from 28 to 639 in. per mile.

EXPERIMENTAL PROTOCOL AND DATA COLLECTION

All test sections were selected, marked, and formed into two routes--one in Pennsylvania and one in Florida. Each section was then measured with a Mays Ride Meter.

Panel members, in groups of three or six, were given detailed instructions on how to rate and then were driven over the route to individually rate each section's ride quality. Mean panel ratings were computed from the individual ratings for each test section for each panel.

TABLE 1 Summary of Experimental Plan

Rating Scale	Weaver/AASHO
Panel	63 Pennsylvania-licensed drivers (3 groups of 21 each) 21 Florida-licensed drivers 21 Florida experts
Sites	34 in Pennsylvania 31 in Florida
Vehicles	2 Pennsylvania K-cars 2 Florida K-cars 1 Pennsylvania subcompact car
Vehicle speeds	One per site equal to the operating speed of the site (except for a subset used in the vehicle speed experiment)
Panel instructions	Given uniformly to all subjects

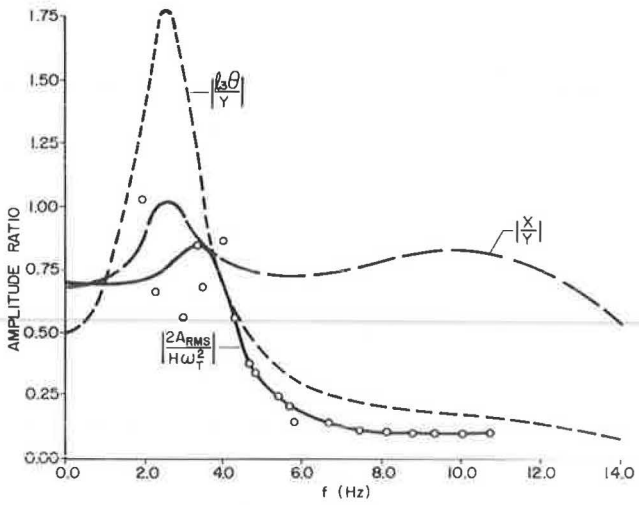

FIGURE 11 Normalized rms acceleration versus frequency for H = 0.5 in.

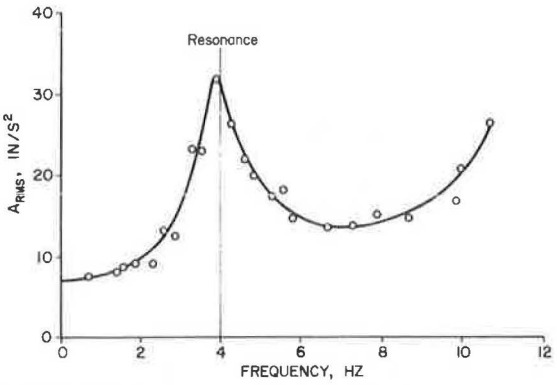

FIGURE 12 Rms acceleration versus frequency for H = 0.5 in.

CONCLUSIONS

Although it was expected that tire traction is reduced at higher frequencies (i.e., higher vehicle speeds or shorter wavelength), the loss was not expected to be as much as 30 percent at 11 Hz (a wavelength of 7.3 ft at 55 mph) for a track height of 0.5 in., peak-to-peak. Second, the traction loss was larger for the higher amplitude track. This would appear to be a logical trend, although more than two track heights would be necessary to obtain an exact relationship.

It was found that the average coefficient of friction was independent of the phases of the various components. Because all the factors are simply ratios of first order functions, this also appears to be a reasonable result. The minimum coefficient of friction is lower than μ_{avg} by a constant offset, independent of frequency. Under special conditions, such as stability during steering, this minimum value may be critical. As long as the braking duration covers several wavelengths, the average coefficient of friction will most likely dominate. This is in agreement with past work (1,2).

The rms acceleration data match the theoretical model fairly well except for the magnitudes at resonance. The reason for this is most likely the low value of damping used to obtain the theoretical resonances. In terms of the model of the present system, the only improvement might be to obtain the actual value of the damping coefficient and verify the inertias and spring constants. This should allow a better matching between the theoretical and experimental values of resonances and the magnitudes at these points.

For the system itself, an improvement should be made with respect to the pneumatic cylinders. They add the proper static loading to the system but, under dynamic conditions, they act as a spring when they should act as an inertia. This moves the first natural frequency up from the desired 1- to 2-Hz range into the 4-Hz range. A possible solution would be to replace the cylinders with lead weights hung on the test frame arm, as calculated by Benvin (3).

Further work will be conducted using a 1980 Pontiac Phoenix suspension system. Its lighter frame and MacPherson strut suspension should produce results that will be relevant for today's down-sized cars. Also, a roughness facility under construction at PTI will allow full-scale vehicle tests to further the research into traction loss due to roughness. Also, a special report by Task Group 1 of TRB Committee on Surface Properties-Vehicle Interaction is being prepared on The Influences of Roadway Surface Discontinuities on Safety. This report will also add to the knowledge of traction loss (safety) as affected by road roughness.

LIST OF SYMBOLS

A	The combined cross-sectional area of the pneumatic cylinders.
C_s	The linear viscous damping coefficient of the shock absorber.
F	The horizontal friction force between the tire and the track surface due to braking.
f_i	The ith natural frequency in hertz.
H	The peak-to-peak amplitude of the test track in inches.
I_o	Mass moment of inertia of the test frame.
K_p	Linear spring coefficient for the pneumatic cylinders.
K_s	Linear spring coefficient for the torsion bar.
K_t	Linear spring coefficient for the test tire.
ℓ_i	The ith lever arm dimension in inches.
m_F	The mass of the Toronado frame.
m_T	The mass of the wheel assembly.
N	The normal load at the test tire.
P_o	The spring force of the pneumatic cylinders.
R	The radius of the test tire.
T	The torque on the test tire due to braking.
TS	The absolute tangential velocity of the test frame.
u	Vertical displacement of the test frame at the point above the wheel assembly, ℓ = 66 inches.
V_o	The combined volume of the pneumatic cylinders.
W_i	The weight of the test frame.
W_F	The weight of the Toronado frame.
W_T	The weight of the wheel assembly.
W_S	The absolute tangential velocity of the test frame based on the test wheel.
X	Vertical displacement of the wheel assembly.
Y	Vertical displacement of the test track.
Z	Vertical displacement of the test frame at the point where the accelerometer is mounted, ℓ = 22 in.
λ	Wavelength of the test track, in inches.
μ	The kinematic coefficient of friction between the automobile tire and the test track.
θ	The rotational displacement of the test frame in radians.
ζ	The damping ratio for the system.

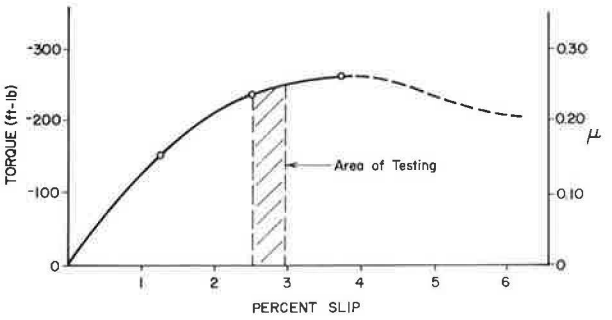

FIGURE 6 Tire traction versus percent slip.

shows that the rigorously precise $\mu(t)_{avg}$, which retains the phases in torque and normal load until the final step in the calculations, is only 0.29 percent less than μ_{avg}. Any phase shifts between the torque and the normal load are averaged out by the use of μ_{avg}. Therefore, in the following calculations μ_{avg} will be used.

It was found that the minimum coefficient of friction, μ_{min}, was offset from μ_{avg} by a constant increment, $\Delta\mu = 0.04375$ (see Figure 7). Because the normal load, N_{avg}, is an essentially constant 1,200 lb, the relationships between torque and frequency, and μ_{avg} and frequency, are identical. The two curves shown in Figures 8 and 9 indicate the relationships of both torque and coefficient of friction with increasing track frequency for both track amplitudes used. Both curves decay in an exponential manner. Figure 10 gives a combination and normalization of these curves to show the effect of track amplitude on the coefficient of friction. The data indicate that the higher amplitude track produces a greater loss of traction over the entire frequency range.

In Figure 11, the solid curve is the root mean square (rms) acceleration of the frame at a point directly above the test wheel, normalized by the input frequency of the track, $(H/2)w^2d$, and plotted against the frequency for H = 0.5 in. The dotted and dashed curves are the theoretical normalized rms accelerations for the test frame and the wheel assembly, respectively. Figure 12 gives the absolute plot of the rms acceleration versus frequency for the test frame where the accelerometer is mounted, at ℓ = 22 in. Scatter in the data at low frequency makes it difficult to draw a smooth curve through the data (Figure 11). However, Figure 12 shows that a smooth curve does indeed exist.

From visual observations during the operation of the system, it appears that the fundamental resonant frequency of the quarter-car model is about 4 Hz, and the tire assembly experiences resonance at about 11 to 12 Hz. The experimental plot in Figure 12 appears to verify both of these observations. The experimental plot in Figure 11 agrees fairly well with the theoretical curve. The only error is for the magnitude at resonance, and the primary reason for this is probably the low value of theoretical damping used.

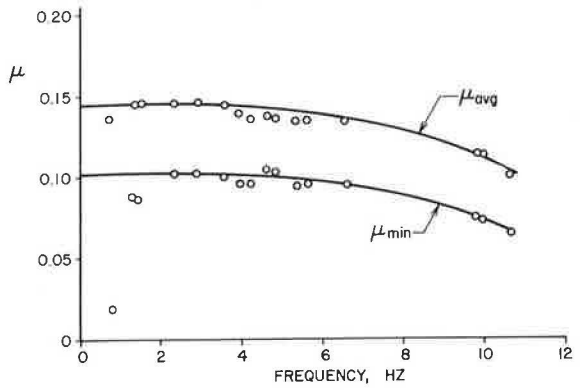

FIGURE 7 Variation in μ versus frequency.

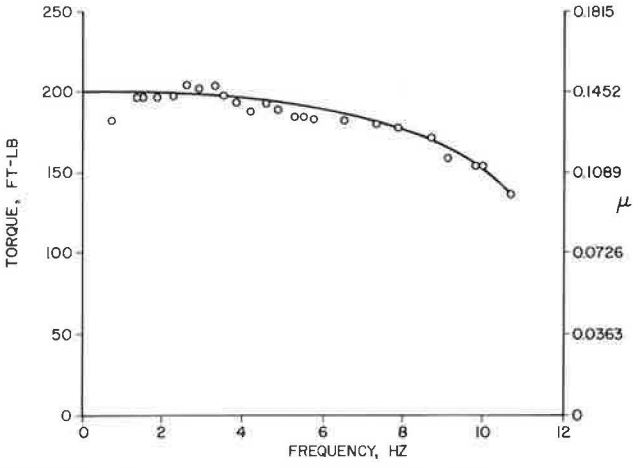

FIGURE 9 Traction versus frequency for H = 0.5 in.

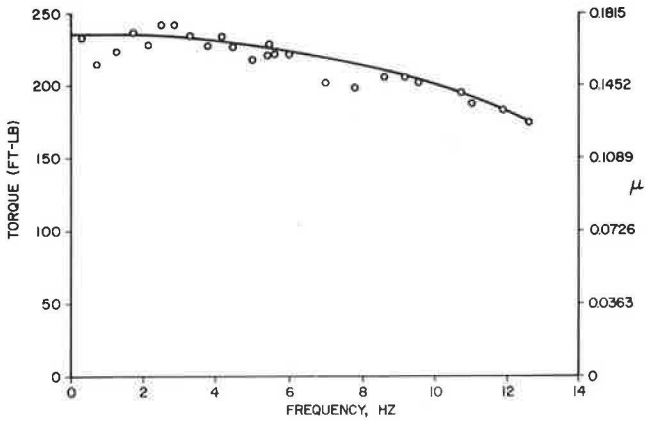

FIGURE 8 Traction versus frequency for H = 0.25 in.

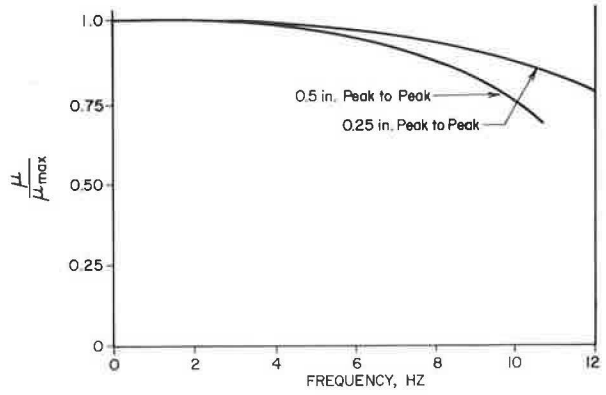

FIGURE 10 Traction versus frequency for both amplitudes.

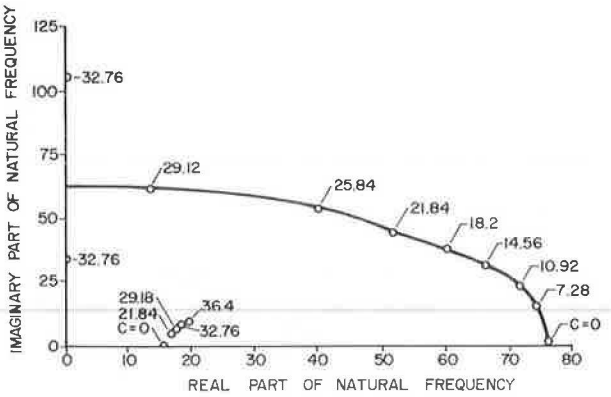

FIGURE 4 Natural frequencies versus damping factor.

cided to choose the highest value of C_s that still allows the resonances to approximately match the experimental resonances. This value is C_s = 14.56 lb-sec/in., and the corresponding natural frequencies and damping ratios are:

f_1 = 2.48 Hz and ξ_1 = 0.309, and
f_2 = 10.65 Hz and ξ_2 = 0.382.

The time-varying component of the normal load may be calculated as:

$$N(t)_T = K_E(Y - u) \tag{7}$$

where K_E is the equivalent spring coefficient for the system. It was experimentally measured to be 320 lb/m.

From the accelerometer mounted at ℓ_2, $\ddot{Z}$ is obtained. For small values of θ, the following approximations can be made:

$$\ddot{Z} = \ell_2\ddot{\theta} \tag{8}$$
$$\ddot{U} = \ell_3\ddot{\theta} \tag{9}$$

For $Y(t) = H/2 \sin(W_d t)$ the system is driven at the frequency W_d so that:

$$U = (-\ddot{U}_2/W_d) \tag{10}$$

therefore,

$$N(t)_T = K_E\,[Y(t) + (\ell_3/\ell_2)/(\ddot{Z}/W_d^2)] \tag{11}$$

and the total normal load becomes:

$$N(t) = N_0 + N(t)_T \tag{12}$$

It is essential to maintain the relative phases of Z and Y(t) during the recording of these values, otherwise the normal load, N(t), would be meaningless. As in the steady state case, the time-varying braking force, F(t), may be calculated as:

$$F(t) = T(t)/R \tag{13}$$

The time-varying coefficient of friction, $\mu(t)$, may then be calculated as:

$$\mu(t) = F(t)/N(t) \tag{14}$$

TESTING

Data were collected for two different amplitudes of track over the frequency range from 1 to 12 Hz. Figure 5 shows the instrumentation used to monitor the system and collect data.

The track speed tachometer was used to obtain the desired track frequency. The wheel speed tachometer was used to set the wheel braking slip with reference to the track speed by the following equation:

$$\%\,\text{slip} = [(TS - WS)/TS] \times 100 \tag{15}$$

The desired loading on the pneumatic cylinders was set by a pressure regulator. The lap reference counter has a microswitch that sent a signal every time the test frame passed a certain point on the track. The accelerometer measures the vertical acceleration, $\ddot{Z}$, of the test frame. The microswitch signal allows the relative phase of the accelerometer signal and the track amplitude to be determined. This is essential if the dynamic normal load, N(t), is to be calculated correctly using Equation 11. Finally, the torquemeter measures the torque at the test wheel for use in Equation 13.

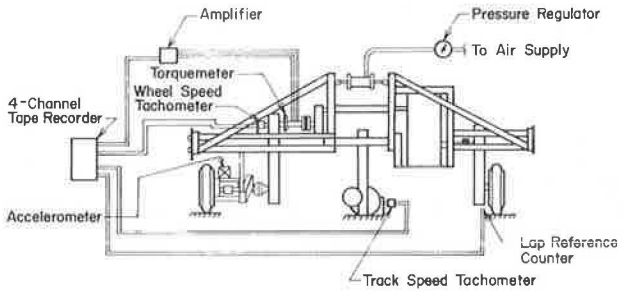

FIGURE 5 Instrumentation for data acquisition.

The torque, acceleration, lap counter, and track speed signals are continuously recorded by a four-channel tape recorder. The wheel speed only has to be measured once each time the percent slip is set, which is only when a new set of concrete slabs is put in place. Therefore, a special data set is taken at the start of each new track set, with the wheel speed replacing the lap counter signal.

The data were recorded and then digitized using an EAI 680 analog computer interfaced with a PDP DEC 10 digital computer. The data were then processed using the calibration curves to convert the signals into meaningful units of force, velocity, and acceleration.

RESULTS

In this section the physical results and the trends in the data recorded on the system are discussed. The variation in the coefficient of friction for changes in the braking slip is shown in Figure 6. The solid curve represents actual data recorded for this project. The dotted curve is the theoretical extrapolation to higher slip values based on Benvin's data (3). The maximum traction possible occurs at approximately 4 percent slip. The tests were run at between 2.5 and 3.0 percent slip.

Consider the relationship between $\mu(t)_{avg}$ and μ_{avg}. Comparison of the results for

$$\mu(t)_{avg} = [T(t)/R \times N(t)]\ \text{avg}$$

versus

$$\mu_{avg} = T_{avg}/(R \times N_{avg})$$

be considered. The circular track is equipped with pressure cylinders that can apply additional loading to the Toronado suspension. The pressure cylinders, along with the natural weight and inertia of the test arm frame, supply a known normal load, N, at the wheel equal to that of the front right quarter of a Toronado under both static and dynamic conditions.

The circular track test frame is equipped with a variable ratio gear train which, when adjusted from equilibrium, applies a braking slip between the drive wheel and the test wheel. This creates a braking torque, T, on the test wheel, which can be measured using an in-line torquemeter. Under steady state operating conditions, with a given percent slip and cylinder loading and with the flat track in place, the horizontal braking force, F, between the tire and the track surface is

$$F = T/R \tag{1}$$

[Note: For explanations of the variables used in the equations, please refer to the List of Symbols at the end of this paper.]

The coefficient of friction, μ, between the tire and the track surface is:

$$\mu = F/N \tag{2}$$

When a sinusoidal track surface is used, the values of torque and normal load will vary sinusoidally about a constant value. A simple procedure would be to assume that, over several revolutions of the system at steady state, the average values of F and N will equal their constant values. Therefore, these average values, F_{avg} and N_{avg}, could be measured and used to calculate the coefficient of friction, μ. However, a more rigorous procedure was chosen which stores both the constant values and the variations in magnitude and phase in the values of torque and normal load. Throughout the calculations of the coefficient of friction, an average value of μ may be the same as that calculated by the simpler procedure; but it is possible that the dynamics of the system, especially at resonance, could result in phase shifts in the relative peaks of F and N, which would affect the instantaneous, and possibly even the average, values of μ. This procedure yields the average value of μ as well as the instantaneous maximum and minimum values. These values may turn out to be as important as the average value.

To perform this procedure, the vertical acceleration of the frame was measured to determine the changes in the normal load, N(t), due to inertial loadings. The time-varying torque, T(θ), was recorded by the torquemeter just as for the steady state case.

To calculate the time-varying normal load, N(t), from the acceleration data, the dynamics of the system must be considered. The free-body diagram in Figure 3 represents the test arm, with the Toronado suspension reduced to a 2-degrees-of-freedom system.

The summing of moments about 0 for the static case yields

$$\Sigma M_0 = P_0\ell_3 + W_1\ell_1 + W_F\ell_3 = N_0\ell_3 \qquad (N_0 = 1{,}257 \text{ lb}) \tag{3}$$

This is the steady state value of the normal load.

The summing of moments about point 0 for the dynamic case yields the differential equations of motion for the system:

$$(I_o + m_F\ell_3^2)\ddot{\theta} + C_S\ell_3^2\dot{\theta} + (K_S\ell_3^2 + K_p\ell_4^2)\theta = K_S\ell_3 x + C_S\ell_3\dot{x} \tag{4}$$

$$m_T\ddot{x} + C_S\dot{x} + (K_T + K_S)x = K_S\ell_3\theta + K_T Y + C\ell_3\dot{\theta} \tag{5}$$

The equations were solved using the mode superposition method. Assuming the general solutions:

$$x(t) = \bar{x}e^{jwt}$$
$$\theta(t) = \theta e^{jwt}$$

where w is complex, and substituting all known values into Equations 4 and 5, the resulting characteristic equation is obtained:

$$1{,}379{,}028.8 - (6{,}103.8 - 8.79 \times 10^{-4}C_S^2)\,w^2 + w^4 + j(3{,}375.4\,C_S w - 4.739\,C_S w^3 \tag{6}$$

The roots of this equation are obtained by setting it equal to zero. The roots are the natural frequencies for the system. Because the damping term, C_S, is difficult to determine accurately, a computer program was written to solve Equation 6 for a range of values of C_S between 0 and 36.4 lb-sec/in. Figure 4 shows the resulting root locus plot.

A typical damping ratio for a quarter-car would be on the order of $\xi = 0.8 - 1.0$. This would correspond to a value of C_S between 37.7 and 47.1 lb-sec/in. A value this high produces meaningless roots for the system. Thus, for the analysis, it was de-

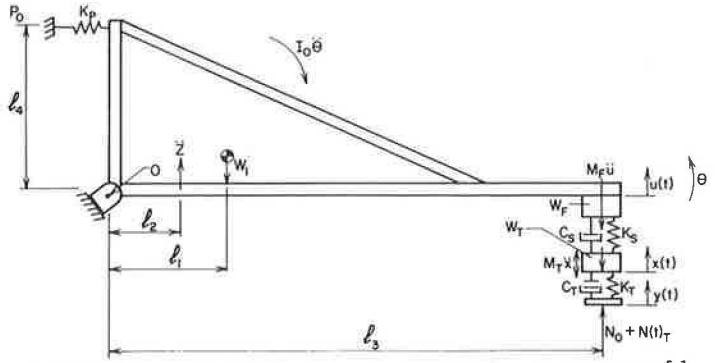

FIGURE 3 Free body diagram for the test frame and wheel assembly.

Traction Loss of a Suspended Tire on a Sinusoidal Road

JEROME S. CAP and J. C. WAMBOLD

ABSTRACT

It has been known for some time that automobiles lose a significant percentage of their traction when exposed to a sinusoidal road input, that is, a washboard road, above certain speeds. Similarly, when an automobile is on a four post shaker, it is common practice to use an approximately 10-Hz shaker frequency, and then push the automobile by hand to position it on the shaker. Early studies of a laboratory test with a fixed axle showed that there is significant loss in traction at higher amplitudes or higher frequencies (shorter wavelengths or high speeds), or at a combination of the two. Presented in this paper are the results of a study on the effects of sinusoidal roads on the traction of the right front quarter-car assembly of a 1968 Oldsmobile Toronado using the circular track apparatus at the Pennsylvania Transportation Institute. The results show that as much as 30 percent of the automobile's traction is lost at frequencies of 11 Hz (as compared to a flat track), and that the rate of decay increases rapidly by this frequency. Furthermore, the loss of traction increases for larger input amplitudes; 11 Hz is comparable to a vehicle traveling at 55 mph on a road with roughness at a 7.3-ft wavelength.

It has long been known that, when an automobile attempts to stop on a washboard road, the braking traction is greatly reduced in comparison to the traction on a flat road. Preliminary work by Ingram (1) produced test data showing this loss of traction as a function of the input roadway frequency and amplitude. Ingram's work was done with a mounted tire that was allowed to slip on a flat plate to simulate braking while the plate was moved sinusoidally up and down to generate the road input. The effect of traction loss on cornering has been demonstrated by Quinn (2).

The purpose of the present study was to examine the effects of road roughness in the range from 1 to 12 Hz on the coefficient of friction between automobile tires and the road by using a more realistic quarter-car model. To accomplish the testing segment of the study, the Circular Track Apparatus (3), located at the Pennsylvania Transportation Institute of Pennsylvania State University, was used (see Figure 1). The circular track consists of a 14-ft-diameter test track on which a test suspension can be operated at various speeds and percent braking slip. For this set of tests, the right front suspension system from a 1968 Oldsmobile Toronado was used (see Figure 2). A special track surface was fabricated using sets of 16 concrete slabs (4). The slabs were cast with computer-generated, banked, sinusoidal surfaces so as to react with the tire

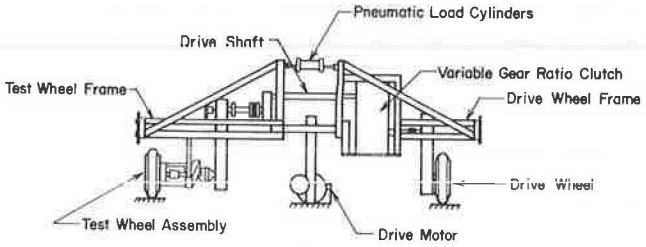

FIGURE 1 Circular track apparatus.

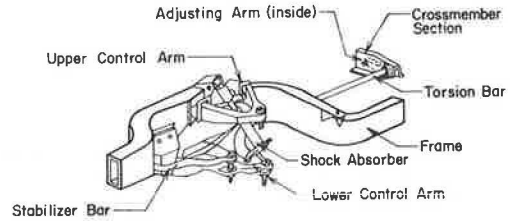

Quantity	Description
1	15-inch-diameter Wheel
1	Right Front Drive Axle Assembly
1	Shock Absorber
1	Front Wheel Ball Bearing
2	Hub Assembly O-Rings
4	Upper and Lower Control Arm Bushings
1	Right Front Output Shaft
1	Bearing Seal

FIGURE 2 Toronado suspension system.

like a straight road with sinusoidal bumps. Five sets of slabs were made: two different wavelengths, λ = 16 in. and λ = 32 in., at two different amplitudes, 0.25 in. and 0.5 in., peak-to-peak; and one set of flat blocks, $\lambda = \infty$. The first four complete track sets permitted continuous testing over the frequency range from 1 to 12 Hz at two different amplitudes. The flat track set was used to collect reference data for comparison with the sinusoidal tests. The slabs were painted with an antiskid paint to ensure that all surfaces were the same and that any changes of the tire/track coefficient of friction thus would be due only to the variations of test parameters and not to any variation in the track surface.

THEORETICAL CONSIDERATION

The principles of the tests are straightforward and will be discussed in this section. First, the static and dynamic simulation of the quarter-car model will

TABLE 2 Overview of Key Variables

Experience	Panel	Number	Sites	Vehicle	Speeds	Null Hypothesis
Panel regionality	21 Pennsylvania	1-a	Florida	K-car[a]	1 per site	No difference between the mean ratings for regionally different panels
	21 Florida	1-b	Florida	K-car[a]	1 per site	
Vehicle size	21 Pennsylvania	1-a	Pennsylvania	K-car[a]	1 per site	No difference between the mean ratings obtained from either vehicle
	21 Pennsylvania	2	Pennsylvania	Subcompact[b]	1 per site	
Vehicle speed	21 Pennsylvania	1-a	Pennsylvania	K-car[a]	1 per site	Different speeds have no effect on subjective appraisal of ride quality
	21 Pennsylvania	3	Pennsylvania	K-car[a]	1 per site but 6-8 site speeds changed	
Expert/laymen	21 Pennsylvania	1-a	Pennsylvania	K-car[a]	1 per site	No difference between the mean ratings made by expert and laymen panels
	22 experts	4	Pennsylvania	K-car[a]	1 per site	

[a]All K-cars were as identical as possible (age, mileage, tires, tire pressure).
[b]Front wheel drive.

DATA ANALYSIS

The analysis of the effect of vehicle size, vehicle speed, expert versus untrained raters and panel residence (regionality) on mean panel ratings is summarized in Table 3.

TABLE 3 Data Analysis

Analysis	Effect
Vehicle size	Mean panel ratings are unchanged when vehicle size is changed (compact versus subcompact).
Vehicle speed	Mean panel ratings are unchanged by normal changes in vehicle speed (extreme changes can cause some effect on panel ratings).
Experts versus untrained raters	Both types of panel members subjectively rate pavement sections the same
Panel regionality	Regionality has no effect on smooth roads but has a small, statistically significant effect on rougher roads. The average difference is about 0.5 scale units.

In each case, a two-way analysis of variance was used to test the hypothesis that there was no effect of the primary variable (vehicle size, vehicle speed, expert versus untrained or panel residence) on mean panel ratings.

CONCLUSIONS

The major results of this experiment can be summarized as follows:

1. There is a small, but significant effect of panel regionality (i.e., area of residence) on subjective ratings of rough roads but no effect on smooth roads.
2. There is no significant effect of vehicle size (intermediate-compact and subcompact) on subjective ratings.
3. There is no effect of vehicle speed on subjective ratings (at least for speeds within a normal driving range).
4. There is no significant difference between subjective ratings provided by "experts" and subjective ratings provided by untrained (in road evaluation) laymen. (However, highly critical, regionally diverse experts will provide statistically different ratings.)

ACKNOWLEDGMENT

This work is extracted from the results obtained under NCHRP Project 1-23, Pavement Roughness and Rideability. A complete coverage of the preceding material will be contained in the final report for this project (1).

REFERENCE

1. M. S. Janoff, et al. Pavement Roughness and Rideability. Final Report. NCHRP Project 1-23, TRB, National Research Council, Washington, D.C., in preparation.

Abridgment

Correlation of Subjective Panel Ratings of Pavement Ride Quality with Profilometer-Derived Measures of Pavement Roughness

M. S. JANOFF, P. S. DAVIT, and J. B. NICK

ABSTRACT

Results of a series of comparative, statistical analyses that were accomplished to relate subjective ratings of pavement ride quality to profilometer-derived measures of pavement roughness are reported. The goal was to develop preferred methods of analysis that can be used to develop transforms that will allow subjective ratings to be predicted from objective measures. The major conclusions are that: (a) it is possible to determine those specific frequency bands that are most related to subjective ride quality and (b) the correlations between the profile power levels in these frequency bands and the mean panel ratings are very high, indicating excellent agreement.

Some of the results of a series of comparative, statistical analyses that related subjective ratings of pavement ride quality to profilometer-derived measures of pavement roughness are briefly summarized. The intent of these analyses was to develop preferred methods of analyses that combine subjective ratings and physical profiles, and that can be used to develop transforms that will allow subjective ratings to be predicted from objective measures.

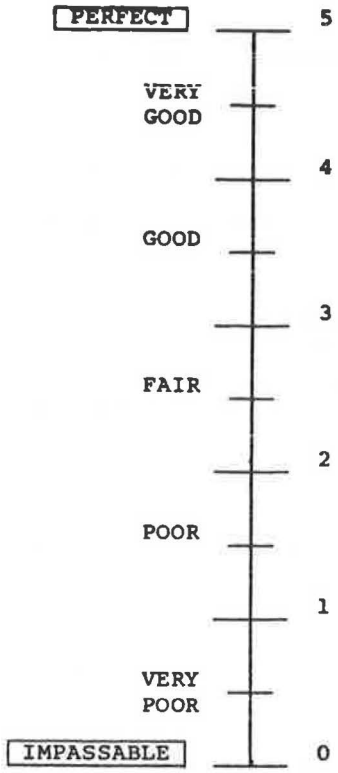

FIGURE 1 Weaver/AASHO scale.

EXPERIMENTAL DESIGN

Twenty-one panel members were used to subjectively rate the ride quality of 18 bituminous pavement sections of uniform length and spanning a wide range of roughness. The Weaver/AASHO scale shown in Figure 1 was employed for all subjective ratings. Roughness was measured, with a GM profilometer and Mays Ride Meter, concurrent with the panel ratings. The test sections spanned a range of roughness of 25 to 327 in. per mile and the mean panel ratings spanned a range of 1.20 to 4.26 on the 0 to 5 scale.

DATA COLLECTION

The panel members were divided into groups of three, given detailed rating instructions, and then driven over the 18 test sections; each test section was individually rated by each panel member and mean panel ratings were computed for each test section. Profiles and response type roughness was collected concurrent with the panel ratings.

DATA ANALYSIS

The profiles were digitized and a fast Fourier transform (FFT) was applied to compute profile power. The power was then graphed to visually compare the 18 test sections. In general, as power rose--indicating a rougher pavement--the mean panel ratings decreased, indicating a loss of ride qual-

TABLE 1 Regression Analyses

Objective Measure of Roughness	Correlation Coefficient[a]
Mays Ride Meter	-0.76
1/4 car index	-0.69
Profile power	
(0.0029 to 3.0 cy/f)	-0.33
(0.09 to 1.5 cy/f)	-0.92
(0.2 to 0.4 cy/f)	-0.92
(0.09 to 3.0 cy/f)	-0.92
(0.02 to 3.0 cy/f)	-0.90
(0.4 to 3.0 cy/f)	-0.87

[a]When correlating mean panel rating (subjective measure of ride quality) with each objective measure of road roughness in column 1.

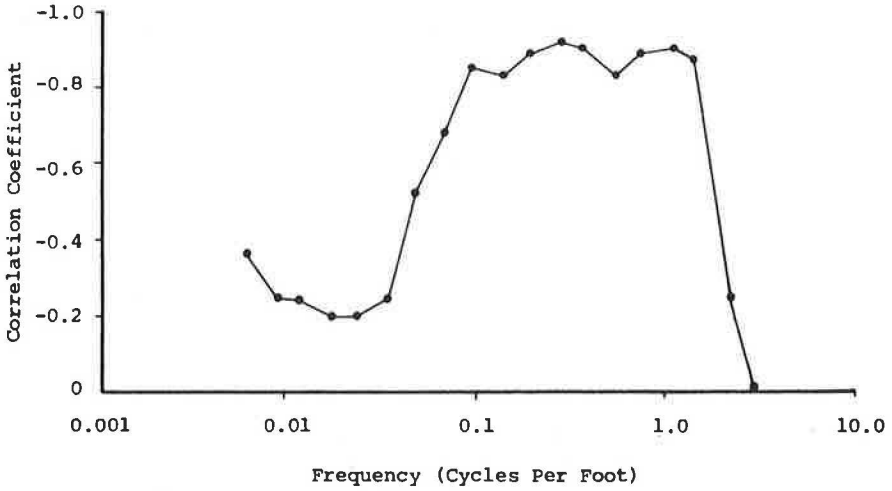

FIGURE 2 Results of correlating power with mean panel ratings for individual one-half octave bands.

ity. However, the correlation coefficient was quite low (-0.33). Simple roughness measures such as the Mays Ride Meter provide somewhat better correlations (-0.76).

In restricted bands of frequencies, however, the correlation of mean panel rating and profile power was quite high, as indicated in Table 1, often exceeding -0.90.

The power was computed in each of 18 one-half octave bands from 0.0029 to 3.0 cycles per foot and correlated with mean panel ratings as illustrated in Figure 2.

The correlations are extremely high between 0.09 and 1.48 cycles per foot and fall off outside this range. The total power in this band when correlated with mean panel rating yields a correlation coefficient of -0.92.

CONCLUSIONS

The one-half octave analysis indicates that it is possible to identify a specific frequency band (or bands) where profile power is highly correlated with subjective ratings of ride quality. A transform can thus be developed that allows the user to accurately predict subjective appraisals of ride quality (i.e., mean panel ratings) from physical measures of the pavement profile.

ACKNOWLEDGMENT

This work is extracted from the results obtained under NCHRP Project 1-23, Pavement Roughness and Rideability. A complete coverage of the preceding material will be contained in the final report for this project (1).

REFERENCE

1. M.S. Janoff et al. Pavement Roughness and Rideability. Final Report. NCHRP Project 1-23, TRB, National Research Council, Washington, D.C., in preparation.

Microprocessor-Based Noncontact Distance Measuring Control System

JIUNNJYH WANG, J. C. WAMBOLD, and J. J. HENRY

ABSTRACT

A microprocessor-based noncontact ranging system is discussed, which, along with a computer-based videographics system, constitutes a noncontact texture profiling system developed at the Pennsylvania Transportation Institute. Consisting of a 6502-based single board computer and a Polaroid ultrasonic circuit board, the ranging system is used to monitor the displacement between a traveling test vehicle and the road surface. The texture measurement is performed by the videographic system, which is capable of acquiring data only when it is within a range of ± 1.2 mm from the pavement. Because the system is mounted in a moving vehicle, it is continuously moving up and down relative to the pavement and, consequently, a ranging device is needed to trigger the data acquisition only when the system is in range. Because the system is to run at highway speeds, the ranging system needs to operate at a sampling rate of 40 per second with a resolution of 0.3 mm or better. The final system achieved a rate of 60 samples per second with a resolution of 0.17 mm. A high resolution of the videographic system is achieved because the ranging system eliminates the need for a large depth of field. In addition, the ranging system is capable of data processing, self-calibration, and controlling, and thus has the potential for other applications such as road roughness measurement, liquid level sensing, and any general noncontact displacement measurement.

In a noncontact texture measurement system described elsewhere in this Record by Her et al., an optical system consisting of a stroboscopic light source and lens assembly is used to project a strong beam of light (in the shape of a long, thin strip) with a sharp edge down to the road surface. The projected light area on the road surface is then taken as a picture by the TV camera and stored as a digitized picture in the LSI-11 processor. The processor performs an edge detection algorithm of the digitized picture and, after angle correction, stores it as a profile of the texture. Because all of the apparatus is maintained on a vehicle moving at 40 mph, bouncing of the vehicle will result in the whole system, lens assembly and TV, constantly going in and out of focus.

A ranging system is needed to solve the problem. There are three functions provided by this ranging system.

1. The ranging system closely monitors the displacement between the vehicle and the road surface and is able to indicate when the system is in focus and to fire the strobe. Thus, a sharp picture is guaranteed whenever a picture is taken.

2. The ranging system determines when the video signal of texture image is available and when it should be acquired and processed before the image fades. This is done by issuing a command to the LSI-11 processor, which hosts the video-digitizer.

3. The texture image in the picture is always at the same position because the picture is always taken at a fixed position, the focal position. This facilitates the processing of the texture image as the processor is able to search for the image more efficiently.

With some modifications, a ranging system designed for these purposes can also be applied to road roughness measurement.

PRINCIPLE OF SYSTEM OPERATION

The speed of sound in a homogeneous medium is constant for a constant set of environmental conditions. Therefore, with each unknown distance, there is an associated time interval determined by the speed of sound in that particular medium. If the time interval can be measured, it can be converted into distance with respect to sound speed at that set of ambient conditions. However, the correct speed of sound is not always available for time-to-distance conversion, especially when ambient conditions such as temperature, humidity, and windspeed keep changing. A measurement error results unless the correct speed of sound at that ambient condition is used for time-to-distance conversion. Another measurement error comes from the varied vehicle speeds. As shown in Figure 1, the sound path is V-shaped. Different vehicle speeds result in a different sound path and time interval for a fixed distance between the vehicle and the road surface (path A for a slower vehicle, path B for a faster vehicle). The distance D' as measured by the moving vehicle without correction can be found to be (1):

$$D' = DV_c/(V_s^2 - V_v^2)^{1/2} \quad (1)$$

where

D = distance between vehicle and road surface;
V_v = vehicle speed. In the case where wind is present, this represents the magnitude of vector sum of vehicle velocity and sound velocity component in the direction of vehicle motion;

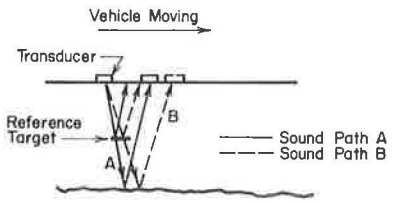

FIGURE 1 Sound path for measurement.

V_c = speed of sound used by computer for time to distance conversion; and

V_s = speed of sound at that set of environmental conditions.

It is shown that D' is a function of the speed of sound and the vehicle speed. Under normal operating conditions with V_v ranging from 0 to 60 mph, D = 40 cm, and V_s = 343 m/s at 20°C, an intolerable error of as much as 1.2 mm, which is equal to the allowed system depth of focus, could occur.

This problem can be overcome in this design by placing a fixed calibration target at a predetermined distance d. Because the distance d measured by the moving vehicle is

$$d' = dV_c/(V_s^2 - V_v^2)^{1/2} \quad (2)$$

the true distance between vehicle and road surface can be obtained by calculating D'/d' x d = D. Therefore, the distance measuring can be free of errors caused by environmental variations and vehicle speed changes.

Both the measurement of time intervals and the time-to-distance conversion were performed by a 6502-based microcomputer. In operation, a certain number of sound pulses are transmitted toward the road surface, and the resulting echoes from the calibration target and the road surface are detected. The elapsed time intervals between initial transmission and echo detection are recorded by a timer under computer control and stored in memory for conversion. The system clock frequency is 1 MHz, and the counting error is no more than 1 μs, which corresponds to a resolution of 0.17 mm, well within the tolerance needed for this project.

SYSTEM DESCRIPTION

Two primary components constitute the Polaroid ultrasonic ranging unit: an acoustical transducer and an ultrasonic circuit board (2). Together, these components are capable of detecting the presence and distance of objects within a range of approximately 0.9 to 35 ft.

The principal component in this device is the transducer, which acts as both loudspeaker and microphone. It has been designed to transmit the outgoing signal and also to function as an electrostatic microphone in order to receive the reflected signal.

The ultrasonic circuit board electronic system controls the operating mode (transmit/receive) of the transducer. It is composed of three major sections that control transducer operation and allow information gathered by it to be used as desired. Among the sections are a digital circuit, an analog circuit, and a power section.

Figure 2 shows a block diagram of the ultrasonic ranging unit. An appropriate drive signal initiates the transmission of an ultrasonic pulse by the transducer. When the unit is activated, the transducer emits a sound pulse, then waits to receive the echo returning from whatever object the sound pulse has struck. The emitted pulse is a high-frequency, inaudible "chirp" lasting for 1 ms and consisting of 56 pulses at 4 carefully chosen, ultrasonic frequencies: 60, 57, 53, and 50 kHz. Occasionally, a single frequency could be cancelled because of certain target topographical characteristics and no echo would be reflected. The use of four frequencies overcomes that possibility.

A crystal-controlled clock in the digital circuit generates the ultrasonic frequencies that comprise the pulses transmitted by the transducer. After generating the chirp, the operating mode of the transducer changes from loudspeaker to microphone to detect the returning echo. Upon receiving the echo, the transducer converts the sound energy to electrical energy, which is amplified by the analog circuit and then detected by the digital circuit to produce the time it takes from transmission to get the echo-received signal.

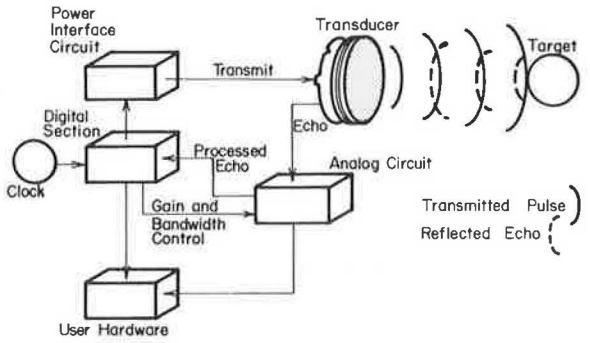

FIGURE 2 Block diagram (transmitting and receiving).

The waveforms presented in Figure 3 illustrate the pertinent timing relationships of the following:

1. Power (VSW) is a drive logic signal that initiates the transmit-receive cycle by supplying the ultrasonic circuit board with the VSW signal. The VSW signal has to reach a low level before a new cycle can be initiated.
2. Transmission (XLG) is the digital logic drive for the transmitted signal. It consists of 8 cycles at 60 kHz, 8 cycles at 57 kHz, 16 cycles at 53 kHz, and 24 cycles at 50 kHz, for a total of 56 cycles, and lasts for a period of about 1 ms. All timing relationships between the transmitted signal and the received echoes are determined from the leading edge of this signal.
3. Amplified echo is useful for observing the reflected echoes.
4. Processed echo is useful if echoes other than the first are of interest.
5. Detected echo (FLG) is the signal that indicates that the echo has been received.

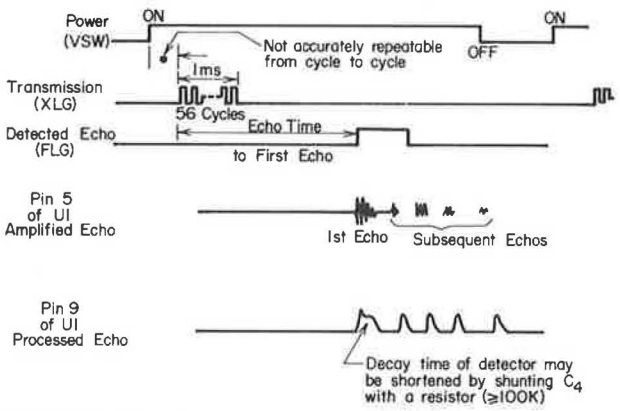

FIGURE 3 Wave-forms.

Because the purpose of the ranging system for the texture project is to closely monitor the displacement between the vehicle and the road surface, sonar response time and the measuring rate of the ranging system have an important effect on the performance of the system. The effects of these two factors are discussed below.

Sonar Response Time

Because of finite sound velocity, there is always a measurement error caused by time delay if the detected object is moving with respect to the transducer, as in the case of the texture project. Assuming the transducer at the height of D is bouncing at f Hz with an amplitude A, it can be found that the maximum error E due to sonar response delay T_d is

$$E = \pm A \sin(\pi f T_d) \qquad \text{where } T_d = 2D/\text{sound speed} \tag{3}$$

This maximum error occurs when the vehicle is passing through the vehicle static equilibrium position, which is also the vehicle system focal position. It is clear that the shorter the distances between transducer and calibration target and road surface are, the smaller the lag effect and error will be. Thus, to reduce the time delay, the transducer and calibration target should be placed as close to the road surface as possible. The only limit on the position of the calibration target is that it should not hit the pavement as the vehicle bounces up and down; 20 cm is taken as a reasonable distance between pavement surface and calibration target. The position of the transducer is limited to the transmitting pulse duration of the ultrasonic circuit board. The leading edge of the reflecting echo can only be detected after the transmission duration period is over and the lasting echo vibrations caused by the transducer holder have been damped out. The ultrasonic circuit provides a pulse duration of 1 ms, which is followed by 3 ms of echo reflecting from the transducer holder. That means the distance between the transducer and the calibration target will be too long (70 cm) to be favorable as far as the response time and space are concerned. Therefore, it was necessary to reduce the pulse duration of the original ultrasonic circuit board in order to place the transducer closer to the calibration target and reduce the measurement error.

Through hardware and software techniques, the ultrasonic circuit board was modified to have an 80-μs pulse duration, which consists of 4 pulse cycles at 50 kHz. This enabled the transducer to be placed 20 cm above the calibration target and resulted in a time delay of 2.4 ms. With the vehicle bouncing at f = 2 Hz with amplitude A = 10 cm, the maximum error is found to be E = ± 1.5 mm. This amount of error is intolerable; however, it will be corrected during the data processing as will be discussed later.

Measuring Rate

The measuring rate or sampling rate affects the accuracy of estimation and the quality of the acquired picture. With the larger sampling rate, the displacement can be monitored more closely, and better estimation and control result.

Because there is a power dissipation problem, the recommended measuring rate for the ultrasonic circuit board is 5 times per second. This is too low to fulfill the performance requirement, because the moving vehicle will bounce at a frequency as high as 20 Hz. This problem also was solved by reducing the transmission pulse duration. It is during the pulse duration that a large current is induced, generating heat that must be dissipated. Therefore, the solution to the sonar response time problem also solved the sampling rate problem without causing further heat dissipation requirements. A measuring rate of 60 times per second was achieved, and the performance of the ranging system was greatly improved.

SYSTEM IMPLEMENTATION

The noncontact texture measurement system comprises the modified ranging unit, an LSI 11/23 processor, television camera, a strobe, and a 6502-based single board computer that coordinates the functions of all the other components. Figure 4 shows the system block diagram. The single board computer provides the drive signal for the ultrasonic circuit board, detects the transmission and echo signal from the ultrasonic circuit board, and records the time interval for data processing. After data processing is completed and a new picture is to be taken, the single board computer will fire the strobe and synchronize the grabbing of the picture with the vertical sync of the television camera by issuing a timely command to the LSI processor.

A 6522 VIA (Versatile Interface Adapter) (3) in the single board computer acts as an interface between the CPU and other system components. The interface block diagram is shown in Figure 5.

The transducer holder and calibration target are attached to a frame, which is placed in line with the television camera and lens assembly. A detailed drawing of the transducer holder is shown in Figure 6. An almost sound-transparent foam is used to prevent dirt and spray from causing damage to the transducer during operation.

One main program and an interrupt request (IRQ) service routine constitute the system software; however, a collection of data processing routines is contained in the IRQ routine. The system software serves two functions. The first function involving measurement data generation and recording is treated first; the second function involving data processing and real-time control is discussed next.

The main program and most of the interrupt request service routine, as shown in Figures 7 and 8,

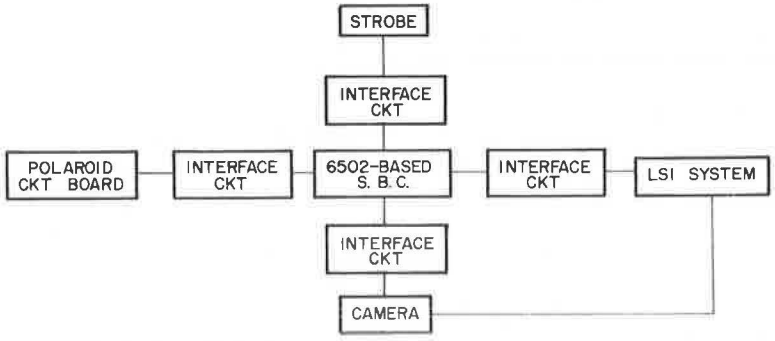

FIGURE 4 System block diagram.

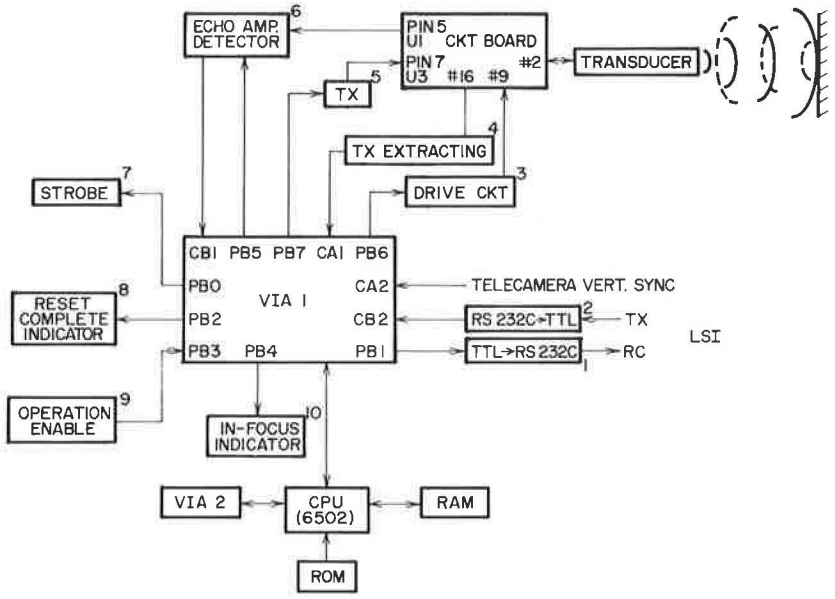

FIGURE 5 Interface block diagram.

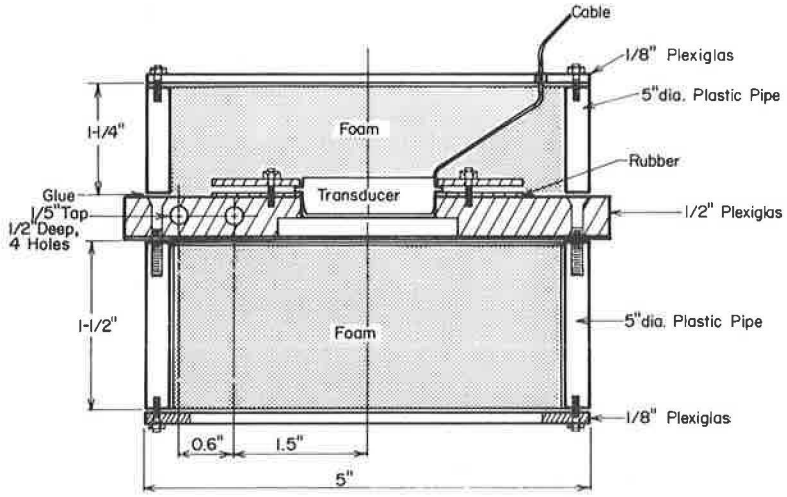

FIGURE 6 Transducer holder.

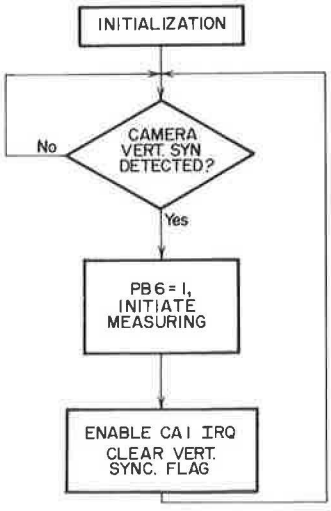

FIGURE 7 Main program flow chart.

perform the measuring and data recording. The description of these two modules is as follows.

Main Program

The main program does the initialization, which assigns program variables with predetermined values and sets up the proper operation mode for the VIA I/O port, timers, and interrupt controls. The measuring cycle is synchronized with the television camera field-scanning cycle (60 Hz). After a vertical synchronization signal is detected, the measuring cycle is initiated by providing a drive signal to the ultrasonic circuit board through pin 36 of the VIA. Then the program clears the vertical synchronization flag and executes a waiting loop until a new vertical synchronization is detected and a new operating cycle starts. During this waiting loop, interrupt requests from the ultrasonic circuit board (due to the transmission signal and the reflection echo signals) will occur and the IRQ routine is called.

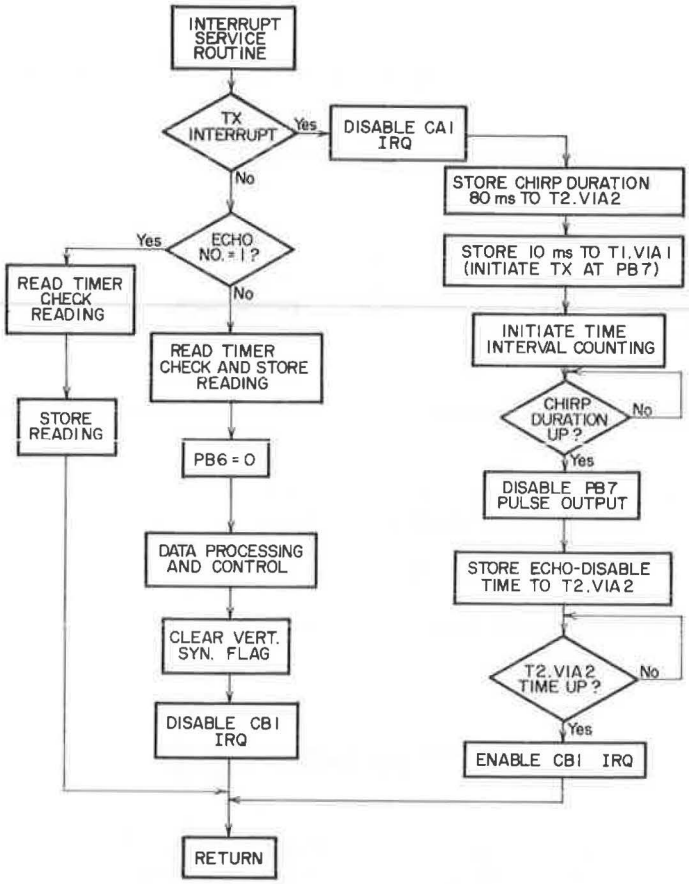

FIGURE 8 IRQ routine flow chart.

IRQ Service Routine

Three interrupt requests will occur during each measuring cycle as follows:

1. Interrupt request from the transmitting signal: the transmitting signal of 1-ms duration from the ultrasonic circuit board is routed to the VIA to generate an interrupt request instead of driving the transmitting power amplifier as originally designed. This service routine is called to generate 4 cycles of the 50-kHz pulse, which is output to the ultrasonic circuit board as the transmitting signal. Counting of the time interval is initiated at this stage.
2. Interrupt request by the reflecting echo from the calibration target: this interrupt service routine will record the timer reading as the basis for calibration. Because the 16-bit timer is composed of two 8-bit/byte timers and each timer is read separately, readings have to be checked for each data point.
3. Interrupt request by the reflected echo from the road surface: in this service routine, the timer reading is recorded and the drive signal at PB6 is cleared in order to initiate the next measuring cycle. Measured data from 2 and 3 are then used in the data processing and control function.

Four routines perform the data processing and control function. The system software flowchart in Figure 9 shows the relationship between these routines. The data generation routine provides the data necessary for these processing routines.

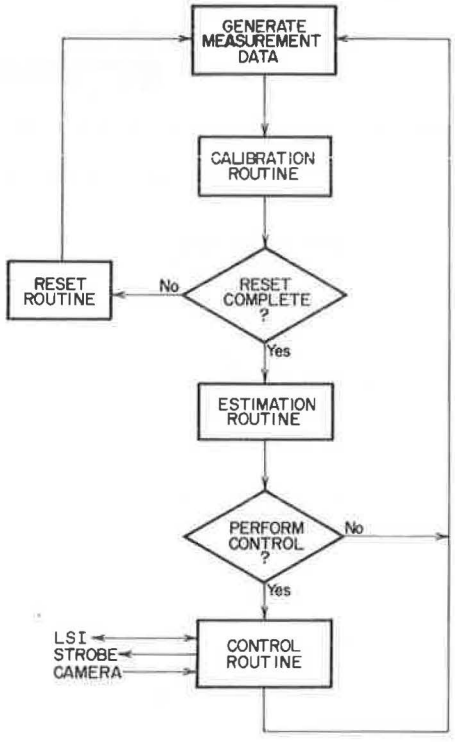

FIGURE 9 Data processing and control flow chart.

Calibration Routine

Because the speed of sound changes due to environmental conditions, and because the vehicle speed may also change during operation, a calibration procedure is necessary for each measurement cycle. This calibration is done by dividing the time interval of the detected echo from the road surface by that from the calibration target, which is placed 20 cm away from the transducer.

Reset Routine

The reset routine is called just after a new operation starts and before the vehicle moves. The function of this routine is to get the best focal length that will yield the best texture image and store it in memory as a standard focal length for use by the data processing routine. Because of the system transient response after power-on, the measurement results are discarded until 30 measurement cycles have been completed. The system is then believed to be stable and 10 measurements are collected. A procedure is applied to delete the maximum and minimum values of these 10 data, and the average of the other 8 measurements is taken as the standard focal length for the system.

Estimation Routine

To obtain the best texture image during the operation with the vehicle bouncing up and down, this routine predicts the time when the system will be in focus so that the control function can be performed at that time. The three most recently measured data points are collected and processed in the following way: (a) If all three measurements are within a 1.2-mm deviation from the standard focal length, the control function is performed immediately without doing an estimation, because the system lies well within the focus range. (b) If these conditions are not met, an estimation is performed, using a first-order Taylor series expansion formula as follows:

$$FL = f(t + \Delta t) = f(t) + f'(t)\Delta t \qquad (4)$$

where

$f(t)$ = current vehicle position,
FL = standard focal length,
Δt = time interval predicted, and
$f'(t)$ = rate of change in vehicle position.

The use of a first-order formula is justified by the fact that $f''(t)$, the rate of change of $f'(t)$ as the vehicle passes through the vehicle static equilibrium position, is negligible and so are the higher order terms.

It should be noted that near the vehicle equilibrium position $f(t)$ is actually the vehicle position 1.2 ms before an echo is received because of the sonar response delay discussed earlier. Also, it takes about 0.8 ms to perform the data processing up to this point; therefore, if Δt is smaller than 2 ms, it means that the system already passed the focal position and processing stops. On the other hand, if Δt is larger than 18 ms, it means that one more measurement can be taken and a better estimation might result; therefore, the processing procedure ends here.

If Δt is between 2 and 18 ms, the time interval of t-2 ms is loaded into the computer timer and counting is initiated. When this time interval elapses, the control routine is called.

Control Routine

The control routine first fires the strobe so that an instant image of the texture is burned on the camera vidicon. This image will remain clear for at least one frame period (32 ms) because of exposure to a strong light source. The control routine will then issue a timely command to the LSI processor to freeze the acquired picture for later image processing. Because the strobe may be fired at any time between frame acquiring periods, an undesired picture with partial texture image might be acquired if the freeze command is issued to LSI immediately after the strobe is triggered. Therefore, in order to acquire a picture with a complete texture image, the freeze command is issued only after a camera vertical sync signal is detected, which means a new frame with complete texture image will be acquired.

OPERATIONAL CONSIDERATIONS

Because of the self-calibration function in this ranging system, temperature fluctuations and wind gusts during operation will cause no effect on the accuracy of measurement. However, a temperature difference may exist between the sound path immediately adjacent to the surface and the ambient environment. This problem can be solved if the reset procedure is performed at the proper location so that surface temperature effect is incorporated into the calculation of the standard focal length. If the surface temperature has significantly changed since the reset function was performed, it may be necessary to repeat the reset function, depending on the quality of the picture.

Figure 10 shows an estimation of the worst case of the traffic noise spectrum at the acoustic transducer (4, Ch. 2). Figure 11 shows the free-field receive response for the ultrasonic transducer.

The ultrasonic transducer is designed to operate above 20 kHz, and because traffic noise above 20 kHz is insignificant, the ranging system is not susceptible to traffic noise. The transducer holder also helps shield the transducer from traffic noise.

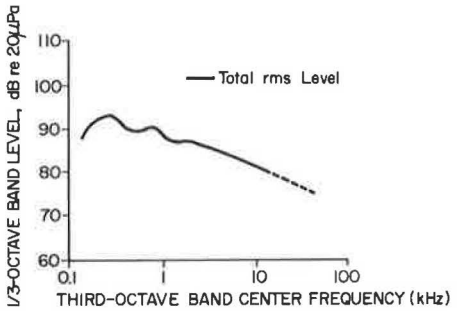

FIGURE 10 Estimated worst case traffic noise spectrum at the ultrasonic transducer.

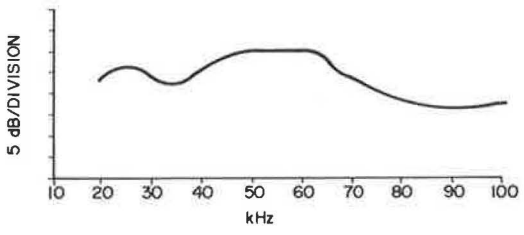

FIGURE 11 Free-field receive response.

Because 2 to 18 ms may elapse between the time a measurement is taken and the time a picture is taken, because of the estimation requirement, the distance between the acoustic footprint and the pavement surface where the picture is taken may range from 3.5-31.5 cm. If there is an abrupt change in pavement surface, such as a pothole or slope changes, which is unpredictable, a poor quality picture might be taken.

CONCLUSIONS

This microprocessor-based ranging system has performed satisfactorily in the texture project. If it is necessary to further improve the resolution and accuracy, the existing 1-MHz processor can be replaced with a higher frequency processor. If a 2-MHz microprocessor were used, the resolution would be improved to 0.08 mm, all data processing and control functions could be done faster, and better control quality could be achieved.

The Polaroid ranging unit is easy to use as an ultrasonic transmitting and receiving device. However, it has two drawbacks as far as this system is concerned. One is the power dissipation problem, and the other is the uncertain time interval between the VSW signal and the leading edge of the transmission signal, XLG (see Figure 3). Six to seven ms are wasted during this period. Adding 3 ms of sonar response time to this time interval, the maximum measuring rate can only reach 100 Hz, even if the power dissipation problem is solved. Thus, if a faster measurement is required, as in the road profilometer application, it would be necessary to design a new ultrasonic transmitting and receiving device.

Other applications include an electronic dipstick for sensing liquid level, machinery control, general noncontact displacement, and focusing instrumentation. An additional application is to sense approaching objects in safety areas. Most of these uses can be applied in the field of robotics.

ACKNOWLEDGMENTS

This paper is based on a research study conducted at the Pennsylvania Transportation Institute, Pennsylvania State University, under the sponsorship of the Federal Highway Administration, U.S. Department of Transportation. A full discussion of the study may be found in the final report for the project.

REFERENCES

1. J.J. Henry and J.C. Wambold. Pavement Surface Texture--Significance and Measurement. The Pennsylvania Transportation Institute, Final Report. U.S. Department of Transportation, Sept. 1983.
2. Polaroid Ultrasonic Ranging Unit Manual. Polaroid Corporation, Cambridge, Mass., 1980.
3. AIM 65 Programming Manual. Rockwell International, Pittsburgh, Pa., 1978.
4. J.M. Lawther. Feasibility Study for an Improved Acoustic Probe for Road Roughness Profiling. FHWA-RD-80-171. FHWA, U.S. Department of Transportation, July 1981.

Representation of Pavement Surface Topography in Predicting Runoff Depths and Hydroplaning Potential

G. WARREN MARKS, RICHARD S. HUEBNER, and JOSEPH R. REED

ABSTRACT

The sensitivity of the prediction of runoff depths and hydroplaning potential to variations in the elevation information used to define the pavement surface topography has been investigated. Different grid densities of elevation points, ranging from 8-in. to 36-in. spacing, and different levels of elevation data precision, ranging from 0.0003 ft to 0.05 ft, were evaluated. Topographic data, with elevation readings to 0.1 mm, were collected at a grid density of 4 in. over a 12- ft by 50-ft section of severely rutted roadway pavement. Runoff depths were computed using a one-dimensional, steady state computer model, employing a kinematic wave approximation. Maximum water depths for the severely rutted section were approximately 1 in. Predictive equations based on recent hydroplaning studies were used to estimate hydroplaning speeds. The results for the single section of pavement show that for a state-of-the-art prediction of runoff depths and hydroplaning potential, it appears adequate to collect elevation data points at a precision of 0.01 ft with a grid spacing of 36 in., being sure to include elevation points in the wheelpaths. It is recommended that additional test sites be observed and analyzed, especially under the conditions where maximum water depths range between 0.01 and 0.1 in. In this range, a more refined elevation precision and grid spacing may be required under certain circumstances.

Hydroplaning is a phenomenon in which a tire is completely separated from a pavement surface by a fluid layer, resulting in a reduction of the friction force at the tire-pavement interface to nearly zero. The primary factors influencing hydroplaning are the pavement surface, the vehicle and its operation, and the environment (typically rainfall). Presence of a fluid layer on the pavement is largely a function of the surface texture and topography in combination with significant rainfall accumulation and runoff. The friction characteristics of the tire-pavement interface differ considerably when the pavement is damp from when it is flooded with water. When the uplift resulting from fluid pressures within the tire-pavement contact zone exceeds the vertical load of the vehicle, the tire moves upward to maintain a dynamic equilibrium of the forces. Under these conditions, a gust of wind or a change in roadway superelevation or vehicle direction can create an unpredictable and uncontrollable sliding of the vehicle. Other variables influencing this phenomenon are the tire design, tread wear, tire-inflation pressure, and vehicle speed.

Efforts in the measurement of pavement surface topography have for the most part been directed toward the evaluation of road roughness. Road roughness is defined as the deviation of a pavement surface from a true planar surface with characteristic dimensions (e.g., roughness amplitude and frequency) that affect vehicle dynamics, ride quality, dynamic pavement loads, and pavement drainage (1). Road roughness is measured by two general types of equipment: profilometers, which measure the above characteristic dimensions directly, and response-type equipment, which measure surface roughness as a dynamic response of the measuring equipment to that roughness. There are two features of typical road roughness measurement that make it unsuitable for use in the measurement of pavement surface topography for the prediction of hydroplaning potential. Road roughness measurement is generally along only one of the wheelpaths, with some systems measuring both wheelpaths. This amount of data transverse to the roadway is inadequate to define where water may accumulate in the formation of hydroplaning fluid layers. Second, the profile reference datum for road roughness measurements is a moving, arbitrary datum, not tied precisely to true vertical (the direction of gravity). Thus, the roughness measurements do not in general yield correctly referenced topographic data (2).

Recent development of noncontact surface probes includes acoustic, infrared, white light, laser, and microwave radiation sources. The trailer-mounted System for Inventorying Road Surface Topography (SIRST), presently under evaluation by the Federal Highway Administration (FHWA), uses 12 infrared sensors spaced at 1-ft intervals transverse to the roadway. Pavement surface data points are collected at either 1-ft or 2-ft intervals, depending on whether the vehicle is traveling at 35 mph or speeds up to 55 mph. An inertial reference unit provides roll, pitch, and azimuth orientation, thus allowing for the maintenance of a stable reference datum referred to true vertical. This system has been developed particularly for the purpose of rapidly collecting the pavement surface topography for input to the prediction of hydroplaning potential (3).

In the measurement of road roughness, it is currently considered necessary that profiling equipment be capable of measuring amplitudes down to 0.01 in. (1). Preliminary tests by the Southwest Research Institute of the FHWA infrared sensors system have indicated that the height-sensing accuracy of the system is better than 0.01 in. (3). Although this accuracy is considered necessary for the measurement of road roughness, the accuracy required for the prediction of runoff depths and hydroplaning potential has not previously been investigated. Furthermore, it is of interest to determine the optimum density of the pavement surface data points to evaluate, for example, whether or not a 1-ft lateral and longitudinal spacing of data points is adequate, or

whether a 2-ft or 3-ft spacing would cause any appreciable change in the prediction of runoff depths and hydroplaning potential for a given pavement surface.

Results of a study to evaluate the elevation precision and grid point spacing requirements of pavement surface topographic data collected for the prediction of runoff depths and hydroplaning potential are reported in this paper. This study was conducted in conjunction with the evaluation and modification of the SIRST vehicle and sensors at the Pennsylvania Transportation Institute.

PAVEMENT SURFACE TOPOGRAPHIC DATA COLLECTION

Detailed topographic data of the roadway surface were collected at a 12-ft by 50-ft test site to: (a) establish a part of the topographic standard against which the SIRST data could be evaluated, and (b) provide a topographic data base for use in development of a hydroplaning potential prediction computer program, HYDROP. These data were ideally suited for use in this sensitivity analysis.

Following are the physical characteristics of the test site selected.

1. General location: Pennsylvania Transportation Research Facility Test Track, a controlled access facility.
2. Length and width: 50 ft long by 12 ft (1 lane) wide.
3. Roadway alignment geometry: straight level section.
4. Roadway surface material: bituminous pavement.
5. Pavement surface condition: severe rutting in the wheelpaths.

Selection of the measurement system and procedures used to collect the topographic data was based on the following criteria:

1. Perceived data point accuracy and density requirements of the roadway surface topography for use in predicting hydroplaning potential.
2. Stated data point accuracy and density capabilities of the SIRST vehicle.
3. Available topographic survey instrumentation.

These considerations led to the choice of differential leveling procedures. An automatic level with optical micrometer and level rod was used for the relative elevation measurement of roadway surface points at a spacing of 4 in. in both the longitudinal and transverse directions over the entire test site.

USE OF GRID POINTS

The SIRST vehicle was designed to collect topographic data points at a fixed lateral spacing of 12 in. and at a longitudinal spacing of either 12 in. or 24 in., depending on the speed at which the vehicle is pulled along the roadway.

A uniform grid of discrete topographic data points is a logical organized system to use to approximate a continuous topographic surface. In establishing the topographic surface data base standard, a fixed lateral and longitudinal spacing of 4 in. was used. This dense set of data points could then be used as a reasonable standard of comparison with which to evaluate data for larger grid spacings. The 4-in. spacing of data points had a significant impact on the effort involved in data collection for the topographic data standard. In a 12-ft by 50-ft test site, there are 663 data points at a uniform 12-in. spacing, and an equivalent 5,587 data points at a uniform 4-in. spacing.

In preparing the roadway surface for measurement, circular marks were painted on the roadway at the 4-in. spacing, using a 4-ft by 8-ft plywood pattern board in which 0.25-in. diameter holes had been correspondingly drilled. On the average, 2 hrs were required to lay out the 4-in. spacing marks over a 12-ft by 50-ft test site.

Measurement of elevations continued from fall 1980 into spring 1981. Selected sections of the test site were then remeasured during the summer of 1982. Reference marks were used to reposition the plywood pattern board when weathering made remarking of the points necessary.

MEASUREMENT PROCESS

To collect the elevation data at each of the marked data points, a Leitz/Sokkisha B-2A Automatic level and K&E Metagrad Philadelphia metric level rod were used with a Leitz parallel plate optical micrometer, capable of being read directly to 0.1 mm with estimation to 0.01 mm. The SIRST vehicle is reported to collect elevation information accurate to 0.01 in. averaged over a 4-in. diameter spot. To collect direct topographic data for the standard, level rod readings were reported to 0.1 mm, equivalent to 0.004 in., an increment 2.5 times smaller than the 0.01-in. requirement reported for profiling equipment.

A reference mark was identified to serve as the elevation datum for the topographic data for the site. Rod readings were collected in a uniform manner, with the rod-person moving to consecutive data points in a column, longitudinally along the test site, then returning in sequence along points in the adjacent column. The rod was held plumb using a bull's-eye rod level such that the foot of the rod was at the elevation of the circular paint mark on the roadway surface. Recording of the rod readings was expedited by using a finger-controlled tape recorder to voice-record both the rod reading (to the nearest cm) and the optical micrometer reading (mm and tenths of mm). Each column of 151 data points, covering the 50-ft-long roadway surface, took 15 to 20 min to observe and record. Allowing for rest breaks, the 12-ft by 50-ft test site took 16 hr to survey. The recorded data values were transcribed from the tape recorder onto data forms, then to computer data cards that were checked against the tape-recorded data, and finally read into a data file. This process took approximately 12 hr.

ERROR CONSIDERATIONS

Choice of the least increment for the level rod readings of 0.1 mm was principally based on the reported 0.01 in. accuracy of the SIRST vehicle data. In light of the task of defining the continuous topography of a bituminous or concrete roadway surface, using data points every 12 in. or even every 4 in., such elevation accuracies (0.01 in. and 0.1 mm) are of no practical value. This can be readily demonstrated by noting the variation in elevation over any section of a test site. The 0.1-mm detail is clearly in the noise level compared to the macro variation in topography of the roadway surface.

Error sources of concern are those in which magnitude affect the definition of the road surface topography. Use of the optical micrometer and short sight distances observed with the automatic level, while holding the level rod plumb with a rod level,

removes concern for significant level instrument and rod reading errors, or earth curvature and atmospheric refraction errors.

One important concern is the ability to hold the foot (i.e., bottom surface) of the level rod precisely at the elevation of the circular paint mark. The foot of the level rod is a flat surface approximately 1.7 in. square. Depending on the road surface topography in the immediate area about the circular paint mark, there may be difficulty in placing the foot of the rod precisely at the elevation of the mark. In addition, temporary irregularities in the road surface topography due to such items as loose road chips, also have a significant effect on the rod readings at the required level of accuracy.

With the level rod held plumb over the point of interest, the foot of the rod rests at the top of the pavement surface asperities. However, the reference elevation used to compute the volume of water traveling over the pavement surface must also take into consideration the texture depth of the asperities, determined in this study on a volumetric average basis using a sandpatch test (4). This necessary correction for the texture depth is applied during the data processing in the hydroplaning potential prediction computer program.

The largest error in road surface definition is the variation of the pavement surface with time, temperature, and related environmental changes. These variations result in significant changes in the roadway surface during a single day and over a period of weeks and months.

PAVEMENT SURFACE STABILITY

It is well-known that both bituminous and concrete pavement surfaces tend to expand and contract with environmental changes in temperature and moisture (5). Temperature differentials through the thickness of the pavement to the subgrade cause the pavement surface to warp, often resulting in pavement cracks. Other environmental effects on the pavement and pavement subgrade, such as rainfall and frost heave, give rise to even greater variations in the road surface topography. These deformations change throughout a given day as well as with longer periods of time.

In determining pavement surface variation of the test site after the original measurements were taken in 1980-1981, two sections, each 5 ft long by 12 ft wide (the width of one lane), were remeasured in 1982. Maximum differences of approximately 1 cm were observed in each of the remeasured sections. In the time interval between the two sets of measurements, the test site was subjected to severe heavy truck traffic, in support of other research projects at the test track. It is likely that this significant pavement loading, in conjunction with environmental conditions, caused movement in the surface topography.

Besides changes because of vehicular traffic and environmental effects, these elevation differences may also have been caused by not having the level rod at precisely the same point for both sets of measurements, and also by possible movement of the elevation reference mark. However, use of the pavement surface topographic data in a hydroplaning potential prediction computer program requires the availability of only relative elevation data. Absolute elevation data are not of critical importance. Elevation differences due to possible movement of the elevation reference mark are therefore of no effect, because all elevations of the pavement surface would appear to move the same amount.

GRAPHIC PRESENTATION OF TOPOGRAPHIC DATA

The most efficient means available to portray elevation differences over a topographic surface is through a graphic contour map of the surface. Computer-driven plotter generation of contours for the pavement surface of the test site was accomplished using the computer program package Surface II, developed by the Kansas Geological Survey (6). The plot is presented in Figure 1. The dimensions of the axes are in inches, the contours are labeled in meters, and the contour interval is 5 mm. The severe rutting in the wheelpaths is clearly noted. The maximum rut depth is approximately 6 cm.

The Surface II program is capable of accepting either a regular grid of elevation data values or a data set of irregularly spaced elevation values. Because the data set for the test site was collected on a regular 4-in. grid, the associated elevations were input directly into the Surface II program and the contours generated by a linear interpolation between the grid node values. The connection of like values formed the contour line. Piecewise Bessel interpolation was applied to smooth the contours, using a smoothing band 0.07 in. in width (6).

PREDICTING RUNOFF DEPTHS AND HYDROPLANING POTENTIAL

The topographic measurements enable the definition of a surface over which runoff occurs. Hydraulic analysis of the runoff leads to the prediction of runoff depths (water film thickness). These thicknesses are required to predict hydroplaning potential.

Water film thickness at nodes on the grid was computed using HYDROP, a one-dimensional, steady state, computer model that uses a kinematic wave approximation (7). The model itself is not the main focus of this paper and, thus, only a brief descrip-

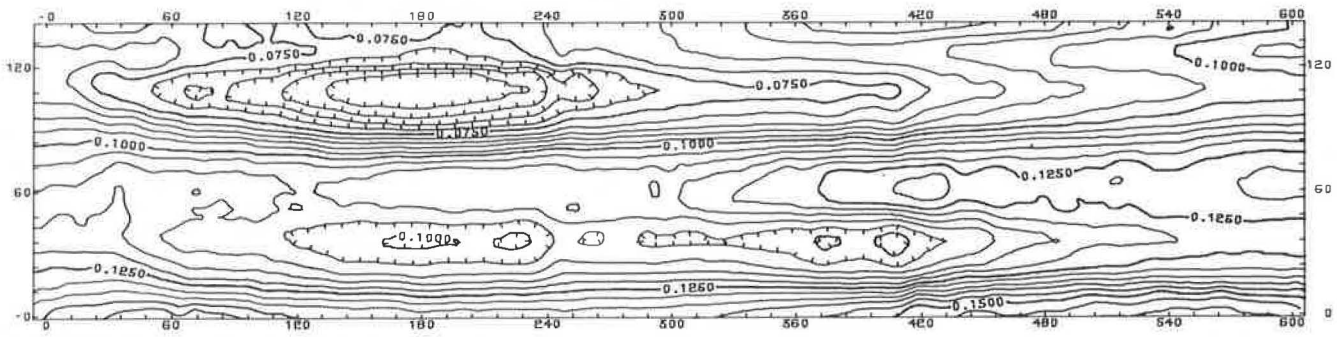

FIGURE 1 Contour plot of the test site pavement surface (perimeter axes in inches, contours labeled in meters, contour interval = 5 mm).

tion of its capabilities is included. The program, developed on an IBM 3081 computer and requiring 350K bytes of total storage for a 24-ft by 50-ft road section using a 12-in. by 12-in. grid, was specifically designed to account for the occurrence of rutting on highway pavements. Provided with the topography of the road surface, the program located the boundaries of areas that contributed rainfall runoff to local depressions. The area within the boundaries was divided into a series of cascading planes and collector channels. The selection of boundaries by the program introduced only minor continuity errors. The nodes where ponding would occur within each depression were also identified. The water surface elevation within each ponded area was determined by the conditions at a single outlet for each local depression. If not ponded, flow in ruts was treated as channel flow. The Chezy equation with Manning's C was used to model channel flow and overland plane flow.

Water depths computed by the Chezy equation or determined by outlet conditions for the ponded areas of the pavement were converted to water film thicknesses by subtracting the average texture depths of the pavement. This was done because the depth variable used in predictive models of hydroplaning speed is usually defined as "water depth above the asperities" (8). It was observed that texture depths vary laterally across a pavement, notably, in rutted areas and out of rutted areas. Thus, texture depths were assigned to each grid column. Manning's roughness coefficient was determined from texture depths (7) but was used in the computation of water depth based on whether a node was within a depression, for example, channel flow in a rut, or not in a depression, for example, overland plane flow.

Two predictive equations were used to estimate hydroplaning speeds at each node. Gallaway et al. (8) using multiple linear regression with a sample size of 1,038 cases found that hydroplaning speed could be expressed as:

$$HPS = SD^{0.04}\, p^{0.3}\, (TRD + 1)^{0.06}\, A \quad (1)$$

where A is the greater of

$$(10.409/WFT^{0.06} + 3.507) \text{ and } (28.952/WFT^{0.06} - 7.817)\, TD^{0.14}$$

where

HPS = vehicle speed at which hydroplaning occurs (mph);
TRD = tread depth in 32nd of an inch;
TD = texture depth in inches (silicon putty method);
WFT = water depth above the asperities in inches (water film thickness);
p = tire pressure in psi; and
SD = spindown in percent

for a range of water film thickness from 0.095 to 0.15 in. Gallaway reported a correlation coefficient of 0.85, indicating that 72 percent of the variation in hydroplaning speed, HPS, could be explained by the equation. For film thicknesses less than 0.095 inches, an equation based on a regression of data points collected by Agrawal et al. (9) was used.

$$HPS = 26.04\, WFT^{-0.259} \quad (2)$$

where HPS is vehicle speed at which hydroplaning occurs (mph), and WFT is water depth above the asperities, in inches (water film thickness). The regression had a correlation coefficient of 0.82, indicating that 68 percent of the variation in hydroplaning speed could be explained by the equation. Summary statistics for pavement sections were generated from computed hydroplaning speeds at each node but typically concentrated on conditions at nodes within the path of travel or wheelpaths.

Predicted waterfilm thicknesses by HYDROP were tested against measured waterfilm thicknesses at seven points on three field sites, using artificial rain-making equipment that produced average intensities of 1.0 to 2.5 in. per hour, spatially. The deviation of predicted values from measured values averaged 10 percent for six of the seven points, with a range of 3 to 15 percent for films of 0.08 to 1.1 in. The results were considered good in light of the uncertainty of the experimental rainfall rate averaged spatially, while HYDROP used the equivalent uniform rate. Pursuit of additional test data was deterred by instrumentation difficulties.

It should be noted that the analysis described here was restricted by several key limitations. First, water depths computed by the one-dimensional model were subject to the definition and location of boundaries for each contributing area. Also, depths within ponded areas were predicated on the assumption of a single outlet for each depression. Second, computed depths are significantly affected by the value chosen for Manning's roughness coefficient. When this study began, there was no conclusive means of selecting appropriate roughness coefficients for flow over pavements. Finally, the weakest parts of the analysis were the predictive equations used to estimate hydroplaning speed. Much more definitive work is required in this area before the results of an analysis of water depths on a pavement surface can be used to reliably predict the speed at which hydroplaning will occur.

VARIATIONS WITH GRID DENSITY AND ELEVATION PRECISION

The topographic data taken at the severely rutted test site, at lateral and longitudinal grid spacings of 4 in. and at the elevation least count of 0.1 mm, provided the basis for two significant evaluations. Comparison of predicted runoff depths and hydroplaning potential for different grid point spacings are presented in Table 1 and those for different elevation precisions are presented in Table 2.

Seven grid point spacings, varying in both the lateral and longitudinal directions from 8 in. to 36 in. are presented in Table 1. Computer run time for the 4-in. grid spacing was too excessive for it to be included. Evaluation of the sensitivity of the hydroplaning potential and runoff depth predictions to these different grid point spacings gives an indication of how far apart the elevation data points can be before the hydroplaning potential prediction is affected. It also points out the importance of having elevation data points in the wheelpath. The minimum hydroplaning speed, averaged over three consecutive data points, is 43 mph for all cases with elevation data in the wheelpath. This leads to the conclusion that as long as the elevation data includes points in the wheelpath, the data points may be as far apart as 36 in., with no degrading effect on the prediction of the minimum hydroplaning speed.

It is further noted from Table 1 that the maximum water film thickness and total depression storage vary greatly for cases without elevation data in the wheelpath. For cases with elevation data in the wheelpath, maximum water film thickness varies up to 14 percent, and total depression storage varies up to 28 percent, as the grid spacing increases.

Evaluation of the sensitivity of the hydroplaning potential and runoff depth predictions to various levels of precision of the grid point elevation data

TABLE 1 Sensitivity of the Prediction of Runoff Depths and Hydroplaning Potential for Different Grid Point Spacings (elevation precision = 0.0003 ft = 0.1 mm, rainfall intensity = 1 in. per hr)

	Grid Point Spacing (lateral x longitudinal)						
	8 x 8 (in.)	8 x 8 (in.)	12 x 12 (in.)	12 x 24 (in.)	24 x 24 (in.)	24 x 24 (in.)	36 x 36 (in.)
Elevation data in wheelpath	No	Yes	Yes	Yes	No	Yes	Yes
Maximum water film thickness (in.)	0.998	0.968	0.956	0.965	0.277	0.834	0.990
Total depression storage (ft^3)	2.4424	2.9839	2.5091	2.4345	0.9711	2.1555	2.6142
Percent of wheelpath below 55 mph	52.9	67.1	65.3	65.3	11.1	58.0	55.6
Minimum hydroplaning speed at a single point (mph)	43	43	43	43	46	43	43
Minimum hydroplaning speed, average of three consecutive points (mph)	43	43	43	43	46	43	43
Continuity error (% of total)	3.075	0.823	2.333	1.833	4.333	1.667	5.469
Computer run time (sec)	1,333	1,593	200	37	13	11	6

TABLE 2 Sensitivity of the Prediction of Runoff Depths and Hydroplaning Potential for Different Elevation Precisions (grid point spacing = 12 in. x 12 in., rainfall intensity = 1 in. per hr)

	Elevation Precision					
	0.0003 (ft)	0.0005 (ft)	0.0010 (ft)	0.0050 (ft)	0.0100 (ft)	0.0500 (ft)
Maximum water film thickness (in.)	0.956	0.967	0.965	0.948	0.946	1.166
Total depression storage (ft^3)	2.5091	2.4861	2.4895	2.5642	2.4581	2.6375
Percent of wheelpath below 55 mph	65.3	66.3	66.7	64.6	66.3	29.3
Minimum hydroplaning speed at a single point (mph)	43	43	43	43	43	43
Minimum hydroplaning speed, average of three consecutive points (mph)	43	43	43	43	43	43
Continuity error (% of total)	2.333	2.333	1.916	1.499	0.999	8.334
Computer run time (sec)	199	197	182	164	166	76

are presented in Table 2. These cases were all run at a grid point spacing of 12 in., in both the lateral and longitudinal directions. The various levels of elevation precision were established by rounding off the original elevation data (collected at a least count of 0.1 mm = 0.0003 ft) to the precision level indicated. It is noted that the minimum hydroplaning speed, averaged over three consecutive elevation data points, is 43 mph, for elevation precision ranging from 0.0003 ft to 0.0500 ft. The maximum water film thickness and total depression storage vary up to only 2 percent for elevation precision ranging from 0.0003 ft to 0.01 ft. At the elevation precision level of 0.05 ft, however, the variation in maximum water film thickness is 22 percent.

It is concluded from this evaluation that, for the state-of-the-art prediction of runoff depths and hydroplaning potential, it is adequate to collect elevation data points at a precision of 0.01 ft, with a grid spacing up to 36 in., being sure to include elevation points in the wheelpaths.

It is noted that these results have been obtained from the analysis of a single test site that was severely rutted, where the maximum water film thickness was approximately 1 in. The relative insensitivity of the minimum hydroplaning speed to large grid point spacings and elevation precision is largely due to the relative insensitivity of Equation 1 to water film thickness and to changes in water film thickness obtained for the given test site. Preliminary results from the analysis of a second test site, with maximum water film thickness approximately 0.06 in. and with maximum uniform pavement slope of 1.8 percent, appear to confirm these elevation precision and grid spacing requirements. However, it is recommended that additional test sites be observed and analyzed for further understanding of the relationships described, especially under conditions where maximum water film thickness ranges between 0.01 and 0.1 in. In this range, a more refined elevation precision and grid spacing may be required under certain circumstances.

ACKNOWLEDGMENTS

Appreciation is extended to the Federal Highway Administration for its sponsorship of the research from which this paper emanated. Also, the authors are grateful to personnel of the Pennsylvania Transportation Institute and the Department of Civil Engineering of The Pennsylvania State University for their support during the course of this study.

REFERENCES

1. J.C. Wambold, L.E. DeFrain, R.R. Hegmon, K. McGhee, J. Reichert, and E.B. Spangler. State of the Art of Measurement and Analysis of Road Roughness. In Transportation Research Record 836, TRB, National Research Council, Washington, D.C., 1981.
2. J.R. Darlington. Evaluation and Application Study of the General Motors Corporation Rapid Travel Profilometer. Report R-731. Michigan Department of State Highways, Lansing, April 1970.
3. J.D. King and S.A. Cerwin. System for Inventorying Road Surface Topography (SIRST). Report FHWA-RD-82-062. FHWA, U.S. Department of Transportation, Aug. 1982.
4. J.J. Henry and R.R Hegmon. Pavement Texture Measurement and Evaluation. ASTM Special Technical Publication 583. American Society for Testing and Materials, Philadelphia, Pa., pp. 3-17, 1975.
5. E.J. Yoder and M.W Witczak. Principles of Pavement Design, 2nd. Wiley, New York, 1975.

6. R.J. Sampson. Surface II Graphics System. (Revision One), Manual of the Kansas Geological Survey, Lawrence, 1978.
7. J.R. Reed and D.F. Kibler. Hydraulic Resistance of Pavement Surfaces. Journal of Transportation Engineering, ASCE, Vol. 109, No. 2, pp. 286-296, March 1983.
8. B.M. Gallaway, D.L. Ivey, G. Hayes, W.B. Ledbetter, R.M. Olson, D.L. Woods, and R.F. Shiller, Jr. Pavement and Geometric Design Criteria for Minimizing Hydroplaning. Report FHWA-RD-79-31. Texas Transportation Institute, Texas A&M University, College Station, 1979.
9. S.K. Agrawal, W.E. Meyers, and J.J. Henry. Measurement of Hydroplaning Potential. Report FHWA-PA-72-6. The Pennsylvania Transportation Institute, University Park, 1977.